TECHNISCHE UNIVERSITÄT WIEN
Vienna University of Technology

Master Thesis

Robust model to determine the epicenter of a seismic event by means of amplitude measurements.

carried out at the
Department of Geodesy and Geoinformation
Research Group of Geophysics
of the Technischen Universität Wien

under the guidance of
Em. O.Univ.Prof.Dipl.-Ing. Dr. Ewald Brückl

by
María del Puy Papí Isaba, Lic.
mppisaba@gmail.com / Maria.Papi-Isaba@zamg.ac.at

Vienna, 12. 05. 2016

Author's signature

Supervisor's signature

Acknowledgement

Firstly, I would like to thank my thesis supervisor Em. O.Univ.Prof.Dipl.-Ing. Dr. Ewald Brückl of the research Group of Geophysics of the department of Geodesy and Geoinformation at the Technischen Universität Wien. The door to Prof. Brückl's office was always open whenever I ran into a troublesome spot or had a question about my research or writing. He consistently allowed this paper to be my own work, but steered me in the right direction whenever he thought I needed it.

Besides my supervisor, I would also like to extend my gratitude to the Amt der NÖ Landesregierung, Abteilung Allgemeiner Baudienst for providing the funding that led to the realization of this master's thesis under the project "Analyse und Weiterentwicklung des seismischen Steinschlag / Felssturz Alarmsystems im Bereich des Steinbruches Spitz". Sincere thanks are also given to Dr. Josef Kaim Bau- und Sprengunternehmung GmbH. I would like to express my gratitude to Herr Dr. Schweigl and Herr Dipl-Ing. Bertagnoli in particular, without whose participation and input the field test, and therefore also the application of the method, could not have been successfully conducted.

I would like to sincerely thank all the colleagues in the geophysics research group, especially Dr. Adrián Florez-Orozco, BCs Theresa Maierhofer, Ing. Walter Loderer, Dr. Johanna Brückl, Dr. Stefan Mertl, Dr. Ingrid Schlögel, Dr. Werner Schwatal and Sonja Böcksteiner, who greatly helped me in many different aspects of my work.

And last but not least, I would like to express my sincere gratitude to my family and friends. Particularly, to my partner and friend, Ignacio, and parents, Francisco and María Puy, who always supported me and encouraged me to work harder and to go beyond myself in every aspect of my life.

Abstract

In this study, a robust new method to locate medium and low magnitude scale earthquakes is presented. This method is based on an empirical model of the ground motion obtained from amplitude data. Firstly, the amplitude is recorded at each station of the seismic network. Secondly, the maximum resultant amplitude within a time window is computed. Subsequently, the maximum resultant amplitude is back-projected to every grid-point covering the whole area of interest while applying an empirical amplitude – distance relation. The number of operating seismic stations in the local network equals the number of back-projected amplitude at each grid-point. This method introduces the new idea of selecting the minimum back-projected amplitude at each grid-point for further analysis. We refer to these back-projected ground velocities as pseudoMagnitudes. In case no detectable seismic event occurred, the spatial distribution of the minimum pseudoMagnitude constrains the magnitude of weak earthquakes hidden in the ambient noise. In the case of a detectable event, the spatial distribution of the pseudoMangitudes shows a significant maximum at the grid-point nearest to the actual epicenter. The application of this method is restricted to the area confined by the convex hull of the seismic station network. Additionally, one must ensure that there are no dead traces involved in the processing. This new method is almost wholly insensitive to outliers (data from locally disturbed seismic stations). This is possible due to the method of obtaining and storing a Pack-Projection Matrix, independent of the registered amplitude, for each seismic station. As a direct consequence, it is possible to save computational time for the calculation of the pseudoMagnitude at every grid-point.

The capability of the method was firstly demonstrated by using synthetic data. In addition, a first impression of the importance of the network distribution is derived from the results obtained from the synthetic test results.

Following, this method was applied using 43 local earthquakes of low and medium magnitude scale (1.7 < magnitude scale < 4.3). These earthquakes were recorded and detected by the seismic network ALPAACT (seismological and geodetic monitoring of Alpine PAnnonian ACtive Tectonics) within the period 2010/06/11 to 2013/09/20. The method gave accuracies of less than 10km for about 27% of the events for the [1-10Hz] band-pass filter and about 18% for the [1-5Hz] filter. On the other hand, about 68% of the events for he [1-10Hz] filter has a deviation from the epicenter location provided by ZAMG of 11km to 30km, whereas for the [1-5Hz] 63% of the events are to be found in this range. Moreover, the estimated epicenter in this thesis for the strongest event turned out to be 4km away from the one taken as real.

Finally, the method was applied to data recorded in the quarry of Spitz (NÖ-Austria). An existing seismic warning system did not fulfill the expected efficiency and reliability standards since the ratio of well-detected events to undetected events or false alarms was not satisfactory. The aim was to analyze how a seismic warning system must be designed in order to overcome these deficiencies. A small-scale seismic network was deployed in the Spitz quarry to evaluate the possibility of improving the early-warning rockfall monitoring network by means of seismic observations.

Zusammenfassung

In dieser Studie wird eine neue robuste Methode zur Lokalisierung niedriger und mittlerer Erdbebenstärken vorgestellt. Dieses Verfahren basiert auf einem empirischen Modell der Bodenbewegung, welches aus Amplitudendaten gewonnen wird. Zunächst wird an jeder Station des seismischen Netzes die Amplitude aufgezeichnet. Anschließend wird die maximal aufgezeichnete Amplitude innerhalb eines Zeitfensters berechnet. Nun wird diese maximale Amplitude auf jeden Rasterpunkt projiziert, welcher in die zu untersuchende Fläche fällt, während eine empirische Amplituden–Distanzbeziehung angewendet wird. Die Anzahl der seismischen Stationen in dem lokalen Netzwerk-Betrieb ist gleich der Anzahl der zurückprojizierten Amplituden an jedem Gitterpunkt. Durch die Auswahl der kleinsten, von den verschiedenen Stationen an die jeweiligen Gitterpunkte zurückprojizierten Amplituden wird eine sogenannte SourceMap erzeugt. Falls kein nachweisbares seismisches Ereignis aufgetreten ist, begrenzt die SourceMap die pseudoMagnitude von schwachen Erdbeben, die sichin Hintergrundgeräuschen verbergen könnten. Im Falle eines nachweisbaren Ereignisses, zeigt die räumliche Verteilung der pseudoMagnituden in der SourceMap ein signifikantes Maximum an den Gitterpunkten welche am nächsten zum Epizentrum liegen. Die Anwendung dieses Verfahrens ist auf den Bereich innerhalb der konvexen Hülle des seismischen Stationsnetzes beschränkt. Darüber hinaus muss man sicherstellen, dass keine toten Spuren in der Verarbeitung beinhaltet sind. Im Gegensatz zu Methoden, die auf der L2 Norm basieren, ist diese neue Methode unempfindlich gegenüber Ausreißern, also Daten von gestörten seismischen Stationen. Da ein Großteil der erforderlichen Berechnungen nur einmal und vorab durchgeführt wird, eignet sich die Methode gut für real-time Auswertungen.

Die Leistungsfähigkeit der Methode wurde zunächst mit synthetischen Daten demonstriert.

Danach wurde diese Methode auf 43 lokale Erdbeben niedriger und mittlerer Stärke angewendet (1,7 < Richterskala < 4,3). Diese Erdbeben wurden durch das seismische Netzwerk ALPAACT (Seismological and geodetic monitoring of ALpine-PAnnonian ACtive Tectonics) im Zeitraum von 11. Juni 2010 bis 20. September 2013 aufgezeichnet.

Schließlich wurde das Verfahren auf Daten, welche im Steinbruch Spitz (NÖ-Österreich) aufgezeichnet wurden, angewandt. Es wurde demonstriert, dass die neue Methode die Grundlage für ein verlässliches Steinschlagwarnsystem bilden kann.

Contents

Table of Contents

1. Introduction 1

2. Study areas and challenges 3
2.1. The southern Vienna Basin and the Mur-Mürz Valley 3
2.2. Seismic network at Spitz (NÖ) quarry 4

3. Theoretical robust model. Attenuation model of seismic waves 7
3.1. The amplitude behaviour 7
3.2. Use amplitudes 10
3.3. Magnitude scales 10

4. Earthquakes location methods 13
4.1. Location of earthquakes based on travel time data:
Circle methods 13
4.2. Location of earthquakes without picking phases 17
4.3. Kanamori method 18

5. Method based on pseudoMagnitudes 19
5.1. Data processing (Seismon and pSysmon softwares) 20
5.2. Computing of the ground motion model 20
5.3. Construction of the Back-Projection Matrix (BPM) 21
5.4. Construction of the Back-Projection Amplitude Matrix (BPAM) 21
5.5. Generation of the SourceMap 22
5.6. Seismic event detection 25
5.7. Code sequence (Step by Step process) 26

6. Simulation with Synthetic Data 27
6.1. Test with Synthetic Data 27
6.2. Data processing and synthetic result (Source Map) 29

7. Application to ALPAACT earthquake database 37
7.1. Empirical ground motion model obtained from ALPAACT
network data 42
7.2. PseudoMagntude calibration 49
7.3. Localization example of seismic events at ALPAACT network 50

8. Application to seismic monitoring of rockfalls at Spitz quarry (NÖ, Austria) 59
8.1. Field trial with a new seismic monitoring system 59

8.2. Seismic data processing and analysis 64
8.3. Detection and localization of rockfalls 70
8.4. Terrestrial laser scanning survey 75
8.5. Analysis and evaluation of the earlier warning system 78
8.6. Avoid false alarms 81

9. Conclusions 85

10. References 89

List of Figures 93

List of Tables 97

Source Code 99

1. Introduction

The aim of this master's thesis is to present a robust new method to detect and locate medium and low magnitude earthquakes based on amplitude measurements from seismic network measurements. Rapid, robust and reliable assessment of source characteristics of medium and low earthquakes is an important task for seismic hazard assessment and mitigation in densely populated and developed regions.

The development of a reliable warning system requires a technical solution, which can determine earthquake parameters as robust and quickly as possible without risk of errors caused by false picking of P- and S-wave arrivals, loss of station data, and similar problems resulting from the seismic network design. A robust and quick method for detection and location of seismic events based on seismic amplitude observations is proposed in order to solve and improve different warning systems, and it is oriented towards multiple applications and settings, such as local seismic networks, as well as landslide, mine, and quarry monitoring.

In order to investigate and solve these challenges, this paper is organized as follows:

In section 2, the study areas where the method will be tested are introduced and described. Firstly, this concerns the local network of ALPAACT (Seismological and Geodetic Monitoring of Alpine-Pannonian ACtive Tectonics) in Austria and secondly, the rockfalls warning network situated in the Spitz quarry.

In section 3, the necessary mathematical background for the method based on amplitude recording is reviewed. The functional model of seismic amplitude and the description of its behavior and properties is presented. The amplitude behavior of a seismic signal depends on the distance between the source and the monitoring station. The decrease of amplitude when increasing distance from the source is referred to as ***attenuation***. It is, in part, due to the geometry of propagation of seismic waves, and partly due to the anelastic properties of the material though which they travel. Depending on the media (homogeneous-inhomogeneous, elastic-anelastic, etc) and the type of wave that travels through the media, the amplitudes of the waves decrease with distance due to geometrical spreading as a potential law r^a. a is the power-law parameter to be determined by means of a ground motion model. In this section, the term pseudoMagnitude is also introduced. It will form the basis of the estimations, and will define the empirical ground motion model.

In section 4, the robust method to determine the epicenter of a seismic event from amplitude measurements is presented and justified. To derive the method, we take advantage of the fact that any small seismic sources can produce indefinitely large amplitudes as long as they are located close enough to the sensor of the seismic station. The basic concepts introduced in the new method are: Back-Projection Matrices (BPA), Back-Projection Amplitude Matrices (BPAM), and obtention of maximum resultant ground velocities in sliding time windows covering the whole period of interest amplitudes. It will be shown that the ordered minimum Back-Projection Amplitude values are insensitive to changes in maximum velocity amplitude recordings, resulting in a very robust result.

Section 5 contains a preliminary experiment that shows the capability of the method using synthetic data. The results provide the earliest evidence not only on the potential of the new method, but also on its limitations and therefore an outlook towards additional studies that should be conducted.

Section 6 is dedicated to the application of the method to the seismic data of 43 real earthquakes provided by the ALPAACT local network. The method is tested for earthquake localization and the numerical results of the model were compared to a set of real data from ALPAACT with two band-pass frequency filters of [1-5 Hz] and [1-10Hz]. Amplification factors at each site are estimated in order to determine the station corrections.

In section 7, the examination and analysis of the existing seismic warning system of rockfalls, which was performed at the quarry of Spitz (NÖ-Austria), is described. Furthermore, a field test was conducted in the quarry in order to develop a rockfall warning system based on the new method. The purpose of this section is also to explain some of the issues involved while working with the devices and methods of the recent seismic warning system in the quarry of Spitz. A Terrestrial laser scanning (TLS) survey was employed with the intention of detecting volumetric changes along the slope after the occurrence of the rockfalls.

Finally, in section 8, brief conclusions are outlined. At the end of the section, a discussion on how a seismic warning system must be designed to overcome the deficiencies of the robust model in order to detect and locate seismic events and avoid false alarms is presented.

As final remark, a CD is included in the master's thesis as an appendix due to the excessive number of images that were analyzed and obtained during the work.

2. Study areas and challenges

Two different study areas were selected in order to apply and test the method developed in this paper. The first one was chosen with the objective of testing the method for local to regional distances, and real earthquake events detected by the ALPAACT (Seismological and Geodetic Monitoring of Alpine-Pannonian ACtive Tectonics) [Brückl et al. 2013] network, were used. In addition, a seismic experiment at Spitz (NÖ) quarry, which allowed us to test the capability of the location method in micro-seismicity environment, was performed. Both tests allowed us to evaluate the new location method and its potential to be integrated into an earthquake early warning system in high earthquake hazard and risk areas.

2.1. The southern Vienna Basin and the Mur-Mürz Valley

The southern Vienna Basin and the Mur-Mürz Valley are the seismically most active regions in Austria. Most other earthquakes cluster around the Mur-Mürz fault (MM) and the Vienna Basin Transfer fault (VBT) (Figure 2.1).

Due to ongoing convergence between the European Plate from the north and the Adriatic plate from the south, crustal blocks laterally extrude to the east into the Pannonian Basin [Brückl et al. (2010)]. Two sinistral strike-slip faults reveal this process: the Salzach-Enns-Mariazell-Puchberg (SEMP) and the more seismically active MM. The Vienna Basin lies in the northwestern extension of those faults, in the transition of the Eastern Alps to the Western Carpathians. This pull-apart basin that started forming in the Early Miocene is now filled with sediment layers of a few kilometers depth. Here, the SEMP and the MM migrate into the VBT. Under the sediment layers, the Bohemian Massif forms the underground of the Vienna Basin, at depths between 3 and 9 km.

Data provided by the ALPAACT network is used in order to understand seismic activity in the Mürz Valley - Semmering - Vienna Basin transfer fault system in Austria and what makes it such a relatively high earthquake hazard and risk area.

This region is one of the most densely populated and most developed in Austria, including the capital Vienna and its surroundings, with more than 2 million inhabitants and sensitive infrastructure. Seismic hazard assessment and mitigation is therefore an important task. The new method was applied to real

data of 43 local earthquakes of low and medium magnitude $1.7 \leq m_l \leq 4.3$ in order to test its capability, efficiency and operation range.

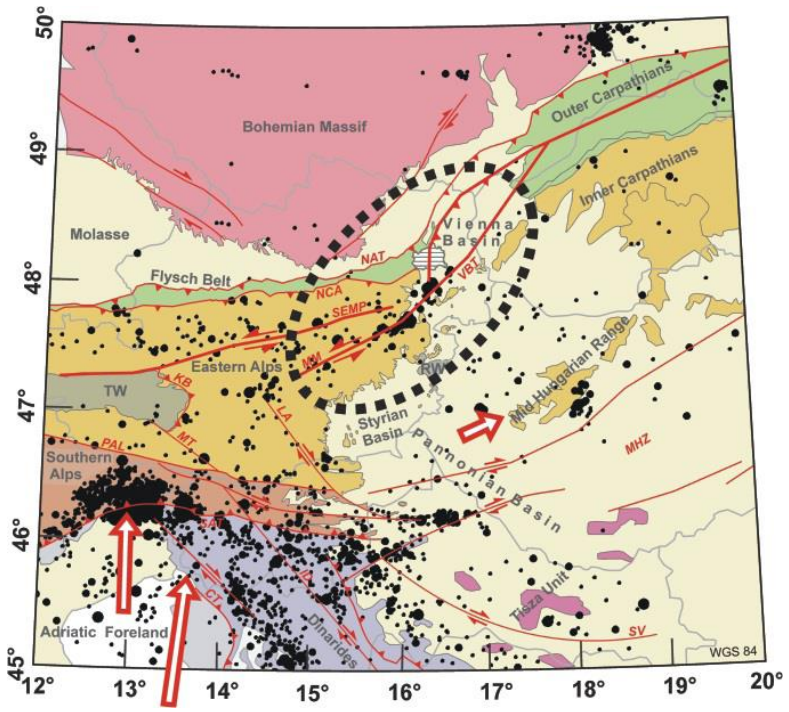

Figure 2.1: Seismicity in Mur-Mürz fault (MM) and the Vienna Basin Fault (VBF)

According to the characteristics of the study area, and the additional computation of the average depth of the 43 studied events, a mean hypocentral depth of 9 km was selected for further computations. An overview of the main tectonic units, faults and seismicity is given in figure 2.1.

2.2. Seismic network at Spitz (NÖ) quarry

The second experiment was performed in a small-scale passive seismic network established at the quarry of Spitz. The overall dimension of the quarry is approximately 200x200 m^2 (long, wide). The height range of this area goes from 261 m (St1) up to 419 m (St3), as seen in figure 2.2. The seismic network comprises seven seismic stations located along the quarry edges, with an average inter-station distance of about 100 m, and acquiring data in continuous mode so that, the rockfall hazard area is covered.

In the past, significant rockfalls occurred in the quarry of Spitz, Niederösterreich (NÖ). These events posed a danger to persons, railway and road. An alarm system composed of three seismic sensors and a crack monitor was established in 2007. In case of an alarm, a road traffic light was turned on red and competent operational centers were notified. Nevertheless, the ratio of

detected events to non- or false alarms was not satisfactory. Therefore, a robust seismic detection method was implemented for this specific area in order to detect and locate rockfall events.

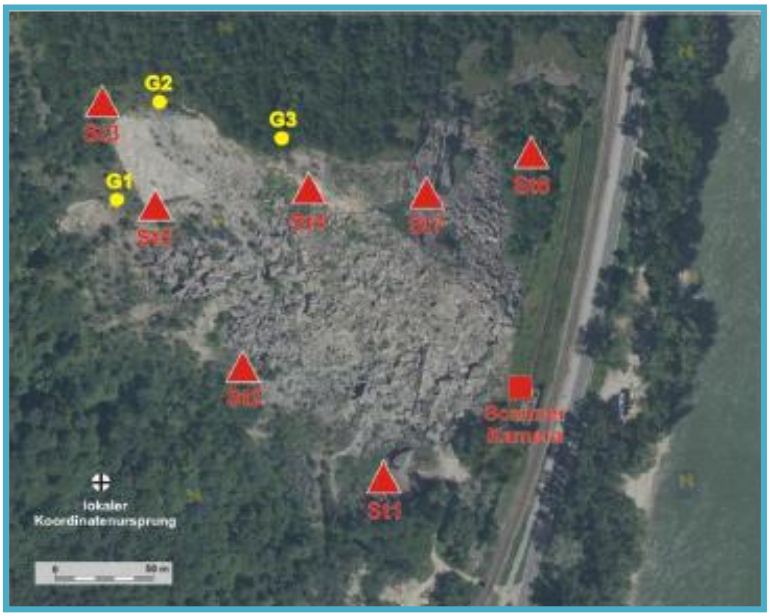

Figure 2.2. Spitz quarry area. Image provided by the Niederösterreich government. Red triangles show the positions where the seismic stations were placed.

The term rockfall covers a wide range of rock volume. For safety reasons, even rock volumes $< 0.001m^3$ may be of interest and monitoring systems have been developed by consulting companies. At the upper limit volumes of up to $10^4\ m^3$ or $10^5\ m^3$ (Hungr et al. 2001) are designated as rockfall. The seismic characteristics of these larger volumes were studied e.g. by Deparis et al. (2008) using recordings of a regional network. A well-documented example of the rockfalls built by one single or a few boulders jumping down the slope was observed at Gradenbach (Brückl et al., 2013). The seismic signature is an irregular sequence of impulsive signals moving down the slope. The strongest impact could be well located by the use of first arrival times and the epicenter agrees well with the location of the main impact.

Furthermore, induced seismic events were recorded for the application of the method with the aim of improving the previous alarm system installed in the quarry and having a real-time automated location routine. The purpose of this field experiment was to study and report some of the issues involved in earthquake detection and location of the impact point of the rockfalls, as well as the strength of the collision, e.g. pseudoMagnitude. Consequently, it allows us to define a robust alarm system, having efficiently defined a threshold value in advance.

3. *Theoretical robust model. Attenuation model of seismic waves*

The basis of the method is a proposal made by Kanamori in 1993. The idea presents the possibility of using the amplitude of the seismic waves (*P*- or -*S* or *body*-waves) to rapidly detect and locate earthquakes, taking into account the geometric spreading of the seismic waves and physical (damping) effects.

In general, source location methods are based on the automated picking, identification and association of the first arrivals of seismic waves, as well as the knowledge of the velocity model between the hypocenter and the seismic station, which allows the calculation of distances between stations and seismic source. In our method, the amplitudes will be our distance indicators, by means of the amplitude – distance relationship resulting from the path effect and other effects from local site geology. Therefore, we must first define a distance amplitude relationship according to the method of Kanamori, considering the behavior of the amplitudes of seismic signals.

The main advantage of locating earthquakes with amplitudes is that the amplitudes are much easier to determine than arrival times, especially in earthquakes and early warning applications. Another advantage is the possibility of improving the early warning monitoring networks due to understanding of the spatial distribution of ShakeMaps parameters. The method allows us to transform a ShakeMap onto a SourceMap.

3.1 The amplitude behavior

The amplitude behavior of a seismic signal depends on the distance between the source and the monitoring station. This leads to different amplitude values from the same seismic event source in different places. The decrease of amplitude when increasing distance from the source is referred to as ***attenuation***. It is, in part, due to the geometry of propagation of seismic waves, and partly due to anelastic properties of the material though which they travel.

When seismic waves travel through the earth, for a spherical wave front (e.g., body-wave propagation in a homogeneous isotropic medium) the surface area grows proportionally with r^2 and for a cylindrical wavefront (e.g., for surface waves) only with distance r. In a ideally elastic medium, the amplitudes of waves decrease with the distance due to geometrical spreading, which depends on factors of (~1/r) for spherical waves (body waves decay is inversely

proportional to the distance). To compare with cylindrical waves, the surface wave amplitudes decrease inversely with the square root of the distance from the source [Udias, A, 1999].

The many processes that influence the shape and amplitude of the seismic signal can be summarized as follows:

- ***Geometric spreading*** *(scattering)*
- ***Anelastic attenuation*** *(anelastic damping)*
- Dispersion
- Phase distortions *(interphase division)*

Geometric spreading

One reason for the decrease in the seismic wave amplitudes with increasing distance is called ***geometric spreading***, and geometrical effects produce it. When considering only waves with small wavelengths compared to the inhomogeneities of the propagation medium (high-frequency approximation), we can assume that the seismic energy only travels along the rays. According to the energy conservation law, the energy flux within a considered ray tube must remain constant although the surface area *dS* of the wavefront related to this ray tube may vary along the propagation path due to focusing or defocusing of the seismic rays. Considering two surface patches of the propagating wavefront *dS1≠ dS2* at different times, which are bounded by the same ray tube, and assuming that v and r are the same at these two locations, then:

$$\frac{\boldsymbol{A_1}}{\boldsymbol{A_2}} = (\boldsymbol{dS_2}/\boldsymbol{dS_1})^{\boldsymbol{1/2}} \qquad (3.1)$$

i.e., the amplitudes (*A*) vary inversely as the square root of the surface area of the wavefront patch bounded by the ray tube. Thus, amplitudes increase due to ray focusing, which is particularly strong at caustics and decrease when the wavefront spreads out.

In a simplified way, we can write for the decay of source amplitude A_0 with distance *r*

$$\boldsymbol{A_k} = \frac{\boldsymbol{A_{0,source}}}{\boldsymbol{r^{\alpha}}} \cdot \boldsymbol{C^k} \qquad (3.2)$$

Where the geometrical spreading term is $\frac{A_{0,source}}{r^{\alpha}}$; $\boldsymbol{r}$ is the distance from the source to the station; α is an exponential factor controlled by the geometric spreading type. In addition, C^k factor is the site amplification due to geology,

among other effects. According to experimental data, α varies between about 0.3 and 3, depending also on the type of seismic wave and distance range considered [Bormann et al, 2002].

The value of exponent α in the amplitude-distance power relation for different ranges of epicenter distances presents an issue. Beyond 10 km epicentral distance, a value of $\alpha \sim 1.6$ relies on the derived results of the national seismological services. For epicentral distances in the range of the network dimensions, the exponent α could be derived from seismic data recorded at the landslide, in local networks as ALPAACT, or in small seismic networks as in the quarry of Spitz.

Wust-Bloch & Joswig (2006), for example, found that for epicentral distances $R < 1\,km$, an exponent of $\alpha = 1$ is appropriate, while the epicentral range $\sim 1\,km < D < \sim 10\,km$ remains experimentally indefinite. Wust-Bloch & Joswig (2006) pragmatically assume a change from $\alpha = 1.6$ to $\alpha = 1.0$ at a distance of 3 km. According to these considerations, we will calculate the empirical parameter (α) for each area studied.

Seismic amplitude model

We consider the amplitude $\boldsymbol{A_k^e(f, r_{i,j})}$ integrated by the following terms corresponding to an event e, on a site *k (station)*

$$\boldsymbol{A_k^e(f, r_{i,j}) = A_{0,source}^e(f) + Distance^e(r_{i,j}, f) + Site_k(f)} \qquad (3.3)$$

$\boldsymbol{A_{0,source}^e(f)}$ is an effect due to the event (e) source size; $\boldsymbol{f}$ is the frequency (5Hz and 10Hz); $\boldsymbol{Distance^e(r_{i,j}, f)}$ is a distance effect, $(a \cdot \log_{10}(r_{i,j}^e))$, an empirical ground velocity – distance relation, which corrects the amplitude as function; $\boldsymbol{r = \sqrt{\Delta^2 + h^2}}$ the hypocentral distance, the epicentral distance (Δ) and focal depth (h).

$\boldsymbol{Site_k(f)}$ is the station effect ($\boldsymbol{C^k}$) due to the geology of the seismometer location. In brief, the amplitude undergoes two major changes, one resulting from the path effect, and another one due to the local site geology from location of the seismometer. The path effect is modeled using a combination of geometrical spreading (decay parameter) and anelastic attenuation function. The amplification or damping of the amplitude depends on the local site geology, structure and evolution of the study area.

3.2 Use of amplitudes

Since the introduction of an intensity scale by Mercalli, isoseismal maps have been derived from macro-seismic observations. This allows for a reliable determination of the epicenter and can even achieve estimates of the focal depth. This method can also be applied to instrumental data on ground motion, using general or locally valid amplitude-distance relations for seismic waves. Kanamori (1993) used accelerometer data and a peak acceleration-distance relation to fit the data recorded during earthquakes at or near the San Andreas Fault. He used a least squares method to determine magnitude and epicenter location, and emphasizes the simplicity of the method, the ability for real time applications, and the reasonable accuracy that could be achieved.

Kanamori's method can be adapted to the location of Landslide Micro-Earthquakes (LMEs) in a straight-forward manner. The approach in this master's thesis is to extend the method to the location of micro earthquakes on a local network, and rockfalls on a passive network. Different from Kanamori's method, we consider ground velocity instead of ground acceleration. Analog to the definition of the local magnitude (m_l), the pseudoMagnitudes derived from the recordings of individual seismic stations in a local grid according to eq. 3.4 is defined.

$$\boldsymbol{pseudoM_e^k = \log_{10}\left(V_e^k\right) + a \cdot \log_{10}\left(r_e^k\right) + C^k} \qquad (3.4)$$

Where $\boldsymbol{pseudoM_e^k}$ is the pseudoMagnitude derived for each event ($\boldsymbol{e}$) and station $\boldsymbol{k}$; $\boldsymbol{V_e^k}$ is the maximum resultant vibration velocity observed at station $\boldsymbol{k}$ for each a certain event $\boldsymbol{e}$; $\boldsymbol{a}$ is the power-law amplitude factor; $\boldsymbol{r_e^k}$ is the hypocentral distance from station $\boldsymbol{k}$ to the event epicenter, and $\boldsymbol{C^k}$ is the station correction, which corrects local seismometer coupling; these are usually considered to be constant, for example, for Landslide Micro-Earthquakes (LMEs).

Therefore, there is one observed parameter ($\boldsymbol{V_e^k}$), one parameter that can be computed from the stations and hypocenter distances ($\boldsymbol{r_e^k}$) and three unknown vectors: the pseudoMagnitude, the station correction and the power-law amplitude factor. The logarithmic scale is used because the seismic-wave amplitudes vary enormously. A unit increase in magnitude corresponds to a 10-fold increase in amplitude of ground displacement.

3.3 Magnitude scales

The detailed understanding and quantification of the physical processes and geometry of seismic sources is one of the ultimate goals of seismology, be it in

relation to understanding tectonics, improving assessment of seismic hazard or discriminating between natural and anthropogenic events. Earthquakes can be quantified with respect to various geometrical and physical parameters such as time and location of the (initial) rupture and orientation of the fault plane and slip, fault length, rupture area, amount of slip, magnitude, seismic moment, radiated energy, stress drop, duration and time-history (complexity) of faulting, particle velocity, acceleration of fault motion, etc. It is impossible, to represent this complexity with just a single number or a few parameters.

Moment Magnitude

There are magnitude scales not based on the ground motion parameters directly, such as the *moment magnitude* (M_w) (eq. 3.6). The best way to quantify the size of an earthquake (or a seismic event) is to determine its seismic moment (M_0), and the shape of the overall source spectrum. This can be done by recovering the source time function from either body or surface waves, but this requires relatively complete modeling of the waveform.

The moment magnitude is related to the seismic moment M_0, which can be derived from the long-period amplitude determined from the displacement spectra of isolated P-waves (Ω_0) (eq. 3.7) [Hanks and Kanamori, 1979].

$$M_w = \frac{2}{3}\log(M_0) - 6.06 \qquad [MKS\ units] \qquad (3.5)$$

$$M_0 = \frac{4\pi\rho {V_p}^3 r\Omega_0}{U_p} \qquad (3.6)$$

Where $\boldsymbol{\rho}$ is the density; $\boldsymbol{V_p}$ the P-wave velocity; $\boldsymbol{r}$ is the hypocentral distance, which only compensates for geometrical spreading (other processes reducing amplitudes with distance are not taken into account); $U_p = 0.52$ is a correction for the mean radiation pattern of P-waves [Aki and Richards, 1980]. An equivalent equation for S-waves also exists.

The low frequency spectral amplitude Ω_0 must be determined from the P-waveform alone, therefore the derivation of magnitudes from seismic moment can only be applied to impulsive waveforms that allow for a separation of the P-wave (or S-wave) phase from other overlapping phases. [Brückl, E, 2015].

Local Magnitude ($\boldsymbol{m_L}$)

It is desirable to have a measure of earthquake size that is much simpler to derive, for example the amplitude of a single seismic phase, such as the P-wave, but they have some limitations. On the other hand, measurements based on wave amplitude are still very useful because of their simplicity and because the

high-frequency shaking in a narrow frequency band is often responsible for damage from earthquakes. [Lowrie, W, 2007]

The concept of *earthquake magnitude*, a relative-size scale based on measurements of seismic phase amplitudes, was developed by K. Wadati and C. Richter in the 1930's.

Magnitude scales are based on two simple assumptions:

1. Given the same source-receiver geometry and two earthquakes of different size, the "larger" event will, on average, produce larger amplitude of arrivals.
2. The amplitudes of arrival behave in a "predictable" manner. That is, the effects of geometric spreading and attenuation are known in a statistical way.

For a more complete review of magnitude scales, see Lay, T. and Wallace, T.(1995)

For example, the Austrian seismological service can calculate m_l using equation 3.8, with A the maximum value of horizontal components $[nm/s]$, band-pass 1 – 10 Hz, the exponent in amplitude-distance power relation $a = 1.66$, and the epicenter distance [degree], and $C = -0.304$.

Networks deployed on a local network, on a passive network and landslides provide a further opportunity to record local earthquakes recorded by nearby seismic observatories. This offers the opportunity to calibrate magnitudes derived from data recorded at the local network, rockfalls on passive network and landslide with local magnitudes m_l provided by the national seismic services.

Our theoretical robust model, which will initially be applied in a test simulation, next to the ALPAACT network and finally to the seismic data recorded at the Spitz quarry, shall be founded on the magnitude expression based on the ground displacement.

Therefore, a calibration will be necessary to convert the pseudoMagnitude values to local magnitude (m_l). A correlation relationship between the local magnitude determined by the Zentralanstalt für Meteorologie und Geodynamik (ZAMG) and the pseudoMagnitude obtained by the model can be derived for the ALPAACT network and applied to the Spitz quarry data later on.

4. Earthquake location methods

4.1 Location of earthquakes based on travel time data: Circle methods

One of the most important tasks in observational seismology is locating seismic sources. Standard earthquake location methods are based on the arrival times of seismic waves (P- or S waves). The unknown focal coordinates are longitude and latitude (or X and Y) of the epicenter, the focal depth Z, and the focal time t_0.

In general, the determination of source location is based on the automated picking, identification and association of the first arrivals of seismic waves (*P- or S* waves) and on the minimization of the residuals between theoretical and observed arrival times of the considered seismic phases, as well as knowing the velocity behavior between the hypocenter and the seismic station.

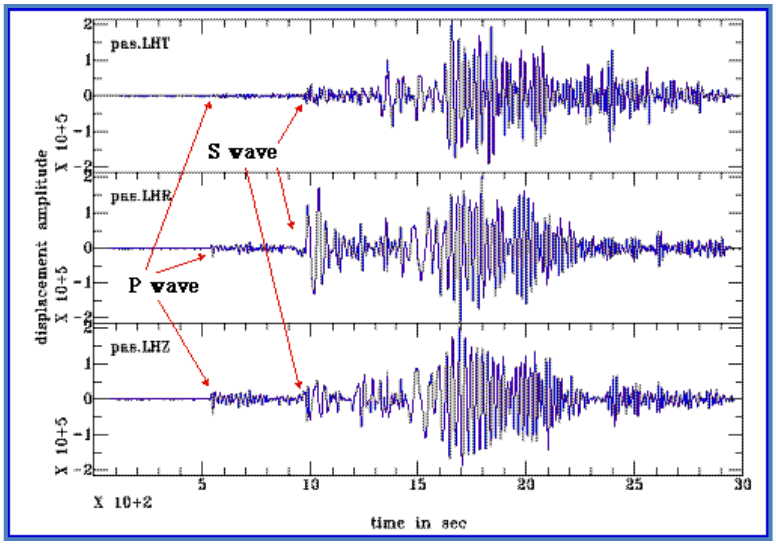

Figure 4.1. Example of a local earthquake phases.

Figure 4.1 shows a good example of a local earthquake's seismogram, where we can clearly see the P and S-phases. However, in most seismograms they are not as easily recognizable.

The coordinates of an earthquake point source are known as the ***hypocenter***. The hypocenter is usually given in terms of latitude, longitude and depth below the surface. The ***epicenter*** is the surface projection of the hypocenter (the latitude and the longitude), and the ***focal depth*** is the depth below the surface. The ***epicentral distance*** is the distance separating the epicenter and the recording seismic station. For large earthquakes, the finiteness of the source

volume is not negligible, and these terms usually refer to the point at which the rupture initiates.

The basic character of seismograms depends strongly on the epicentral distance. At short epicentral distances the character of the seismograms is dominated by the details of the highly heterogeneous crustal structure. At large distances, seismograms are dominated by the relatively simple velocity structure of the deep mantle and core.

In the *entire processing scheme* from automated event detection to automated event location, the first step is usually the application of a phase detector to all available recordings. The consistency of these detections is then checked in order to ***detect an event***. With the purpose of obtaining a first rough P-phase arrival time estimate, a single-station detector, e.g. a simple STA/LTA trigger is applied to all available continuous data streams of a seismic network. Nowadays, continuous data streams are usually transferred to the data centers where a phase detector is applied to the incoming real-time data. Event detectors are configured so that the number of false detections is minimized. On the other hand, the detector has to be sensitive enough to also detect small events. Any phase detector yields a considerable number of false detections and not all P phases are detected. Hence, the consistency of the detections at different stations has to be (manually) checked before the detection of an event is declared.

After a seismic event has been recognized, a phase picking algorithm is applied to the data in order to estimate P- and S-phase arrival times for robust earthquake location. Picking phases is a skill which requires much practice and the phases observed might be somewhat different than initially assumed. With digital recordings, different filters can be used to enhance certain phases and suppress noise; however, this can introduce new problems of phase shift.

At the present time, there is a considerable amount of automated picking algorithms available. Most of these standard algorithms are based on the automated picking, identification and association of the first arrivals of *P* and *S* waves and on the minimization of the residuals between theoretical and observed arrival times of the considered seismic phases. Although current methods can accurately pick *P* onsets, the automatic picking of the *S* onset is still problematic, especially when the *P* coda overlaps the *S* wave onset.

Most of these methods are modified versions of the Geiger (1910) algorithm, which is based on the iterative minimization of the residuals between the theoretical and observed arrival times of the main seismic phases.

Given the location of a seismic source, one can calculate the travel time for any particular phase to a seismic station anywhere in an arbitrary complex velocity model. This type of problem is known as a ***forward model***; arrival times are calculated based on a parameterized model. On the other hand, finding the earthquake location is usually posed as an ***inverse problem***, where we know the arrival time of the phases, but must solve for a source location and origin time that are consistent with the data.

In general, the arrival times of various seismic phases at many seismic stations are required to accurately determine an earthquake hypocenter and origin time. An accurate location can be determined using P and/or S arrival times alone. If the event is at local distances, the two principal phases on the seismogram are P and S. The origin time of the earthquake can be determined with a very simple graphical technique called a Wadati diagram. The time separation of the S and P phase $(t_S - t_P)$ is plotted against the absolute arrival time of the P wave. Since $(t_S - t_P)$ goes to zero at the hypocenter, a straight line fit on the Wadati diagram gives the approximate origin time at the intercept with the P arrival time axis. Figure 4.2 shows an example of a Wadati diagram. The slope of the trend is $m = (\alpha \,/\, (\beta - 1))$, and this can be related to Poisson's ratio as follows:

$$\frac{\alpha}{\beta} = \sqrt{\frac{1-\nu}{\frac{1}{2}-\nu}} \quad \rightarrow \quad \nu = \frac{1 - n/2}{1 - n} \qquad (4.1)$$

Where $n = (m+1)^2$. α is the P-wave volcity and β is the S-wave velocity

Once the origin time (OT) has been estimated, the epicentral distance for the i-th station can be estimated by taking the travel time of the P wave and multiplying it by an estimate of the average P velocity

$$D_i = \left(t_p^i - OT\right) \cdot \alpha \qquad (4.2)$$

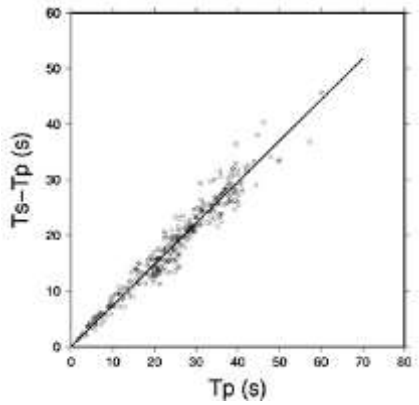

Figure 4.2. Wadati diagram. T_p is the P-wave arrival time; (T_s-T_p) is the difference in time of S and P arrival times.

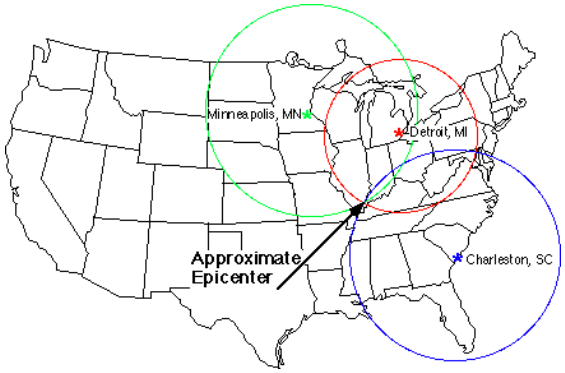

Figure 4.3. Method of circles. The point where the three circles intersect is the epicenter of the earthquake.

The epicenter must lie on a hemisphere of radius $\boldsymbol{D_i}$ centered on the i-th station. In map view this corresponds to a circle of radius $\boldsymbol{D_i}$. Figure 4.3 shows an example of this method for three stations. Since a single hypocenter must account for all three P-wave arrivals, the hemispheres for all stations must intersect at a point. The epicenter can be found by drawing the cord of intersecting sections of the circles. The intersection of the cords will give the epicenter. The focal depth, $\boldsymbol{d}$, can be determined by taking the square root of the difference between the square of propagation distance $\boldsymbol{D_i}$, and the distance along the surface to the epicenter, Δ : $\boldsymbol{d = (D^2 + \Delta^2)^{1/2}}$. Including more observations will give additional intersections that theoretically should pass through the epicenter. In practice, error is always present, both in the data and in the assumptions that ray paths are straight and that the velocity is known perfectly, so scatter in the intersection usually occurs. This method for determining the hypocenter of an earthquake is called ***method of circles.***

Although these current methods can accurately pick *P* onsets, the automatic picking of the *S* onset is still problematic, especially when the *P* coda overlaps the *S* wave onset. Moreover, the performance of automatic pickers is limited when noisy data is present during picking, and phase identification might also be difficult, therefore automated location methods are requested to be noise robust.

After this proposal, more sophisticated methods were developed, taking into consideration the optimization of an objective function in which the arguments are the geometry of the seismic network, the observed arrival times of seismic waves at the station, t^i_{obs}, and the calculated travel times, t^i_{calc}, from a hypothetical hypocenter (X, Y, Z t_0) to station i. Generally, it is also possible to invert the parameters of the seismic structure in the area spanned by the sources (earthquakes) and receivers (seismic stations) simultaneously with the focal coordinates of individual earthquakes. Here it is assumed that either a seismic velocity model for the monitoring area already exists, or at best, a reliable 3D model of V_p and V_s has been derived from a dense local seismic survey. Reliable travel times t^i_{calc}, for each seismic station with index *i* to all nodes of a closely spaced grid in the potential focal area can be calculated in advance.

The focal time t_0 can be calculated from a weighted mean of all differences $(t^i_{obs} - t^i_{calc})$ [Moser et al., 1992]. The most common objective functions, in which the minimization or maximization allow for the determination of the other focal coordinates, are the L2 Norm (eq. 4.3) and the relative probability density function PDF(X, Y, Z) (eq. 4.4), which is based on Bayesian statistics [Tarantola et Valette, 1982]

$$L_2(X,Y,Z) = \sum \frac{\left(t^i_{obs} - t^i_{calc} - t_0\right)^2}{{\sigma_i}^2} \qquad (4.3)$$

$$PDF(X,Y,Z) \sim \exp\left(-\frac{1}{2}\sum \frac{\left(t^i_{obs} - t^i_{calc} - t_0\right)^2}{{\sigma_i}^2}\right) \qquad (4.4)$$

The sum Σ is over all stations i. The standard deviation σ^i takes into account the uncertainties of t^i_{obs} and t^i_{calc}.

Both methods assume a Gaussian error distribution and are sensitive to outliers in variable t^i_{obs}. The use of the L1 Norm could provide a more robust solution. Another path was taken by [Joswig, 2008] with the introduction of so-called nanoseismic monitoring. This method aims to achieve reliable location of earthquakes by making recordings with a S/N (Signal to noise ratio) near to 1. The total dataset is subdivided into subsets that define a mathematically exact solution. Using this procedure and with support from an instructive Graphical User Interface (GUI), an expert can instantaneously check the reliability of individual travel time picks. This method would preferentially be applied to mini-arrays with 4 – 6 stations.

4.2 Location of earthquakes without picking phases

The growing interest in microseismic monitoring applications, particularly for landslides, volcanoes, mining, rockfalls, oil, and gas applications, has led to the recent development of alternative techniques for automated seismic event location, similar to migration techniques used in reflection seismics. These methods are based on the concept of amplitude delay and the sum of seismic waveforms and do not need prior phase picking or phase identification. Bruckl & Mertl (2014) applied a localization algorithm based on the waveform amplitude decay of seismic waves for the localization of rock-falls and landslide movements. The algorithm is based on the amplitude differences between two stations, and it was implemented as a grid-search. Also among the techniques based on waveform amplitudes, we find the Source Scanning Algorithm (SSA) developed by Kao & Shan (2004, 2007), which makes use of a brightness function to localize seismic tremors. Gharti *et al.* (2010) proposed rotating seismic traces to the ray coordinates, computing the envelope and finally performing a stacking along *P* and *S* arrival times. The new feature of these techniques, based on migration, is that it does not require picking phases or phase identification.

4.3 Kanamori Method

The localization using events travel times is successful if, and only if, its first-breaks can be picked reliably. In case this is not possible, Kanamori proposed a method based on amplitude measurements and avoiding picking phases altogether.

This method is applied to instrumental data on ground motion, using general or locally valid amplitude – distance relations for seismic waves. Kanamori (1993) developed a least square method (L2-Norm) to determine the magnitude and epicenter location using accelerometer data and peak acceleration-distance to fit the occurring recorded data at or near the San Andreas Fault. As he remarks, this method is strong in its simplicity, allowing it to be used for real time applications. Moreover, the results obtained with the method can achieve reasonable accuracies.

For simplicity, Kanamori used the peak acceleration-distance relation developed by Joyner and Boore (1981). He scanned the model parameter space (M, φ, λ) to determine the approximate location of the global minimum of the error function. He then used the values of M, φ, λ at that location as the first approximation to determine the final solution using the method of least squares (L2-Norm). As an example of the use of Kanamori's method Ebreischsdorf earthquake ($m_l = 4.3$) is illustrated in figure 4.4.

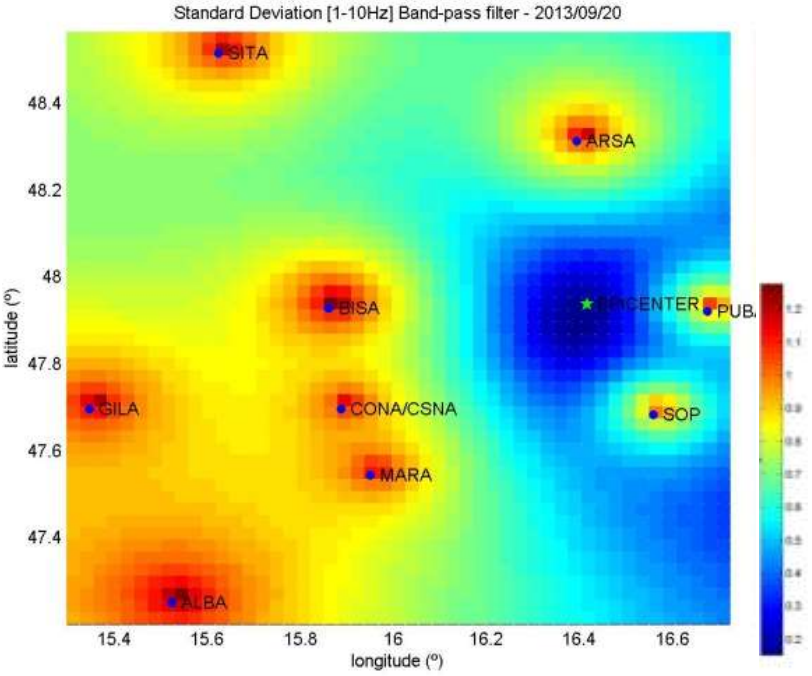

Figure 4.4. Standard deviation map derived from Kanamori´s method. Ebreichsdorf earthquake (2013/09/20). The minimum standard deviation indicates the epicenter location.

5. *Method based on pseudoMagnitudes*

Situations in which reliable phase picking cannot be performed, such as mass movements, rockfall areas, etc. are very common. This is primarily caused by gradually rising amplitudes at the onset of the events or by a small signal to noise ratio. For these events, a localization algorithm based on the amplitude decay of seismic waves was used.

The *basic idea* is that any small seismic sources can produce large amplitudes, as long as they are located close enough to the seismic station sensor. [Papí M. P., Brückl, E., 2016].

The new detection and localization method proposed here is based on an empirical model of the ground motion obtained from amplitude data of earthquakes in the area of interest, which were located using traditional methods. The first step in the method is the computation of maximum resultant ground velocities in sliding time windows covering the whole period of interest. In the second step, these maximum resultant ground velocities are back-projected to every point of a grid covering the whole area of interest while applying an empirical amplitude-distance relation. We refer to these back-projected ground velocities as pseudoMagnitudes. The number of operating seismic stations in the local network equals the number of pseudoMagnitudes at each grid-point. Our method introduces the new idea of selecting the minimum pseudoMagnitude at each grid-point for further analysis.

In case no detectable earthquake occurred, the spatial distribution of the minimum pseudoMagnitudes constrains the magnitude of weak earthquakes hidden in the ambient noise. In the case of a detectable local earthquake, the spatial distribution of the minimum pseudoMagnitudes shows a significant maximum at the grid-point nearest to the actual epicenter. The application of the method is restricted to the area confined by the convex hull of the seismic station network. Additionally, one must ensure that there are no dead traces involved in the processing.

Compared to other methods based on L2, the method presented is almost wholly insensitive to outliers (data from locally disturbed seismic stations). A further advantage is the fast determination of the epicenter and magnitude of a seismic event located within a seismic network. This is possible due to the efficient organization of the data, being able to quickly determine the epicenter. Since obtaining and storing a Back-Projection Matrix (BPM) for each seismic station is independent of the registered amplitude, this makes it possible to apply the method in real time. As a direct consequence, it is possible to save computing time for the creation of a SourceMap.

The method is divided into four steps; the four core processes for event location are presented in the following scheme

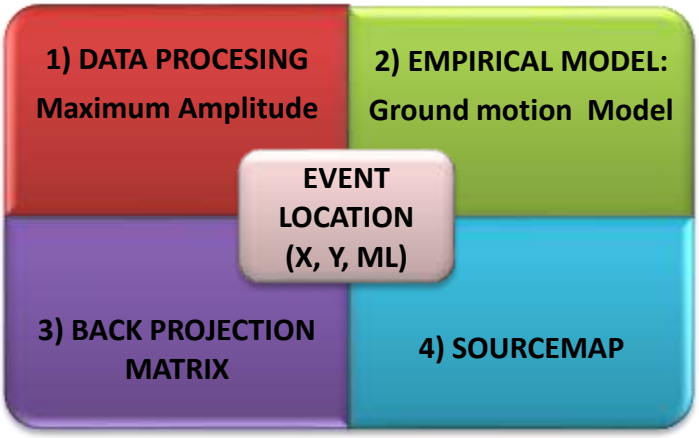

Figure 5.1. Main steps of the localization method.

5.1 Data processing (Seismon and pSysmon)

Firstlythe computation of maximum resultant ground velocities in sliding time windows covering the whole period of interest is performed. The data extraction was conducted using either Seismon (for the ALPAACT network) or pSysmon (for the Spitz quarry study).

The resultant ground velocity (V) for each station in the network was extracted. This was performed by means of the peak-to-peak values of the individual components V_{xpp} , V_{ypp} and V_{zpp} within time frames according to the equation:

$$\boldsymbol{V = sqrt\left(V_{Xpp}^2 + V_{Ypp}^2 + V_{Zpp}^2\right)} \qquad (5.1)$$

The maximum amplitudes are measured in successive time windows of an explicit length (seconds)

5.2 Computation of the ground motion model

A ground empirical model based on the amplitude-decay law and the general definition of magnitude, is defined in the study area. This model describes the ground behavior, and, using the Least Square adjustment, a constant part of the pseudoMagnitude can be computed. This is advantageous for the computation of a Back-Projection Matrix, with the final purpose of obtaining a SourceMap. The ground motion model relates the quantity named pseudoMagnitude to the maximum resultant ground velocities, the source station distance and station corrections according to equation (3.4)

The solution of the system of equations (Least Square Adjustment) was computed under the constraint:

$$\sum_{k=1}^{N} \boldsymbol{C^k} = \mathbf{0} \qquad (5.2)$$

The hypocentral distance correction $\left(\boldsymbol{a} \cdot \mathbf{log_{10}}\left(\boldsymbol{r_e^k}\right)\right)$ can be computed for the local network under study. Nevertheless, other relations for the power law amplitude can be used.

Local earthquakes (epicentral distances from 10-100 km) may have roughly the same frequency content as LMEs, mine monitoring, etc. Moreover, differences in the amplitude-distance correction are negligible and station corrections $\boldsymbol{C^k}$ can be derived from the observed amplitude data.

In our approach introduced in this master's thesis, Peak Ground Velocities (PGV) and not Peak Ground Accelerations (PGA) [Kanamori, 1993] were considered.

5.3 Construction of the Back-Projection Matrix (BPM)

A Back-Projection Matrix (BPM) for each station is created as follows:

$$\boldsymbol{BPM_{i,j}^k} = \boldsymbol{a} \cdot \mathbf{log_{10}}\left(\boldsymbol{r_{i,j}^k}\right) + \boldsymbol{C^k} \qquad (5.3)$$

All matrices define a 2-D Cartesian grid containing the study area determined for all stations. Each grid point represents a potential source location. For computing the BPM for each station, firstly, the distance from each station to every grid point must be calculated $\left(\boldsymbol{r_{i,j}^k}\right)$. Next, the BPM for each station is simply computed as all the parameters are already known.

5.4 Construction of the Back-Projection Amplitude Matrix (BPAM)

The previously computed and stored BPM allows the application of a robust and inexpensive computational method for the determination of the pseudoMagnitude. This is due to the fact that it is not necessary to compute the BPM every time the location and pseudoMagnitude of an event are obtained, but it can be updated by adding the $\mathbf{log_{10}}\left(\boldsymbol{V_e^k}\right)$ to its corresponding $\left(\boldsymbol{BPM_{i,j}^k}\right)$ [Papí, M. P. et. Brückl, E. 2016].

Therefore, a Back-Projected Amplitude Matrix (BPAM) for each station is computed. This is done every time the ground velocity at each station for a particular event $\left(\boldsymbol{V_e^k}\right)$ is registered.

$$\boldsymbol{BPAM_{i,j}^k = \log_{10}\left(V_e^k\right) + a \cdot \log_{10}\left(r_{i,j}^k\right) + C^k} \qquad (5.4)$$

5.5 Generation of the SourceMap

The study area was represented by a rectangular grid. The back-projected amplitudes (velocities) at each grid point for a particular station can be efficiently determined by adding a term $\boldsymbol{\log_{10}\left(A_{i,j}^k\right)}$ to the ***BPM,*** which from now on will be known as *Back-Projected Amplitude Matrix* (***BPAM***).

A specific procedure selects the smallest value of the computed $\boldsymbol{BPAM_{i,j}^k}$ between stations at every grid point (Figure 4.5), e.g. we select the minimum value at each grid point between each two stations BPAM in a sequential algorithm according to:

$$BPpMM_{i,j} = min\left\{BPAM_{i,j}^k\right\} \quad k = 1, \ldots, N \qquad (5.5)$$

where N is the maximum number of stations.

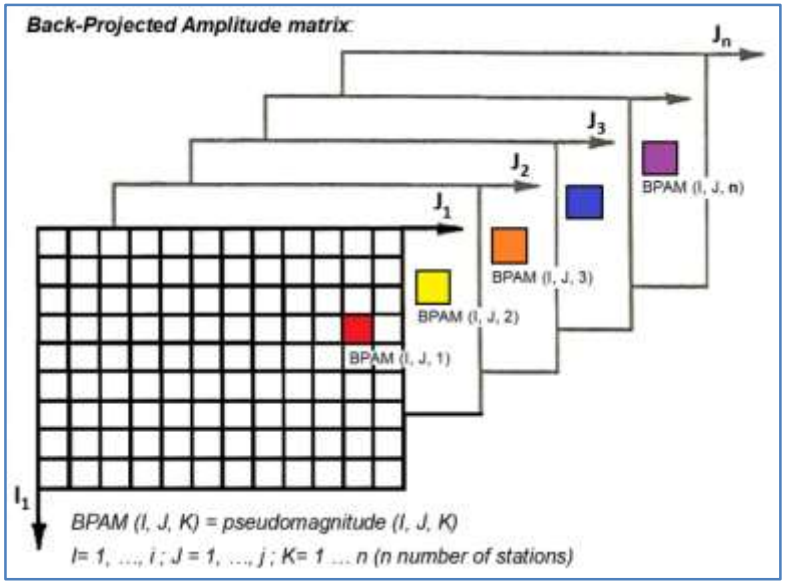

Figure 5.2. BPAM's array

As illustrated in figure 5.3.a), in case of zero noise at every single station, the BPAM for each station must result in the same pseudoMagnitude value, which is derived by the distance-power law, at the epicenter location. On the other hand, figure 5.3.b) shows that even when a highly noisy station is presented in

the network, the epicenter location is still well located due to the selection of the minimum at each grid-point. This fact makes the method very robust against outliers.

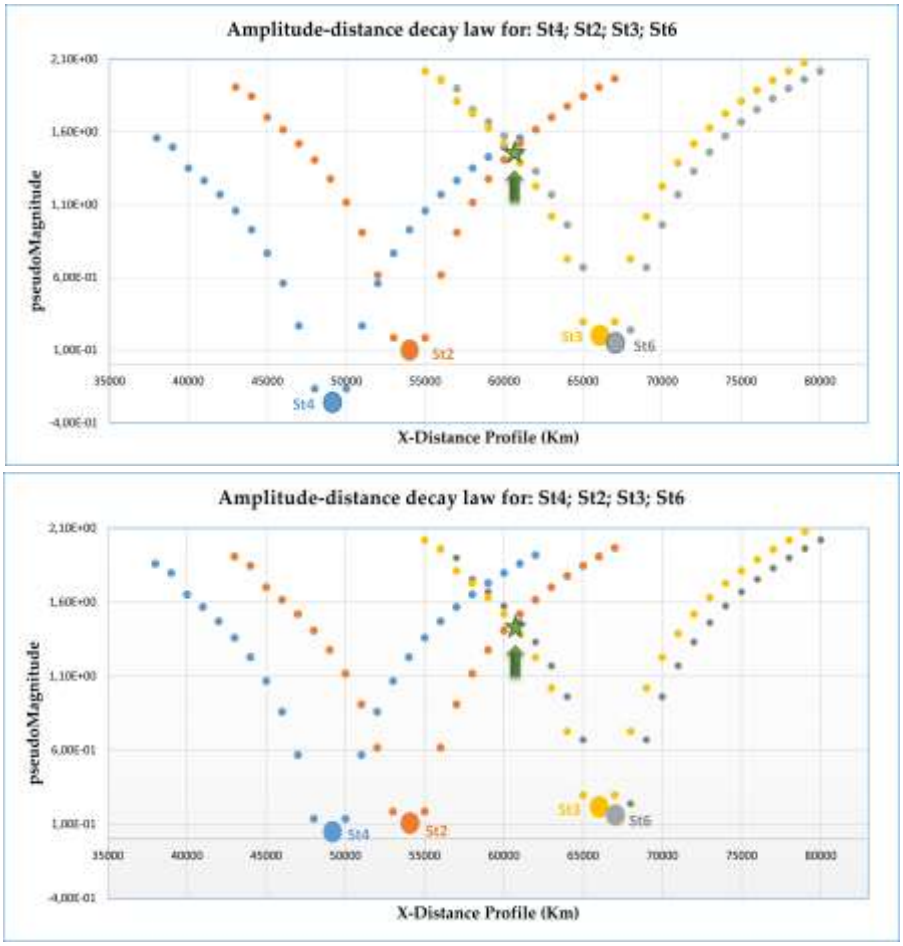

Figure 5.3. Principle of the method. a) Stations without noise. b) Station 4 is noisy, however, the epicenter is still well determined making the method robust against outliers.

The ordered minimum pseudoMagnitude values are insensitive to outliers, and we obtain a very robust result.

The final result (SourceMap) is stored in a pseudoMagnitude Matrix. Finally, the epicenter can be directly seen in the SourceMap. This code was implemented in Matlab®, [Margrave, G. F. 2003].

In case of a lack of a sufficiently strong seismic event, the distribution of pseudoMagnitude values shows the maximum possible pseudoMagnitude hidden in the ambient noise. If the seismic event exceeds a detection threshold, it appears as a local maximum. Confining the study area to the interior of the **convex hull** [Worboys, M. F. et M. Duckham. 2004], which is defined by the station network, the epicenter should be recognized as a global maximum [Rosenberger, A. 2009]. Additionally, one must ensure that there are no dead traces involved in the processing.

The computation of the SourceMap following this methodology only makes sense if, and only if, the epicenter lies inside the network, therefore the concept of *convex hull* is introduced. This is due to the fact that the back-projected amplitude increases continuously (as a power law) with distance from the network. Therefore, local maximums, or even a global maximum, can be found outside the network even when the epicenter lies inside of it. This will lead to incorrect estimates of the location of the epicenter.

Please note that, the convex hull is only a ***mask***, e.g. it does not influence the calculations at all, since it is placed as a mask once all the computations are performed.

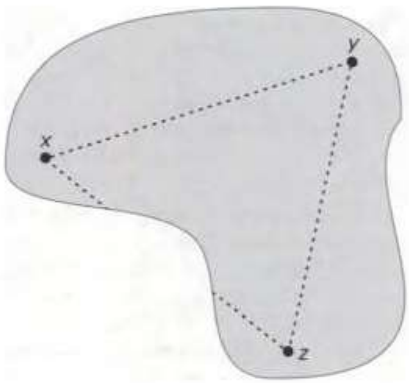

Figure 5.4. Visibility between points x, y and z

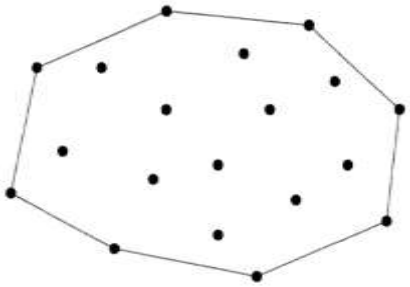

Figure 5.5. Convex Hull of a point set (the points represent the stations).

The essential idea is that a set of points S in the Euclidean plane is convex if every point is visible from every other point within the set. Figure 5.4 shows the visibility relation within a set between the three points x, y and z. Points x and y are visible to each other, as are points y and z. But, points x and z are not visible to each other.

The intersection of a collection of convex sets is also convex, and therefore any collection of convex sets closed under intersection has a minimum member. This leads to the definition of a *convex hull* of a set of points S in $\mathbb{R}^2$ as the intersection of all convex sets containing S. From the above, the convex hull must be unique smallest convex set that contains S (Figure 5.5). A convex hull of a finite set of points is always a polygonal region. [Worboys, M. F. et M. Duckham. 2004]

5.6 Seismic event detection

Once the SourceMap is obtained, a detection threshold/criterion must be defined in order to raise an alarm in case of an earthquake or rockfall.

In the case of the ALPAACT network, the detection step needs further development since all the studied events had already been detected by the network. In this case, the extraction of the maximum and minimum amplitudes was done manually with a single time window once the events were detected. The main challenge in this example would be the implementation of a real time procedure in order to extract the maximum and minimum amplitudes within sliding time windows.

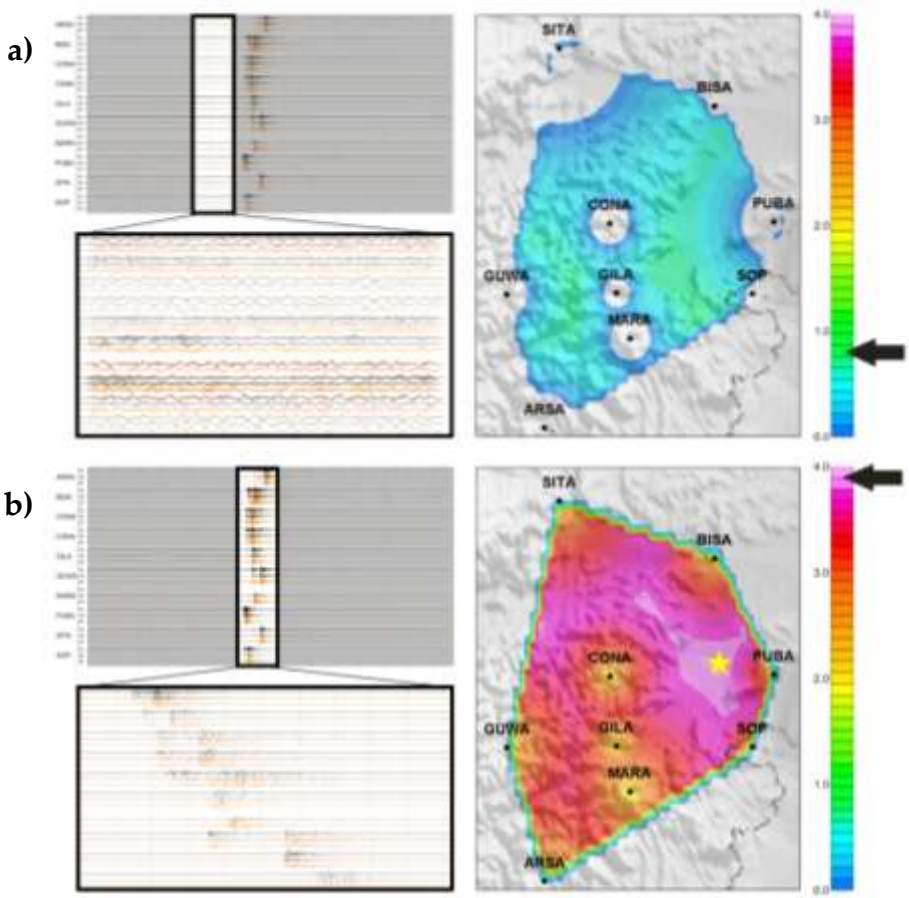

Figure 5.6. Seismogram obtained by Sysmon and SourceMap of the Ebreichsdorf (20/09/2013) event. Black arrows indicate the maximum pseudoMagnitude. The yellow star shows the epicenter. a) Noise in the Time Window. b) Event enclosed by the Time Window.

In figure 5.6.a), one time window before the event is shown, which only contains noise. In contrast, figure 5.6.b) shows a second time window, with the same size as the previous one but this time containing the whole event. As seen from the SourceMap a characteristic increase of the pseudoMagnitude leads to the location of the epicenter. However, further study on the detection method should be performed in order to establish reliable criteria to detect earthquakes.

For that, a significant pseudoMagnitude should be set as threshold value which, when exceeded, should raise an alarm.

However, this is not the case for the Spitz quarry, where a detection criteria was established in order to activate the alarm system. The procedure followed to set the appropriate threshold for the detection in this area is thoroughly explained in section 8.

The main advantage of the derivation of a SourceMap is that, in case of no seismic event occurring, the SourceMap will display a homogeneous color. However, when a seismic event occurs, a characteristic increase of the pseudoMagnitude will indicate the epicenter of the seismic event.

5.7 Code sequence (Step by Step process)

In conclusion, the steps for determining the location of an earthquake can be summarized as follows:

- Extraction of the maximum amplitude at each station for a selected time window in order
- Establishing the ground motion model (attenuation amplitude)
- Computation of the Back-Projection Matrix (BPM). The distance from each station to every grid point must be calculated. (eq. 5.3)
- Obtention of the Back-Projection Amplitude Matrix (BPAM) by adding the amplitude term to the BPM. (eq. 5.4)
- Generating the SourceMap with the computation of the minimum of the Back-Projection pseudoMagnitude Matrices ($BPpMM$). The maximum within the convex hull gives the epicenter of the event.
- Setting the detection criteria. In case of fulfillment of the criteria, the maximum is extracted.

Please note that the codes can be found in the Appendix on the CD

6. Simulation with Synthetic Data

In this section, the equations are not expressed in logarithmic form but in power-law form, however the basis of the method and procedure remains as explained in section 5.

6.1 Test with synthetic data

The simulation technique based on ***Ricker Pulse*** was used to calculate the synthetic maximum amplitude at each of the six stations of the network in order to determine the location of the seismic event. Random noise was added to each station seismogram to generate a more realistic signal.

Synthetic Seismogram: Ricker Pulse

A test with synthetic data was performed in order to explore the sensitivity of our method to degraded data. The simulation technique based on Ricker Pulse was used to calculate the synthetic maximum amplitude at each site of a grid in order to determine the location of the seismic event.

The location of the stations and configuration of the seismic network (six stations in total) are represented in figure 6.2.

Initially, we present the method used to obtain a signal generated from equations that describe the frequency content of the wavelet. There are two types:

1. Ricker wavelets, which are generated directly in the time domain and
2. Klauder wavelets, which are generated in the frequency domain.

Both are called zero phase wavelets (i.e. symmetric) and have minimum delay, i.e. the maximum energy is at the beginning of the wavelet.

Ricker wavelets were implemented in Matlab® with the purpose of obtaining a synthetic seismogram for each of the network stations.

The code requires the temporal sample rate (seconds), the domain frequency (Hz) and the temporal length (seconds) as input. As mentioned before, the Ricker pulse has a simpler form in time-domain and is given analytically by

$$A_{ricker}(t) = \left[1 - 2\pi^2 f_{dom}^2 t^2\right] \cdot \exp\left(-\pi^2 f_{dom}^2 t^2\right) \qquad (6.1)$$

This is the second derivative of a Gaussian, where $\boldsymbol{f_{dom}}$ is the dominant frequency; $\boldsymbol{A_{ricker}}$ is the amplitude of the generated Ricker pulse.

The resulting plot of a Ricker pulse with a time step of 0.01 seconds, a dominant frequency of $10Hz$ and a seismogram length of 1.5 seconds can be seen in figure 6.1. In order to produce a more realistic signal, random noise was added to the Ricker wavelet.

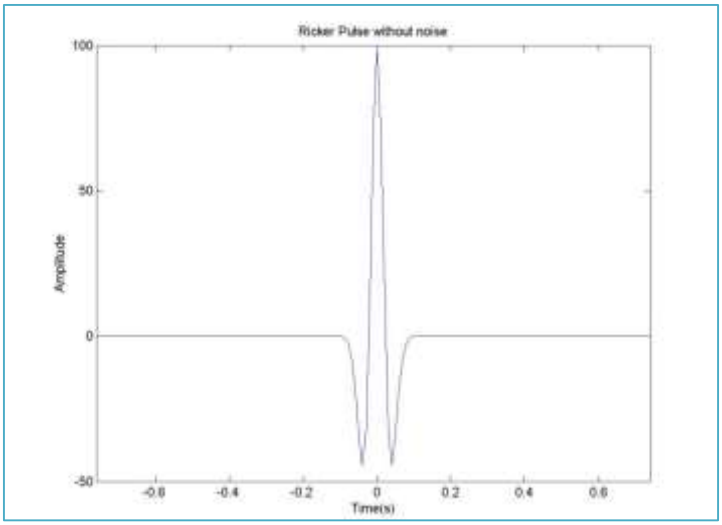

Figure 6.1. Ricker pulse signal for a time step of 0.01 seconds, a dominant frequency of 10Hz and a seismogram length of 1.5 seconds.

Synthetic study area

A hypothetical seismic network was established, in which six stations were well distributed in a $30x30$ km area with a grid point spacing of 0.5 km (Figure 6.2). The stations are marked by colored points, whereas the epicenter is represented by a green star.

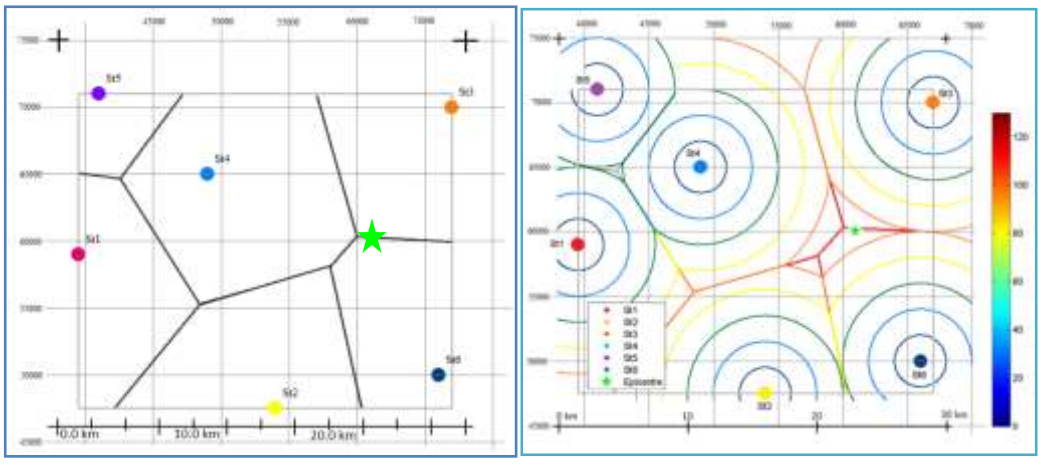

Figure 6.2. a) Voronoi diagram, the sites correspond to the stations from which regions of influence are obtained. b) Voronoi diagram together with pseudoMagnitude values (colors).

6.2 Data processing and synthetic results (SourceMap)

Extraction of the maximum amplitude at each station

A synthetic Ricker pulse originating from the epicenter location was extrapolated to every station by means of a simple attenuation law based on ***the amplitude decay*** within distance and by adding random noise at each station (equation 6.2).

$$\boldsymbol{V_{station}(t) = \frac{V_{souce,ricker}(t)}{r^a} + g(t)} \qquad (6.2)$$

$\boldsymbol{V_{station}(t)}$ is the resultant wavelet at each station; $\boldsymbol{g(t)}$ is a random noise function (varying from 0 to 1); $\boldsymbol{V_{ricker}(t)}$ is the Ricker pulse at the epicenter; $\boldsymbol{r}$ is the hypo-central distance from the station to the source and $\boldsymbol{a}$ is the attenuation factor, for which a value of 1.66 was assumed. This value, which includes all damping effects (e.g. geometric spreading, intrinsic attenuation, reflection and refraction), is based on experiences from seismic experiments at sites with comparable geology and morphological settings, [Brückl, E, et al 2014]. However, in later sections it will be obtained from empirical data.

Once all the seismograms are computed for all stations in the network (Figure 6.3. a) b)) and since the resultant seismogram has already been generated for the synthetic data, the resultant vibration velocity will be directly defined by the peak-to-peak value in the seismogram for a selected time window. For simplicity in the explanation of the method, a time window with same size as the synthetic signal was chosen.

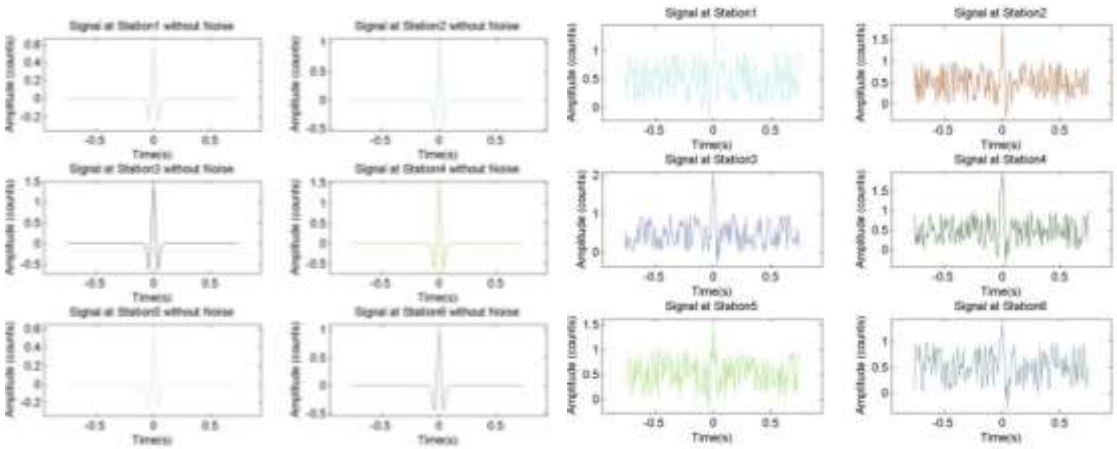

Figure 6.3. Synthetic seismograms a) Wavelet without noise at each station. b) Noisy wavelet at each station.

The resultant ground velocities (V) for each station in the network are presented in table 6.1.

	St1	St2	St3	St4	St5	St6
V(counts)	1,396	1, 970	2,177	1,831	1,790	1,539

Table 6.1. Resultant velocity for the synthetic network stations.

***Definition of the Ground Motion Model*:**

The ground motion model used for the simulation has the power law amplitude-distance relation:

$$V_{source} = V^k \cdot r^{1.66} \qquad (6.3)$$

Equation 6.3 shows the amplitude decay; k corresponds to the station number. From the ground motion model, a synthetic ShakeMap can be defined, in our case based on ground velocity measurements. A ShakeMap is a representation of ground shaking produced by an earthquake. The information it presents is different from the earthquake magnitude and epicenter that are released after an earthquake because a ShakeMap focuses on the ground shaking produced by the earthquake rather than the parameters describing the earthquake source. This means that while an earthquake has one magnitude and one epicenter, it produces a range of ground shaking levels at sites throughout the region depending on distance from the earthquake, the rock and soil conditions at sites, and variations in the propagation of seismic waves from the earthquake due to complexities in the structure of the Earth's crust.

A ShakeMap can also be transformed into a SourceMap to determine the location of the event [Papí M.P. et. Brückl, 2016]. The method developed here determines the source map and location of a seismic event by applying the steps below.

Back-Projection Matrix (BPM)

Firstly, the hypocentral distance must be calculated in order to obtain the BPM. For the synthetic data, it is defined as follows:

$$\boldsymbol{r(km)} = \sqrt{(\Delta \boldsymbol{x})^2 + (\Delta \boldsymbol{y})^2 + (\Delta \boldsymbol{z})^2} \qquad (6.4)$$

With $\Delta x = x_{station} - x_{epicenter}$; $\Delta y = y_{station} - y_{epicenter}$;
$\Delta z = z_{station} - z_{epicenter}$. Since the x and y coordinates are well defined by the location in the plane of the stations and the epicenter, the only term that warrants further discussion is (Δz). A standard depth of 9 km was used for the

theoretical seismic events. This value was taken based on the average depth of the 43 events studied later, which were registered by the ALPAACT network.

In this case, the Back-Projection Matrix (BPM) for each of the stations in the network covering the whole area of interest is defined as:

$$\boldsymbol{BPM_{i,j}^{k}} = \left(\boldsymbol{r_{i,j}^{k}}\right)^{\mathbf{1.66}} \qquad (6.5)$$

The distance $\boldsymbol{r_{i,j}^{k}}$ refers to the distance from station $\boldsymbol{k}$ to all grid points $(\boldsymbol{i},\boldsymbol{j})$. Consequently, since the seismic network consists of six stations, six Back-Projection Matrices will be obtained from equation 6.5. Figure 6.4 shows the Back-Projection Matrices for each station individually.

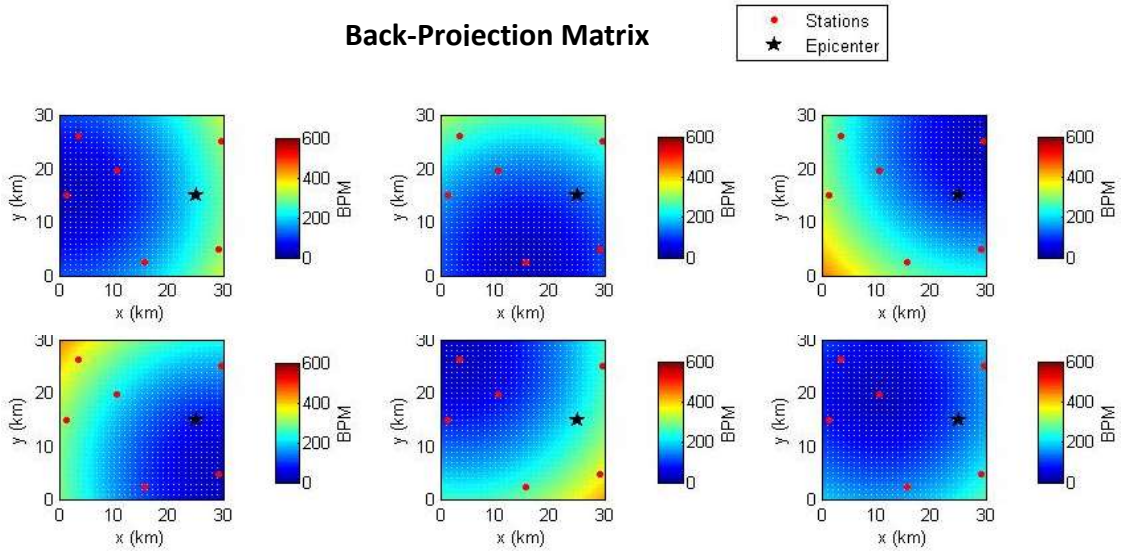

Figure 6.4. Individual Back-Projection Matrices for the six stations used in the simulation.

Back-Projection Amplitude Matrix (BPAM)

Once the BPM is obtained for each station , and after having extracted the resultant ground velocity at each station, the ***Back-Projection Amplitude Matrix*** for all the stations can be computed. The BPAM is easily derived by multiplying the maximum amplitude term for each station by its corresponding BPM:

$$\boldsymbol{BPAM_{i,j}^{k}} = \boldsymbol{V} \cdot \boldsymbol{BPM_{i,j}^{k}} \qquad (6.6)$$

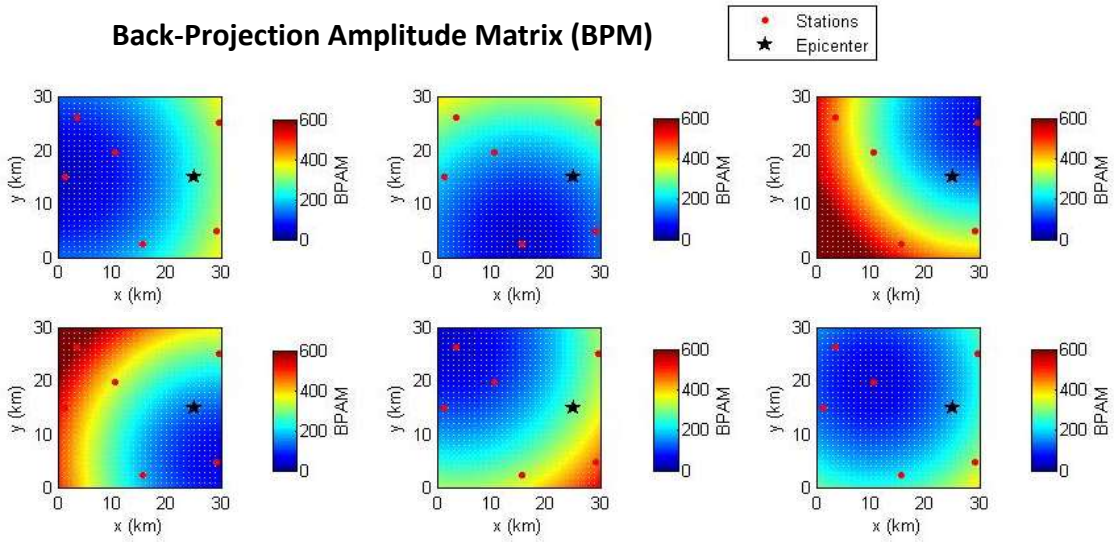

Figure 6.5. Back-Projection Amplitude Matrices from each station individually to every grid point.

SourceMap and epicenter extraction.

After having generated the six grid meshes of the Back-Projection Amplitude Matrices for each station, the minimum at every grid point is computed, e.g. at each grid point there are six different values of the Back-Projection Amplitude and the minimum among these values is taken. We store this information in a resultant matrix (pMBPM) (60*x*60). Selecting the minimum value at each point for each time window will result in a SourceMap, in which the location of the seismic source is shown as a maximum in the case of sufficient signal to noise ratio. The process is illustrated in figure 6.6.

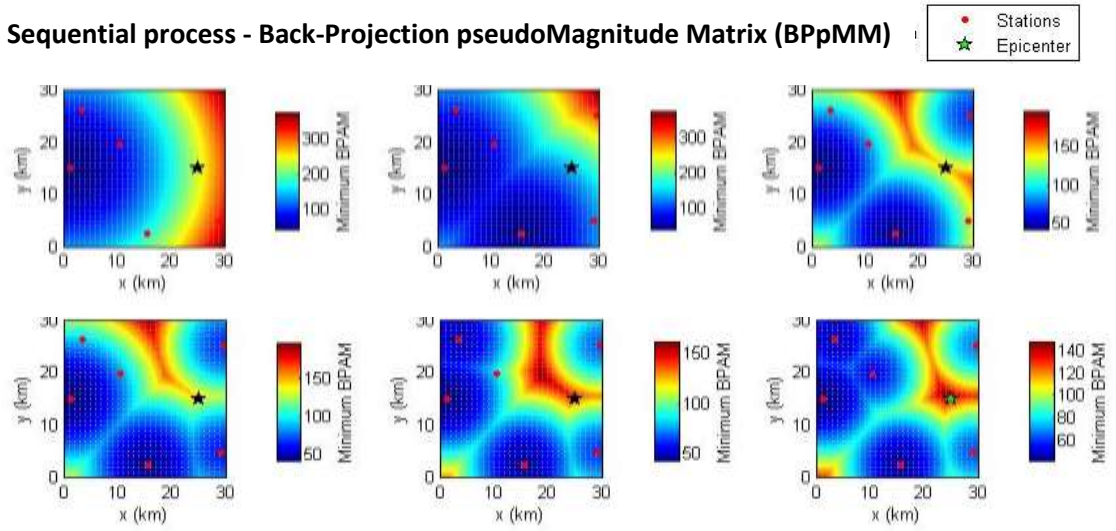

Figure 6.6. Location event: Step-by-step sequential procedure to determine epicenter and maximum pseudoMagnitude of an event.

The more stations there are, the more times the sequence must be followed in order to get Back-Projection pseudoMagnitude Matrix for the seismic network.

As indicated in chapter 4, the convex hull is used since the back-projected amplitude increases as a power-law with increasing distance from the station. Therefore, local maximum or even a global maximum can be found outside the network even when the epicenter lies inside of it. It is important to remember that the convex hull is only a ***mask***, e.g. it does not influence the calculations at all, since it is placed as a mask on top of the data once all the computations are performed.

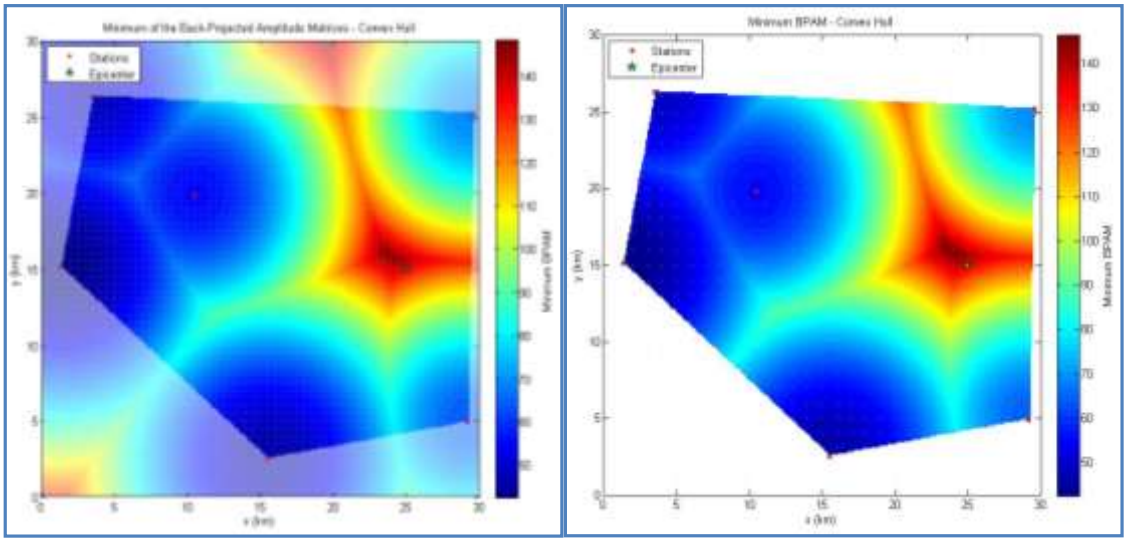

Figure 6.7. SourceMap. a) Mask plus back ground are represented. b) Inner part of the convex hull.

In the final step, the ***maximum value of the BPpMM*** in the grid is extracted and selected as the most likely location of the epicenter. In addition, we obtain an image of the source.

The coordinates of the maximum BPpMM provided by the location method, as well as the epicenter, are presented in table 6.2.

Set Epicenter		Model Epicenter	
X (km)	Y (km)	X (km)	Y (km)
25	15	24.2	15.7

Table 6.2. Theoretical epicenter coordinates and the ones obtained with the model.

Time Window Sequence

If sliding time windows along the whole signal are selected, we will be able to detect whether or not there is a characteristic change in the ground motion within the seismic network and therefore be able to detect seismic events with

consistent results. An example of this is show in figure 6.8, which corresponds to the same synthetic data produced in this section. In this case 5 time windows (TW) have been applied (0.3 seconds each TW), one after the other and with an overlap of a quarter of the time window between them (0.075 seconds).

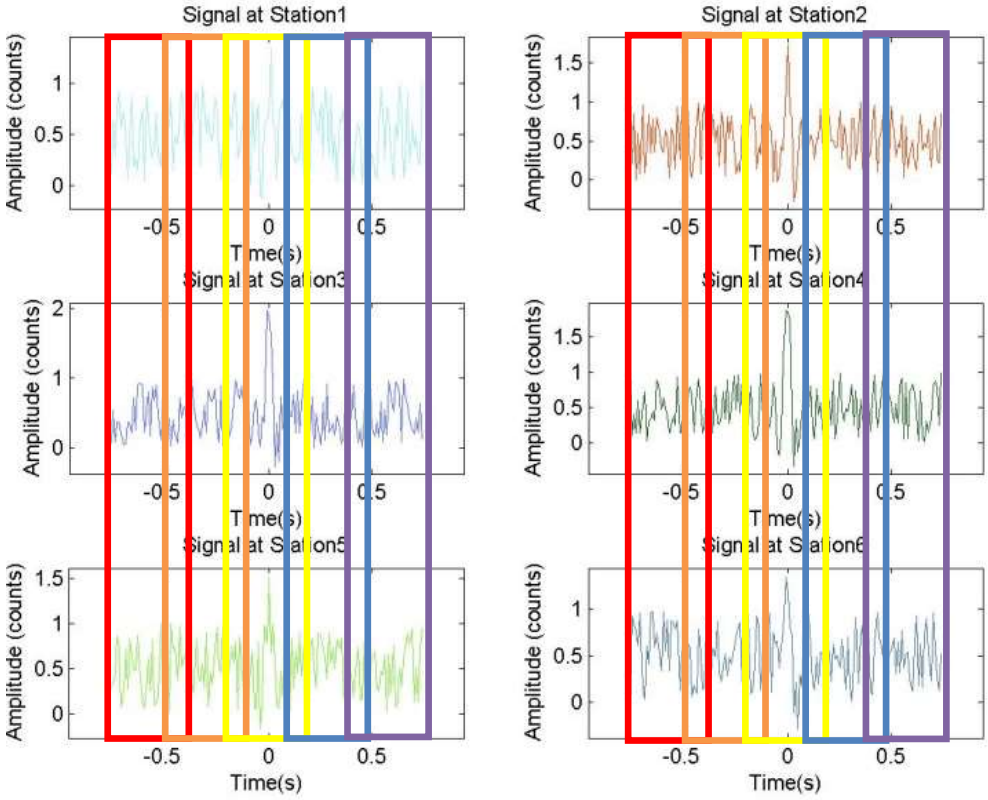

Figure 6.8. Red: TW1. Orange: TW2. Yellow: TW3. Blue: TW4. Purple: TW5.

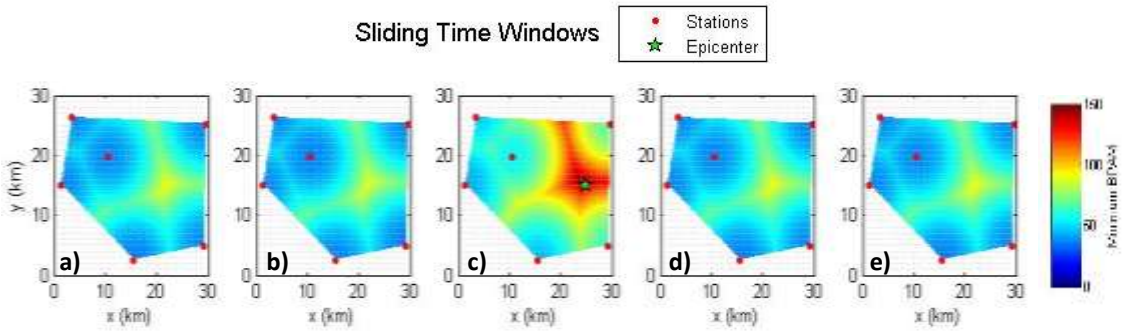

Figure 6.9. Localization using amplitudes of synthetic test data for different sliding time windows.

Since this is a symmetric wavelet and there is no time shift in the arrival times at the stations, i.e. the maximum of the wave at every station is at time $t = 0\ sec$, the maximum energy carried by the wave is contained within TW3, the centered time window. This leads to the maximum amplitude peak being contained in the third time window since the energy of a wave is proportional to amplitude squared.

Figure 6.9 c) shows a characteristic change in the ground motion in comparison to the previous and next TWs. By extracting the maximum back-projected amplitude within the grid for each time window (Table 6.3), we can have, for this specific case with synthetic data, a quantitative result of how high the variation is when a seismic event occurs.

	TW1	TW2	TW3	TW4	TW5
Back-Projected Amplitude	80.85	84.72	135.46	85.19	89.94

Table 6.3. BPA values for each of the five time windows of figure 6.9.

It should be noted that the noise distributions in figures 6.9 a), b), d) and e) are due to the geometry of the network.

The first results of the method applied to synthetic data verify that the method is very robust even when outliers are present in the data. Analyses with many stations showed variable results depending on network geometry and epicenter location.

7. Application to ALPAACT earthquake database

In this part of the master's thesis, the method will be applied to earthquake data from the Vienna Basin. The data were obtained using a local seismic network within the project ALPAACT. The method was applied to data of ***43 local*** earthquakes of low and medium magnitude (1.7 < magnitude scale < 4.3).

The basis of the ALPAACT seismic network is a local long term net dedicated to reach the scientific goals of ALPAACT and the existing net of regional observatories.

The ALPAACT project comprises seismological and geodetic (GNSS) monitoring by dense local networks. The goal of ALPAACT is contribute to a deeper understanding of the complex tectonic processes, especially the relationships between seismic activity (location and source mechanism), geodetically determined deformations, and the geometry of the main tectonic structures.

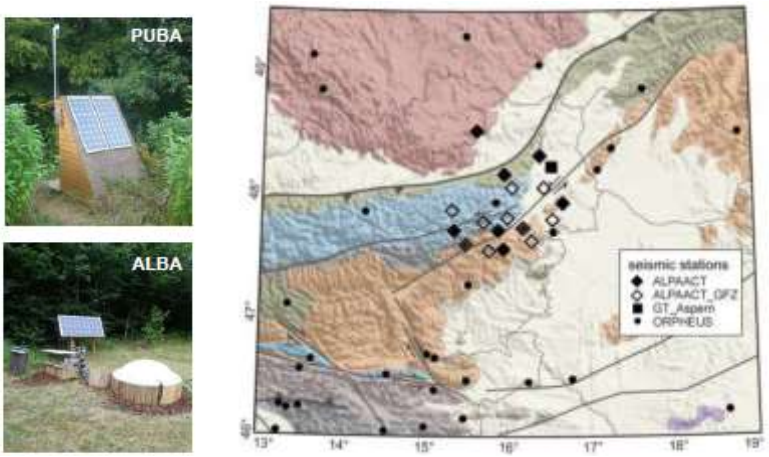

Figure 7.1. Site map of the ALPAACT seismic network.

ALPAACT Seismic network Stations and observatories used in the test)

Broadband data from permanent seismic networks are included in our analysis. A total of 11 stations of the ALPAACT network were used, eight belonging to the ALPAACT network (ALBA, ARSA, BISA CONA, CSNA, GILA, GUWA, MARA, PUBA and SITA) and one belonging to the Seismological Station Network in Hungary (SOP)

ID	Location	Lon(°E)	Lat(°N)	Height (m)
ALBA	Altlenbach	15.9623	48.1592	418
ARSA	Austria	15.5230	47.2505	577
BISA	Bisamberg	16.3946	48.3125	240
CONA	Austria	15.8618	47.9282	1044
CSNA	Austria	15.8588	47.9282	1039
GILA	Grillenber	15.8878	47.6958	643
GUWA	Gusswek	15.3464	47.6963	880
MARA	Mariensee	15.9505	47.5431	1005
PUBA	Purbach	16.6748	47.9210	178
SITA	Schiltern	15.6229	48.5145	373
SOP	Hungary	16.5583	47.6833	260

Table 7.1 Locations of the ALPAACT network stations.

The blue color in the table refers to the ALPAACT_CORE network, which comprises 9 stations, however, only seven of them were used since there was no available data from the other two. These stations were designed for long term operation and were maintained beyond the time frame of ALPAACT. The sample rate of ALPAACT_CORE stations is 100 Hz. Detailed information about the stations of ALPAACT_CORE can be found in the "ALPAACT final report 2008-2013".

Data from seismic observatories of the ORPHEUS–net implemented into the ALPAACT seismic network are listed in Table 7.1 in green. All stations are equipped with broadband sensors. Data from CSNA is continuously integrated into the data flow. Data from the other stations is requested on demand.

Description the data set

The area of study is delimited by [15.0913°, 16.8211°] East of longitude, and [47.3844°, 48.2996°] North of latitude. The stations of the network used here as well as the 43 events analyzed, are presented in the map in figure 7.2.

Event	Date	Time	Magnitude	Longitude (°)	Latitude (°)	Depth (m)
1	2010/06/11	18:47:45	1.8	16.1737	47.8309	12300
2	2010/06/24	17:47:58	2.2	16.4021	47.9413	12500
3	2010/07/18	08:28:51	2.0	16.2515	47.8474	8200
4	2010/07/24	15:58:55	2.0	16.0186	47.7082	8300
5	2010/08/31	08:00:01	2.7	15.0913	47.6479	10300
6	2010/09/11	05:12:46	1.8	16.3076	47.8808	10000
7	2010/10/04	10:29:00	1.7	15.4852	47.5478	6000
8	2010/10/11	19:08:42	2.3	15.3520	48.2561	4900
9	2010/12/09	21:45:59	2.4	16.7443	48.2829	10400
10	2010/12/10	08:32:45	2.5	16.8200	48.2996	4400
11	2010/12/10	08:33:34	2.8	16.8211	48.2858	7500
12	2010/12/18	06:19:55	2.4	16.4241	47.9626	10100
13	2011/01/05	23:52:17	2.6	15.9529	47.6621	9800
14	2011/02/22	00:31:33	2.3	16.1718	47.7615	14200
15	2011/04/19	23:32:31	2.0	16.0087	47.6517	6000
16	2011/06/04	14:36:28	2.6	15.8846	47.6353	5000
17	2011/06/29	05:19:00	2.4	15.7830	47.6402	10000
18	2011/07/02	04:50:07	2.2	15.8601	47.6380	8600
19	2011/07/10	14:51:10	2.2	15.4511	47.5524	7300
12	2011/09/16	20:28:35	1.9	16.1268	47.6899	5000
21	2011/09/28	06:04:04	2.4	16.2105	48.0747	7300
22	2011/10/10	07:52:13	1.8	16.3423	47.7450	6000
23	2011/10/17	06:54:39	1.9	16.2658	47.8498	12200
24	2011/10/31	14:54:20	2.7	16.2426	47.7314	6400
25	2011/11/24	10:14:18	2.3	16.3289	47.7334	8000
26	2011/11/24	10:52:51	2.0	16.3168	47.7352	8000
27	2011/12/06	22:48:11	2.2	16.1694	47.7402	10000
28	2011/12/07	17:53:12	2.0	16.1893	47.8131	12700
29	2011/12/13	03:01:55	1.8	16.1893	47.8131	10000
30	2012/01/10	05:37:26	2.0	15.2649	47.3896	6000
31	2012/01/22	12:04:25	2.1	15.2831	47.3844	10200
32	2012/02/18	16:01:19	1.7	15.8343	47.6723	10700
33	2012/02/24	09:57:39	1.7	16.1995	47.7723	8000
34	2012/04/27	21:26:14	1.7	16.2126	47.7387	14000
35	2012/07/18	21:32:45	1.9	16.1942	47.7452	14500
36	2012/11/15	03:17:38	2.5	16.2304	47.7153	14000
37	2013/01/06	10:56:53	2.7	15.3474	47.455	5000
38	2013/01/25	07:14:34	3.6	16.1658	47.6973	11600
39	2013/05/03	13:00:39	2.0	16.0335	47.663	12200
40	2013/05/17	06:58:05	2.5	16.0735	47.7186	8000
41	2013/06/27	18:59:52	2.7	15.8328	47.6305	113000
42	2013/06/28	08:37:22	2.0	16.1869	47.7899	13200
43	2013/09/20	02:06:33	4.3	16.4164	47.9376	10900

Table 7.2. Information on the analyzed events.

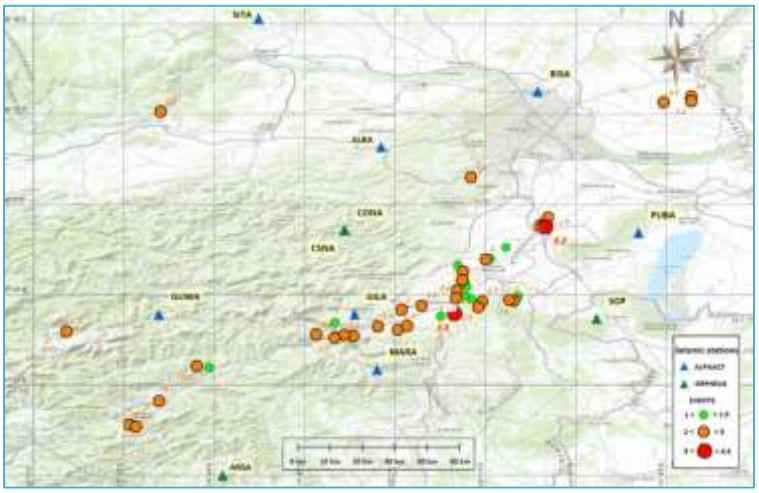

Figure 7.2. Representation of the stations and seismic events in the study. Mercator projection.

In order to compute an empirical robust model to determine the epicenter by means of amplitude data, a total of 43 seismic events (table 7.2), enclosed in the aforementioned period, were selected and analyzed. These events had been already detected and presented in the ALPAACT report 2008-2013 with magnitude values between 1.7 and 4.3.

Amplitude data processing with Seismon

The first step in the method is the computation of the resultant ground velocities for each station and all events (V) in order to obtain the empirical model. However, a prior processing step must be applied to the empirical data in order to filter, detrend, obtain ground velocity in physical units (m/sec), etc.

In the ALPAACT data, two different Bad-Pass filters were used: [1-5Hz] and [1-10Hz]. Therefore, in this section two different models will be obtained for each of the band-pass filters.

The seismic data processing for the ALPAACT network was performed using ***Seismon*** software. ***Seismon*** is a seismological prototyping and processing software dedicated to non-standard seismological studies. It is an open source software project developed by Stefan Mertl (TU Wien), and was designed as a modular program with defined interfaces for specific types of modules. Seismon is written in MATLAB and all input and output data are stored in a MySQL database, which can be accessed by multiple Seismon users simultaneously. Seismon is equipped with tools for communication with the

database, various waveform file conversions, and basic tools for data analysis and visualization.

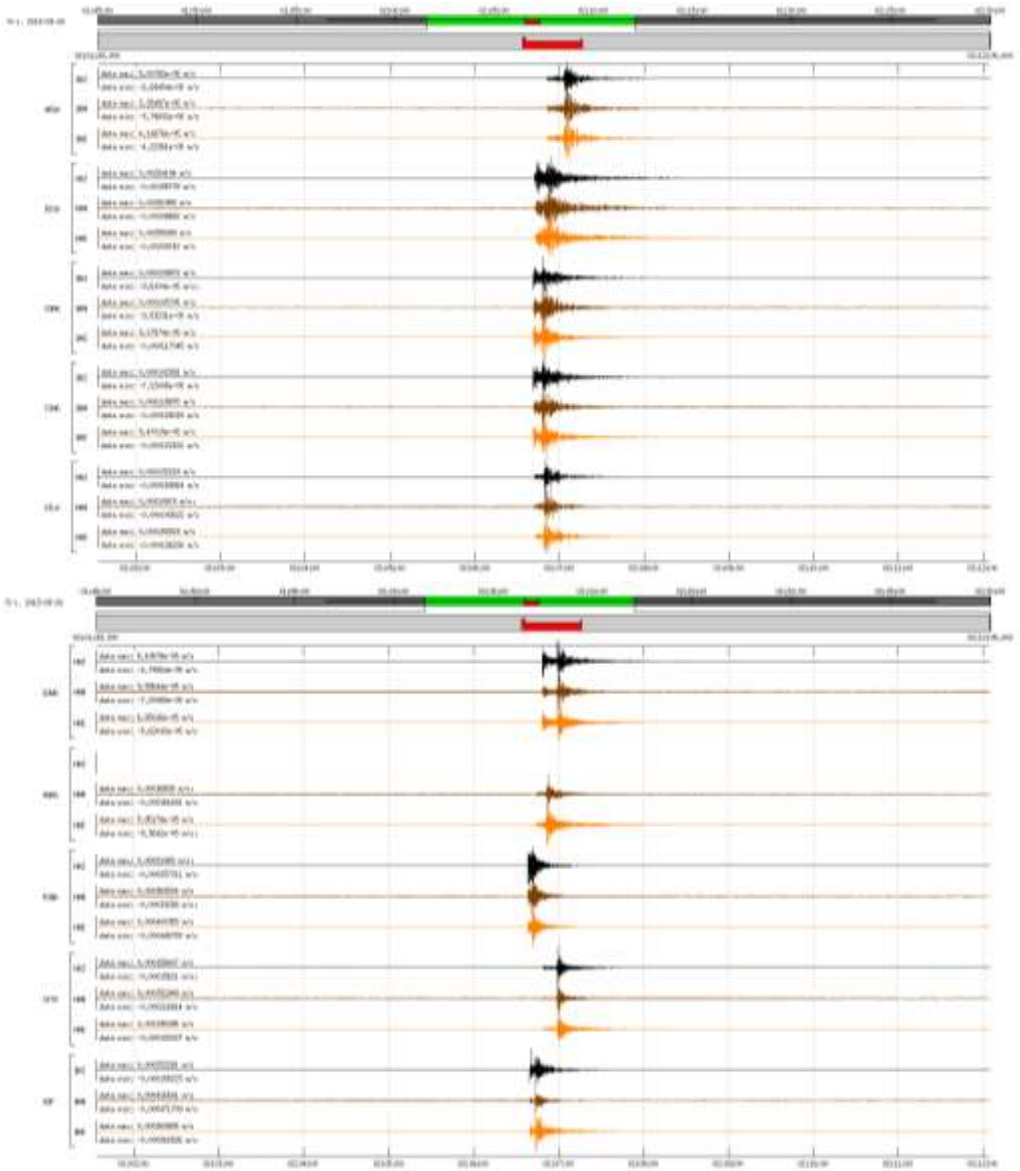

Figure 7.3. Ebreichsdorf (20/09/2013; $m_l = 4.3$) event display with Seismon software.

The resultant ground velocity (V) was obtained using equation (4.5). However, and in contrast to the synthetic data, $\boldsymbol{V_{xpp}}$ in the ALPAACT network corresponds to the EHH seismogram component, $\boldsymbol{V_{ypp}}$ to the NHH component and $\boldsymbol{V_{zpp}}$ to the ZHH seismogram component.

The maximum and minimum amplitudes of the whole wavelet of each event were carefully picked for all stations and all components. In the case of a dead trace, the average (eq. 7.1) of the other two components was assigned to the no data component. As an example, figure 7.3 shows that the ZHH component of the MARA station is dead, therefore the procedure mentioned above was followed for these cases.

$$\bar{x} = \frac{1}{N}\sum_{i=1}^{N} x_i \qquad (7.1)$$

In this case N equals two, which represents the non-dead traces and $\boldsymbol{x_i}$ is the component of each non-dead trace.

Events detected by the ALPAACT network allow an evaluation of the new location method based on recorded amplitudes, i.e. empirical data.

7.1 *Empirical ground motion model obtained from ALPAACT network data*

The empirical model of the ground motion is obtained from resultant vibration velocity data.

Distance computation

Preliminary to making use of seismograms, it is desirable that we should be able to suitably connect the coordinates $\boldsymbol{\theta}$, $\boldsymbol{\lambda}$ and epicenter Q with the corresponding coordinates $\boldsymbol{\theta'}$, $\boldsymbol{\lambda'}$ of an observing station k. Let the variables $\boldsymbol{r}, \boldsymbol{\theta}, \boldsymbol{\lambda}$ and $\boldsymbol{\varphi}$ be:

$\boldsymbol{\theta} \equiv \boldsymbol{Colatitude}$
$\boldsymbol{\lambda} \equiv \boldsymbol{Longitude}$
$\boldsymbol{\varphi} \equiv \boldsymbol{Latitude} \quad \boldsymbol{\varphi = 90° - \theta}$
$\boldsymbol{r} \equiv \boldsymbol{Radius}; \quad \boldsymbol{|r| = 1}$

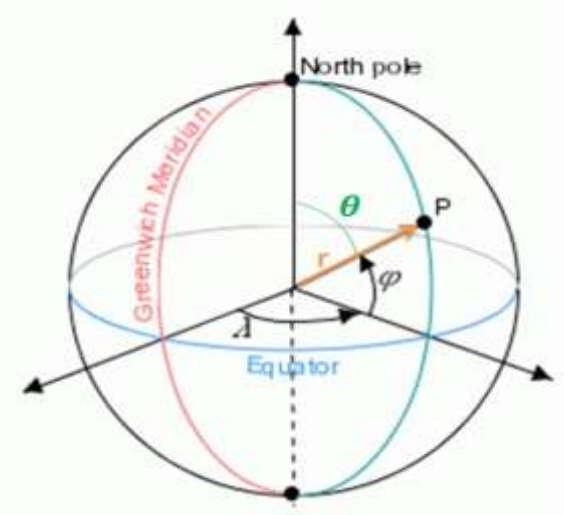

Figure 7.4. Spherical coordinates.

Letting A, B and C be defined by:

$$\boldsymbol{A = \sin\theta\cos\lambda} \qquad \boldsymbol{B = \sin\theta\sin\lambda} \qquad \boldsymbol{C = \cos\theta} \qquad (7.2)$$

and let A', B' and C' be corresponding constants for the station k.

Now the epicentral distance Δ of k from Q can be introduced. It is sometimes measured as the arc-length Q k in kilometers and sometimes as the angle subtended by Q k at Earth's center.

$$\cos \Delta = A \cdot A' + B \cdot B' + C \cdot C' \qquad (7.3)$$

The hypocentral distance can be approximated by:

$$D[^\circ] = sqrt\left((\Delta[^\circ])^2 + \left(\frac{Z[m] \cdot 360^\circ}{2\pi R[m]}\right)^2\right) \qquad (7.4)$$

R is the Earth radius ($R = 6371 \cdot 10^6\ m$); A standard depth of $Z = 9km$ was used for all the events, which was the result of computing the average depth for all 43 studied events.

Please note that the epicentral distances obtained in this work will be slightly different from the real ones since the assumption of a perfect spherical Earth was made. However, for this study this approximation can be taken into account with little influence on the final results, since the main influence for on epicenter location is the network geometry. This fact is based on the results presented at the end of this chapter, in which epicenters are satisfactorily located for most of the cases.

Determination of an empirical model

Least squares adjustment is a model for the solution of an over-determined system of equations based on the principle of least squares of observation residuals.

The functional model, which relates a quantity named pseudoMagnitude to the maximum resultant ground velocities, source station distance and station corrections, can be written as equation (3.4).

The $pseudoM_e^k$ will have a size $(1xp)$, with p being the maximum number of events; C^k will have a size $(1xq)$, q being the total number of stations and a is a vector of size $(1x1)$ e.g. a scalar.

Equation (7.5) can be cast into a standard matrix formation,

$$A \cdot x = l \qquad (7.5)$$

The former equation represents a typical linear inversion problem that can be solved using least squares, maximum-likelihood, or generalized inversion methods.

The matrix A is an $(m \times n)$ forward operator matrix; n is the number of unknowns (source terms, station correction, and the power-law factor) and m is the number of observations. Such a system of equations has a unique solution when the number of independent observations (l) is greater than or equal to the number of unknowns (x).

If the total number of earthquakes is $\boldsymbol{p}$ and the total number of stations is $\boldsymbol{q}$, the over-determined system must be solved by

$$\boldsymbol{x = inv(A^T \cdot P \cdot A) \cdot A^T \cdot l} \qquad (7.7)$$

$\boldsymbol{l}$ is defined as the observations vector and in this case is to be expressed in terms of the resultant amplitudes obtained from the measured amplitudes at each station $(\boldsymbol{k})$ for each event $(\boldsymbol{e})$; $\boldsymbol{A}$ is defined as the designed matrix; and $\boldsymbol{P}$ is the weighting matrix, which equals the identity matrix for the ALPAACT and Spitz quarry studies.

Then the matrices in equation (7.7) can be written as:

The observations (l) vector (with dimensions (255×1) for the band-pass filter [1-5Hz] and (251×1) the band-pass filter of [1-10Hz]).

$$\boldsymbol{l} = \begin{bmatrix} \log_{10}(V_1^1) \\ \log_{10}(V_1^2) \\ \log_{10}(V_1^3) \\ \cdots \\ \log_{10}(V_1^q) \\ \log_{10}(V_2^1) \\ \log_{10}(V_2^2) \\ \log_{10}(V_2^3) \\ \cdots \\ \log_{10}(V_2^q) \\ \vdots \\ \log_{10}(V_p^1) \\ \log_{10}(V_p^2) \\ \cdots \\ \log_{10}(V_p^k) \end{bmatrix}$$

The dimensions of the vector of unknowns (x) are $(55x1)$, e.*g.* $55 = 43events + 11station\ corrections + 1\ power - law\ factor.$

$$\boldsymbol{x} = \begin{bmatrix} pseudoM_1^1 \\ \cdot \\ \cdot \\ \vdots \\ \cdot \\ pseudoM_p^q \\ C^1 \\ \vdots \\ \cdot \\ C^{11} \\ a \end{bmatrix}$$

The design matrix, or matrix of coefficients, has dimensions (255×55) for the 1-5Hz band-pass filter and (251×55) for the 1-10Hz band-pass filter.

$$A = \begin{bmatrix} 1\,0\,\ldots\ldots\ldots\ldots 0 & \cdot & \ldots\ldots\ldots\ldots\ldots & \log_{10}(r_1^1) \\ 1\,0\,\ldots\ldots\ldots\ldots 0 & \cdot & \ldots\ldots\ldots\ldots\ldots & \log_{10}(r_1^2) \\ 1\,0\,\ldots\ldots\ldots\ldots 0 & \cdot & \ldots\ldots\ldots\ldots\ldots & \ldots \\ 1\,0\,\ldots\ldots\ldots\ldots 0 & \cdot & \ldots\ldots\ldots\ldots\ldots & \log_{10}(r_1^q) \\ \ldots\ldots & 0\,1\,\ldots\ldots\ldots\ldots 0 \quad \ldots \quad \ldots & \ldots\ldots\ldots\ldots\ldots & \log_{10}(r_2^1) \\ \ldots\ldots & 0\,1\,\ldots\ldots\ldots\ldots 0 \quad \ldots \quad \ldots & \ldots\ldots\ldots\ldots\ldots & \log_{10}(r_2^2) \\ \ldots\ldots & 0\,1\,\ldots\ldots\ldots\ldots 0 \quad \ldots \quad \ldots & \ldots\ldots\ldots\ldots\ldots & \ldots \\ \ldots\ldots & 0\,1\,\ldots\ldots\ldots\ldots 0 \quad \ldots \quad \ldots & \ldots\ldots\ldots\ldots\ldots & \log_{10}(r_2^q) \\ \cdot & \cdot & \vdots & \vdots \\ \cdot & \cdot & 0\,0\,\ldots\ldots\ldots\ldots 1 & \log_{10}(r_p^1) \\ \vdots & \vdots & 0\,0\,\ldots\ldots\ldots\ldots 1 & \log_{10}(r_p^2) \\ \cdot & \cdot & 0\,0\,\ldots\ldots\ldots\ldots 1 & \ldots \\ & & 0\,0\,\ldots\ldots\ldots\ldots 1 & \log_{10}(r_p^k) \end{bmatrix}$$

Solution for the ground motion empirical model

As stated before, two different models were obtained due to the two Band-Pass filters applied. Table 7.4 contains the resulting pseudoMagnitude values for both models.

Figure 7.5 shows the correlation between the computed magnitude obtained by means of the models and the measured amplitudes after having been filtered (band-pass filters [1-5]Hz and [1-10]Hz). Both graphs show a high correlation between the measured and computed amplitudes, e.g. the computed results are consistent with the velocity model. Furthermore, in the case of the 1-10 Hz band-pass filter, the correlation factor equals 1, whereas for the 1-5 Hz it equals 0.99. Moreover, both graph results are consistent.

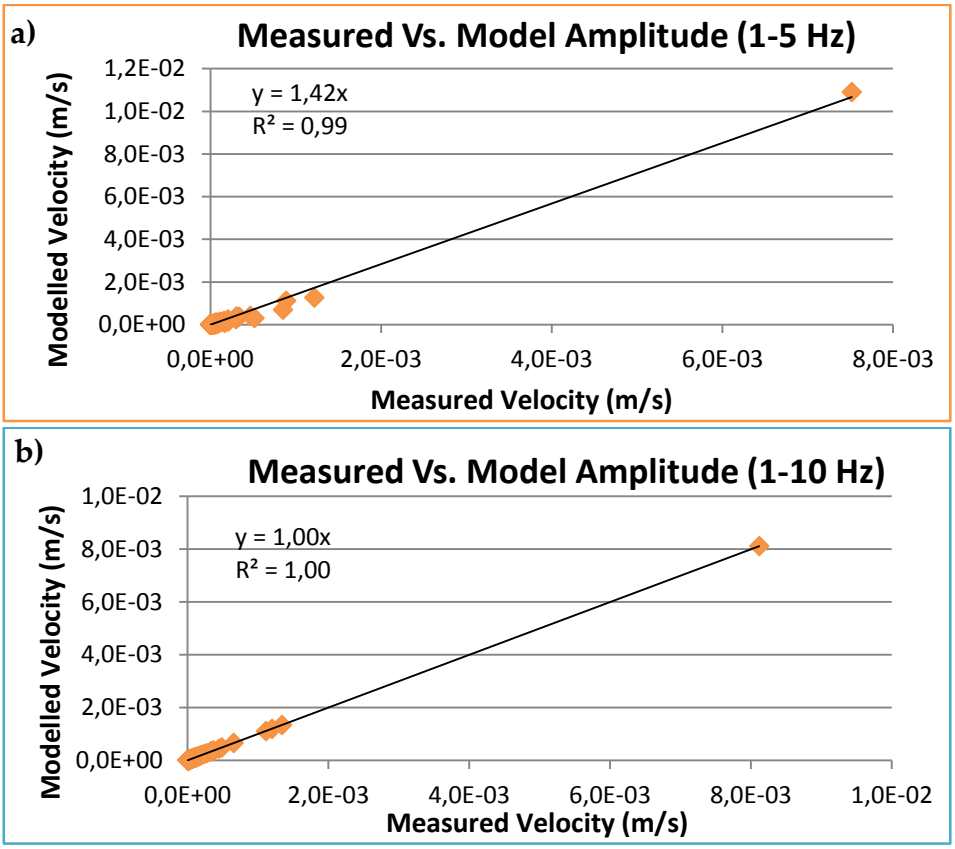

Figure 7.5. Measured velocity versus velocity obtained by the computed model. a) Band-pass filter 1-5Hz and b) Band-pass filter 1-10Hz

The results for the power-law factors were:

	Filter [1-5]Hz	Filter [1-10]Hz
a	1.41	1.61

Table 7.3. Power-law factors for both of the band-pass filters.

Local earthquakes can be recorded by means of observatories deployed nearby a seismic network. This presents the opportunity to calibrate pseudoMagnitudes derived from the recorded data provided by the seismic network, with local magnitudes (m_L) provided by the national seismic services.

In the case of Austria, the seismological service computes the local magnitude (m_L) by means of equation (7.8), where $\boldsymbol{A}$ is the maximum value of horizontal component (in nm/sec) after having applied a band-pass filter between 1-10 Hz; the exponent in the amplitude-distance relation ($\boldsymbol{a}$) has a value of 1.66; Δ is the epicentral distance in degrees; and $\boldsymbol{c = -0.304}$. The value of the exponent $\boldsymbol{a}$ in the amplitude-distance power relation for different ranges of epicenter distances presents an issue.

$$\boldsymbol{m_L = log_{10}(A) + a \cdot log_{10}(\Delta) - c} \qquad (7.8)$$

	Filter [1-5]Hz	Filter [1-10]Hz	ZAMG Magnitude
PseudoMagnitude	-6.45	-6.25	1.80
	-6.01	-5.82	2.20
	-6.23	-6.17	2.00
	-6.38	-6.20	2.00
	-5.12	-4.97	2.70
	-6.29	-6.29	1.80
	-6.34	-6.22	1.70
	-5.81	-5.66	2.30
	-5.95	-5.80	2.40
	-5.73	-5.57	2.50
	-5.42	-5.32	2.80
	-5.67	-5.52	2.40
	-5.36	-5.39	2.60
	-5.99	-5.84	2.30
	-5.94	-5.76	2.00
	-5.30	-5.10	2.60
	-5.57	-5.46	2.40
	-5.82	-5.61	2.20
	-5.74	-5.62	2.20
	-6.25	-6.06	1.90
	-5.83	-5.72	2.40
	-6.17	-6.16	1.80
	-6.24	-6.01	1.90
	-5.00	-4.91	2.70
	-5.81	-5.64	2.30
	-6.12	-5.95	2.00
	-5.77	-5.58	2.20
	-6.00	-5.88	2.00
	-6.26	-6.14	1.80
	-6.14	-6.10	2.00
	-5.76	-5.76	2.10
	-6.28	-6.17	1.70
	-6.60	-6.47	1.70
	-6.53	-6.38	1.70
	-6.28	-6.16	1.90
	-5.40	-5.23	2.50
	-5.30	-5.20	2.70
	-4.33	-4.22	3.60
	-6.27	-6.12	2.00
	-5.50	-5.33	2.50
	-5.45	-5.34	2.70
	-6.01	-5.87	2.00
	-3.72	-3.70	4.30

Table 7.4. Obtained pseudoMagnitude from the two models corresponding to the two band-pass filters (1-5Hz and 1-10Hz).

Amplification factor - Station correction

By application of the least squares estimation, the station corrections were also obtained as an additional parameter. Station corrections can improve the accuracy of pseudoMagnitude calculations in case of near-surface deviations of the calculated pseudoMagnitude, according to our prediction model.

The computed values of pseudoMagnitude for both models (table 7.4) have been corrected using the station correction given in the next table (table 7.5). The station correction range varies from −1.16 to 0.24.[1-5 Hz band-pass filter], and from -1.05 to 0.38 [1-10 Hz band-pass filter].

	1-5 Hz	1-10 Hz
ALBA	-0.1689	-0.3522
ARSA	0.0550	0.1491
BISA	-1.1685	-1.0543
CONA	0.2330	0.3833
CSNA	0.2366	0.3254
GILA	0.1307	0.1925
GUWA	0.2436	0.1688
MARA	0.1389	0.0035
PUBA	0.1928	0.1601
SITA	-0.0937	-0.2707
SOP	0.2004	0.2944

Table 7.5. Computed pseudoMagnitude correction factors of the seismic stations of the ALPAACT network.

Equation (5.2) was established as a constraint. For verification, the station corrections for both of the models were added, which resulted in a value of zero for the band-pass filter of 1-10 Hz and almost zero for the 1-5 Hz filter, as shown in equations 7.10a) and 7.10b).

$$\sum_{k=1}^{N=11} \boldsymbol{C^k}[\mathbf{1-5\ Hz}] = 0.0000 \qquad (7.9a)$$

$$\sum_{k=1}^{N=11} \boldsymbol{C^k}[\mathbf{1-10\ Hz}] = 0.0000 \qquad (7.9b)$$

The station correction characterizes the topography and geology at each station. It provides an idea of the type of terrain; negative station correction values arise for sedimentary soil, such as those seen in BISA, and positive values for hard rock, such as those seen in GUWA. This is due to the fact that seismic waves tend to be amplified when travelling through sedimentary basins, such as in the BISA station, which is located in the Vienna Basin. On the other hand, hard-rock sites cause seismic waves to attenuate, such as at the station GUWA, which is located in the Styrian Mürzsteg Alp. The station corrections are plotted and

countered in figures 7.6. a) and b) for both filters. The high negative value of the corrections for the permanent station BISA, situated at the Vienna Basin, are -1.1685 [1-5 Hz], and -1.0543 [1-5 Hz]. The smallest positive values correspond to stations ARSA and MARA.

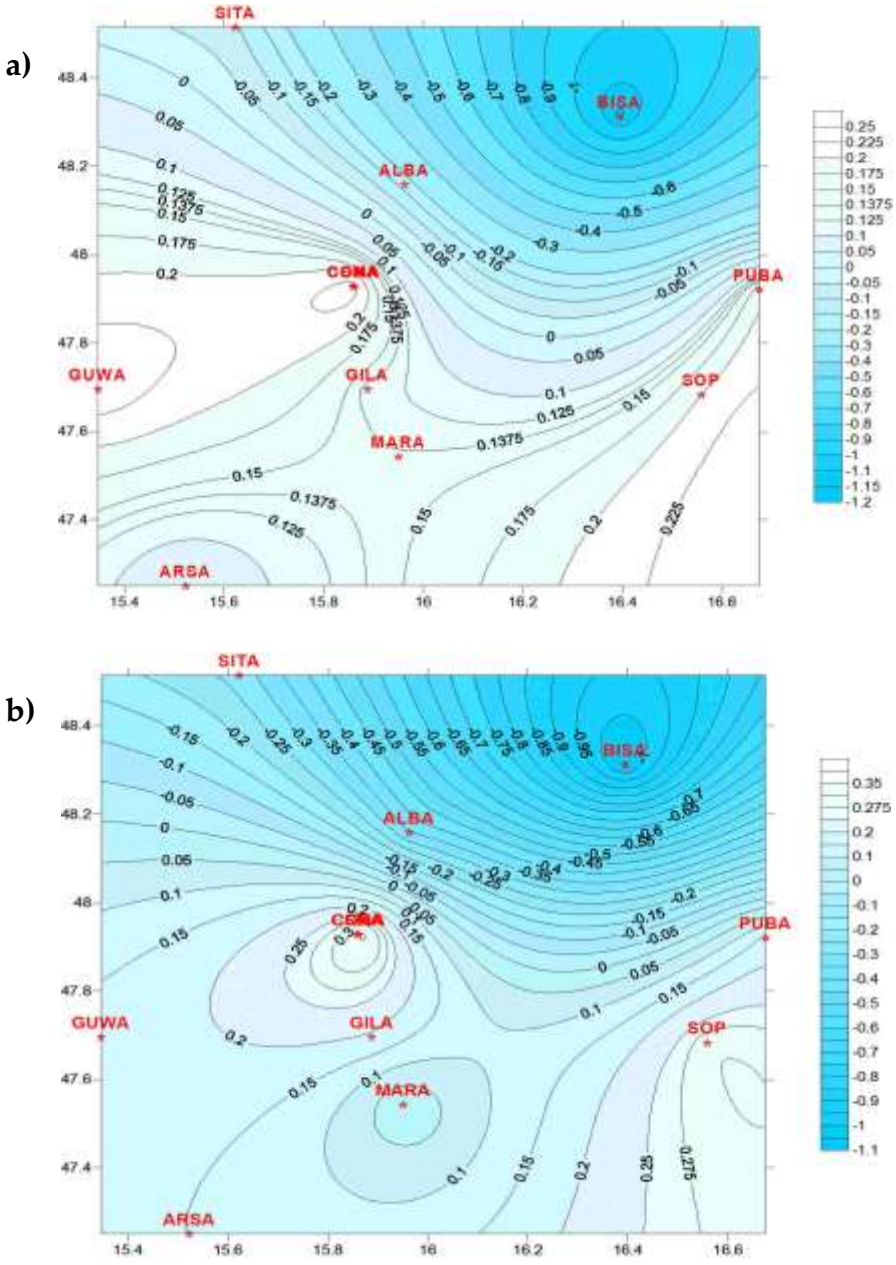

Figure 7.6. Station corrections plotted as contour lines from a Krigin interpolation and station symbols (stars) over the study area for band-pass filters, a) 1-5 Hz. b) 1-10 Hz.

7.2 PseudoMagntude calibration

The figures in 7.7 show the correlation between the local magnitude (m_L), provided by the seismological service of the Zentralanstalt für Meteorologie

und Geodynamik (ZAMG), and the pseudoMagnitudes obtained with the ground motion model, for the two band-pass filters [1-5] Hz and [1-10] Hz respectively.

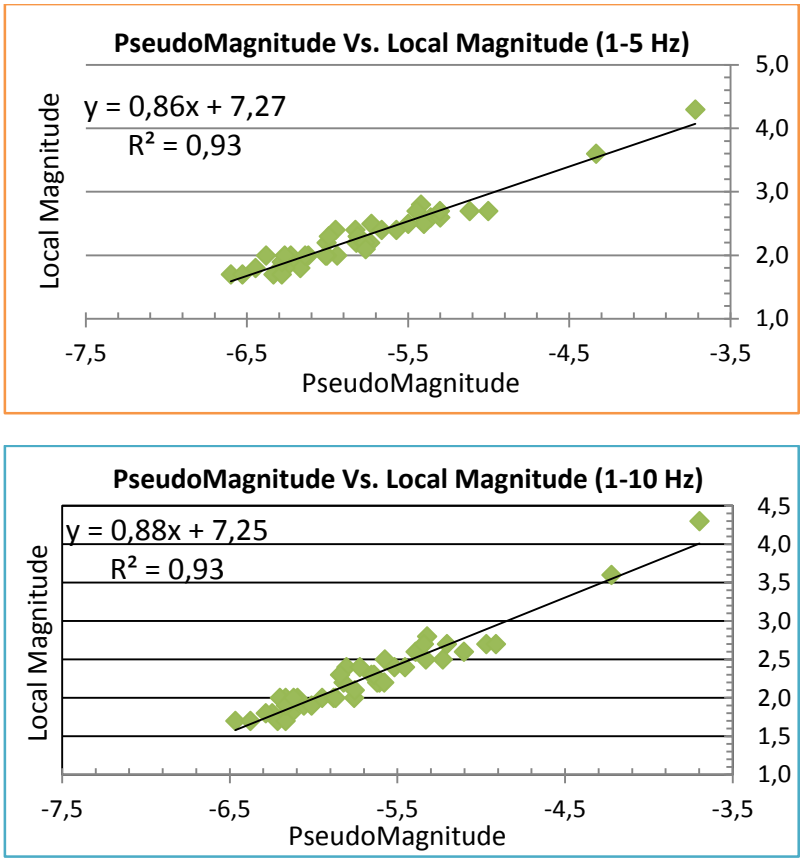

Figure 7.7. Correlation of the obtained pseudoMagnitude with the local magnitude provided by ZAMG. a) Band-pass filter 1-5Hz; b) Band-pass filter 1-10Hz.

For earthquake data, obtained within the ALPAACT project, the following empirical relationship between the local magnitude (determined by the ZAMG) and pseudoMagnitude can be derived using:

$$m_L(1-5\ Hz) = 0{,}86 * pseudoM + 7{,}27 \qquad r^2 = 0.93 \qquad (7.10a)$$

$$m_L(1-10\ Hz) = 0{,}88 * pseudoM + 7{,}25 \qquad r^2 = 0.93 \qquad (7.10b)$$

7.3 Localization examples of seismic events at ALPAACT network

Detection and localization of earthquakes in the ALPAACT network

Once the empirical ground motion models were calculated and the minimum values of the Back-Projection Amplitude Matrix were selected, the location and SourceMap of the earthquakes could be determined according to equation 4.9.

All of the SourceMap plots for both band-pass filters and all events (43) can be found in the Appendix on the CD.

However, some of the results for the [1-5Hz] and [1-10Hz] band-pass filters are presented in this section in parallel (figure 7.9).

For further analysis, the evaluation of the results was performed taking two types of errors into considerations, namely the ***Absolute Error*** and the ***Relative Error***. The ***Absolute Error*** is simply the amount of physical error in a measurement, and will have the same unit label as the measured quantity.

$$\Delta x_{abs} = \left| x_{measured} - x_{accepted} \right| \qquad (7.11a)$$

The ***Relative Error*** is the ratio of the absolute error of the measurement to the accepted measurement. The relative error expresses the "relative size of the error" of the measurement in relation to the measurement itself, and it is considered to be a measure of accuracy. When the accepted or true measurement is known, the relative error is found using:

$$\Delta x_{rel} = \frac{\Delta_{abs}}{x_{accepted}} \qquad (7.11b)$$

This error will be calculated only for the pseudoMagnitude and not for the location (latitude and longitude).

Band-Pass Filter 1-5 Hz ***Band-Pass Filter 1-10 Hz***

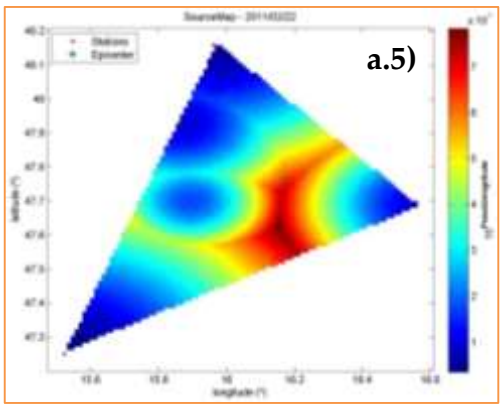

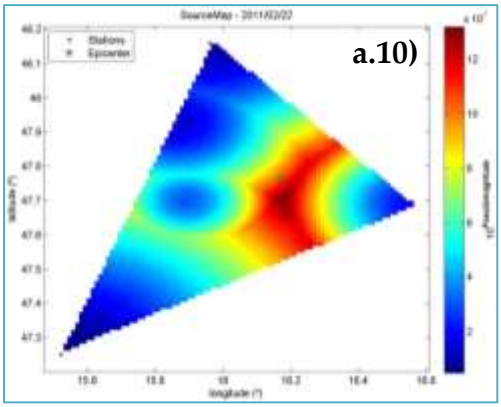

Date	*Time*	m_l	*Longitude*	*Latitude*	*Depth (m)*
Event. a) 2011/02/22	00:31:33	**2.3**	16.1718	47.7615	14200

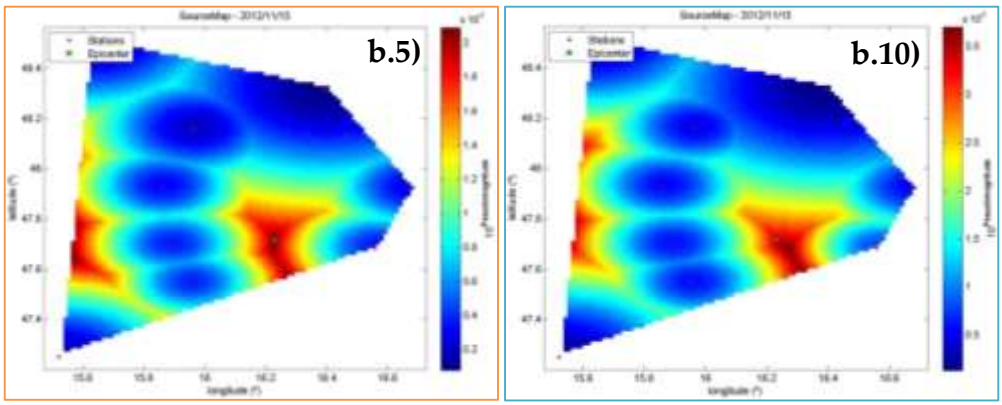

Event. b) 2012/11/15	03:17:38	**2.5**	16.2304	47.7153	14000

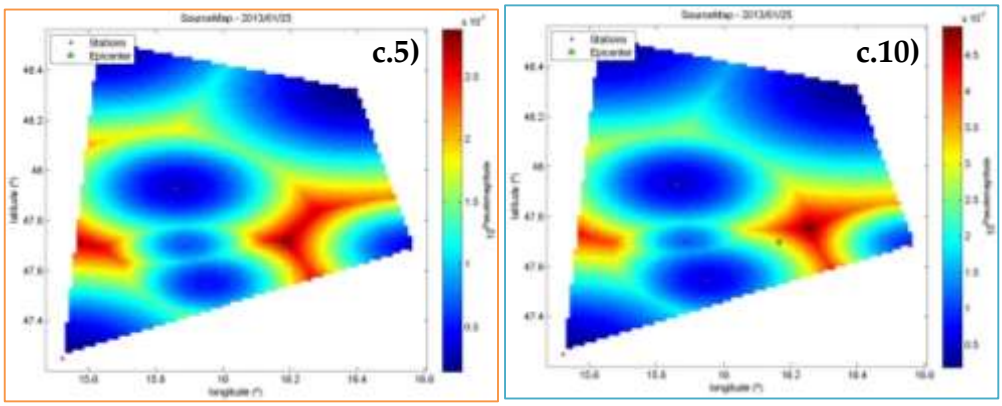

Event. c) 2013/01/25	07:14:34	**3.6**	16.1658	47.6973	11600

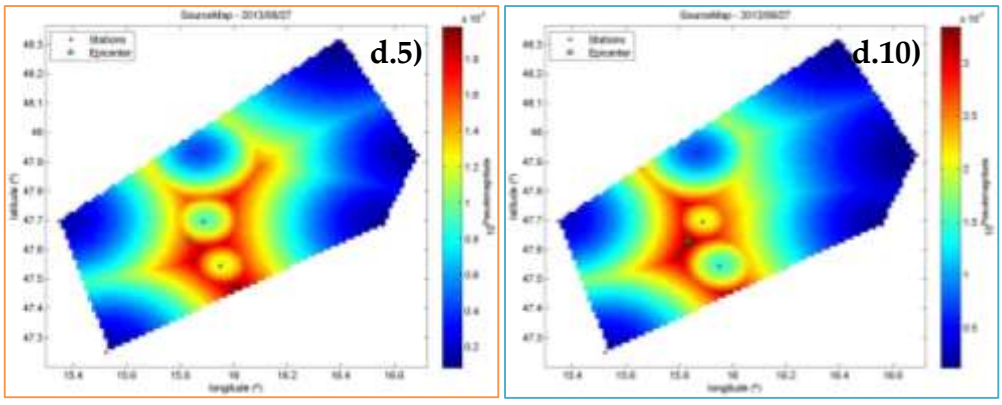

Event d) 2013/06/27	18:59:52	**2.7**	15.8328	47.6305	113000

Figure 7.8 Events a) b) c) and d) Examples of epicenter location with low location error. The .5) and .10) of the labeling refers to the 1-5Hz and 1-10Hz band-pass filters respectively.

Table 7.6 contains the deviation of the computed epicenter for both filters, from the epicenter locations provided by the ZAMG. The deviation is given in degrees and km for both of the band-pass filters used and for the events that lay inside the network.

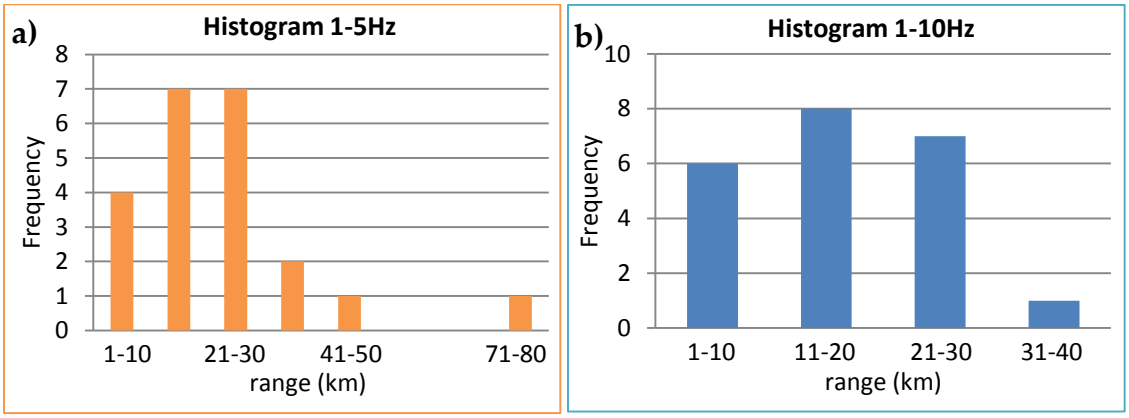

Figure 7.9. Histograms of the error in radial distance (km). a) 1-5Hz Band-pass filter. b) 1-10Hz Band-pass filter

Events marked in blue correspond to the SourceMaps presented in figure 7.8.

Event	$\lambda(°)$	$\varphi(°)$	$\Delta d_{5Hz}(km)$	$\Delta d_{5Hz}(°)$	$\Delta d_{10Hz}(km)$	$\Delta d_{10Hz}(°)$
1	16.2069	47.9647	15	0.1378	13	0.1132
3	16.1496	47.7609	15	0.1337	14	0.1264
4	16.0808	47.5571	18	0.1634	16	0.1440
13	15.7712	47.5979	21	0.1928	26	0.2384
14	**16.1496**	**47.6182**	**16**	**0.1450**	**7**	**0.0617**
15	15.7712	47.7111	27	0.2449	20	0.1764
16	15.7024	47.6182	20	0.1830	22	0.1995
17	16.0579	47.6692	31	0.2764	30	0.2663
20	15.9432	47.6483	21	0.1883	27	0.2419
27	16.3216	47.5877	24	0.2155	22	0.1965
28	16.2069	47.8628	6	0.0527	2	0.0192
29	16.1152	47.8368	9	0.0778	4	0.0405
32	15.5742	47.7654	31	0.2763	31	0.2763
33	16.3075	47.5863	24	0.2151	23	0.2091
34	16.2775	47.5697	20	0.1810	21	0.1864
35	16.2949	48.1236	43	0.3916	13	0.1186
36	**15.5615**	**47.6414**	**75**	**0.6730**	**8**	**0.0718**
38	**16.1840**	**47.7103**	**2**	**0.0223**	**11**	**0.0960**
40	16.1477	47.5174	24	0.2144	18	0.1599
41	**16.0034**	**47.4587**	**27**	**0.2421**	**2**	**0.0140**
42	16.2487	47.8918	13	0.1191	12	0.1038
43	16.4074	47.8481	10	0.0900	4	0.0356

Table 7.6. Coordinates and error in the radial distance (d) of the events which lay inside the network. Band-pass filters 1-5Hz and 1-10Hz.

Tables 7.7 and 7.8 contain the obtained magnitude and the corresponding relative error taking the value provided by the ZAMG as the accepted value. Table 7.7 refers to the [1-5Hz] band-pass filter, whereas table 7.8 refers to the [1-10Hz] band-pass filter.

Event	m_l^{ZAMG}	$10^{PM(5Hz)}$	$PM(5Hz)$	m_l^{5Hz}	abs. Δm_l^{5Hz}	rel. Δm_l^{5Hz} (%)
1	1.8	2.0E-07	-6.7	1.3	0.5	29.1
3	2.0	3.4E-07	-6.5	1.5	0.5	25.9
4	2.0	3.8E-07	-6.4	1.3	0.7	35.2
13	2.6	4.0E-06	-5.4	2.4	0.2	6.5
14	**2.3**	**7.8E-07**	**-6.1**	**1.5**	**0.8**	**36.2**
15	2.0	6.7E-07	-6.2	2.0	0.0	0.3
16	2.6	1.7E-06	-5.8	2.3	0.3	11.3
17	2.4	1.9E-06	-5.7	2.1	0.3	12.9
21	1.9	3.0E-07	-6.5	1.4	0.5	27.2
27	2.2	1.2E-06	-5.9	1.4	0.8	36.1
28	2.0	6.0E-07	-6.2	1.8	0.2	12.0
29	1.8	2.8E-07	-6.5	0.9	0.9	48.0
32	1.7	3.2E-07	-6.5	1.5	0.2	11.0
33	1.7	1.6E-07	-6.8	0.9	0.8	46.3
34	1.7	2.0E-07	-6.7	0.7	1.0	56.0
35	1.9	3.5E-07	-6.5	1.5	0.4	20.5
36	**2.5**	**2.1E-06**	**-5.7**	**2.5**	**0.0**	**0.0**
38	**3.6**	**2.9E-05**	**-4.5**	**2.8**	**0.8**	**22.1**
40	2.5	2.4E-06	-5.6	1.9	0.6	22.8
41	**2.7**	**2.0E-06**	**-5.7**	**1.9**	**0.8**	**30.9**
42	2.0	7.0E-07	-6.2	1.1	0.9	46.0
43	4.3	1.1E-04	-4.0	3.6	0.7	16.2

Table 7.7. Obtained magnitude for events lying inside the network and its relative error, where the value provided by the ZAMG was taken as the accepted value. 1-5Hz Band-pass filter.

According to the results in table 7.6 - 7.8 as well as those obtained from figure 7.9, it is shown that, in general, a better performance is obtained using the [1-10Hz] band-pass filter. For the [1-10Hz] filter, all but one event (95%) have accuracies of less than 30km, whereas for the [1-5Hz] filter this percentage is reduced to 81%. On the other hand, the only event, that is not enclosed in the 1-30km range for the [1-10Hz] filter deviates 31 km from the real position of the epicenter as given by the ZAMG. However, the location spread for the [1-5Hz] band-pass filter is much higher, with one event location being 75km away from the real epicenter.

A good accuracy would be an error of 10 km or less, which in case of the [1-10 Hz] band-pass filter was accomplished by about 27% of the events, while for the [1-5Hz] filter was fulfilled by about the 18% earthquakes. On the other hand, about 68% of the events, for the [1-10 Hz] filter, have a deviation from the epicenter location provided by ZAMG from 11km to 30km, whereas for the [1-5Hz] filter approximately 63% of the earthquakes were enclosed in this range.

$Event$	m_l^{ZAMG}	$10^{PM(10Hz)}$	$PM(10Hz)$	m_l^{10Hz}	$\mathbf{abs.}\Delta m_l^{10Hz}$	$\Delta m_l^{10Hz}(\%)$
1	1.8	3.75E-07	-6.4	1.7	0.1	7.6
3	2.0	4.45E-07	-6.4	1.7	0.3	17.2
4	2.0	7.18E-07	-6.1	1.9	0.1	5.5
13	2.6	3.83E-06	-5.4	2.5	0.1	5.2
14	2.3	**1.32E-06**	**-5.9**	**1.9**	**0.4**	**18.9**
15	2.0	1.24E-06	-5.9	2.2	0.2	8.9
16	2.6	2.98E-06	-5.5	2.5	0.1	5.2
17	2.4	3.00E-06	-5.5	2.4	0.0	2.0
12	1.9	5.21E-07	-6.3	1.9	0.0	1.9
27	2.2	2.62E-06	-5.6	2.1	0.1	6.2
28	2.0	8.40E-07	-6.1	1.7	0.3	14.1
29	1.8	4.89E-07	-6.3	1.4	0.4	23.5
32	1.7	4.95E-07	-6.3	1.7	0.0	2.1
33	1.7	2.77E-07	-6.6	1.2	0.5	29.3
34	1.7	3.61E-07	-6.4	1.1	0.6	32.4
35	1.9	5.66E-07	-6.2	1.6	0.3	15.1
36	2.5	**3.70E-06**	**-5.4**	**2.1**	**0.4**	**14.8**
38	3.6	**4.90E-05**	**-4.3**	**3.3**	**0.3**	**8.5**
40	2.5	3.79E-06	-5.4	2.1	0.4	15.3
41	2.7	**3.34E-06**	**-5.5**	**2.5**	**0.2**	**6.3**
42	2.0	1.21E-06	-5.9	1.6	0.4	22.1
43	4.3	1.32E-04	-3.9	3.9	0.4	10.2

Table 7.8. Obtained magnitude for events lying inside the network and its relative error, where the value provided by the ZAMG was taken as the accepted value. 1-10Hz Band-pass filter.

As was shown in section 6 (in the study with synthetic data), a factor requiring further study is the geometrical distribution of the network. The method is strongly influenced by the distribution of the stations in the network, and certainly also the number of available measuring stations.

The earthquake of Ebreichsdorf, 20 September 2013

Figure 7.10. Ebreichsdorf earthquake location.

The events studied include the earthquake that occurred around ***Ebreichsdorf***, in the southern Vienna Basin, on the 20th of September 2013. This is the strongest registered event presented in this thesis and within the recording period, with a local magnitude of (m_l = 4.3), which was followed by almost 30 aftershocks. (04.06:32 Local Time) in the southern Vienna Basin: Longitude 16.3960 °E, Latitude 47.9012 °N, depth 12km.

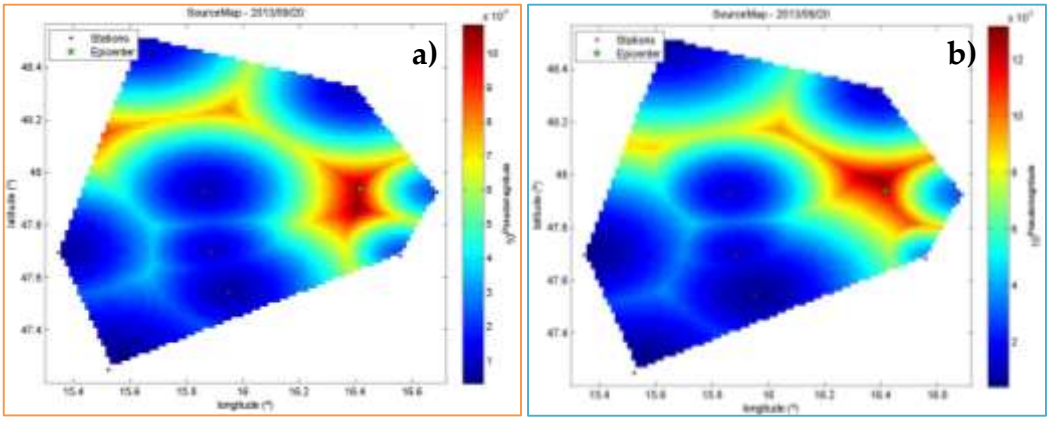

Figure 7.11. Ebreichsdorf SourceMap. a) 1-5 Hz Band-Pass Filter. b) 1-10 Hz Band-Pass Filter.

	ZAMG	BPF 1-5 Hz	BPF 1-10 Hz
$\boldsymbol{\lambda}$(°)	16.4164	16.4074	16.4074
$\boldsymbol{\Delta\lambda_{abs}}$ (°)	-	0.009	0.009
$\boldsymbol{\Delta\lambda_{abs}}$ $\boldsymbol{(km)}$	-	1.0	1.0
$\boldsymbol{\varphi}$(°)	47.9376	47.8481	47.9721
$\boldsymbol{\Delta\varphi_{abs}}$ (°)	-	0.0895	0.0345
$\boldsymbol{\Delta\varphi_{abs}}$ $\boldsymbol{(km)}$	-	9.9	3.8
$\boldsymbol{m_l}$	4.3	3.6	3.9
$\boldsymbol{\Delta m_l^{rel}}$ (%)	-	16.2	10.2

Table 7.9 Ebreichsdorf earthquake coordinates provided by the ZAMG and obtained by the two models.

The results presented for the Ebreichsdorf earthquake (table 7.9) show, as noted before, that a better performance of the network is achieved with the [1-10Hz] band-pass filter. In this event, a total number of 10 stations out of the 11 comprising the network were operative. Moreover, the beneficial geometry together with the position of the epicenter leads to satisfactory location of the earthquake. However, the local magnitude is slightly underestimated.

On balance, the potential of the method is shown in this section. However, further study on the geometrical network aspects needs further study. Furthermore, the detection matter needs additional investigation in order to implement the method in real time for earthquakes detection.

8. Application to seismic monitoring of rockfalls at Spitz quarry (NÖ, Austria)

The aim of this section is to analyse how the seismic warning system installed in Spitz must be designed in order to overcome the present deficiencies in the rockfalls warning system at Spitz quarry .

Therefore, the new developed methodology, which enables the detection and location of rockfalls above a critical size, was applied and tested.

In the context of this thesis, the causes of the unsatisfactory performance of the recent seismic warning system are also examined, along with the extent to which suitable results can be obtained for practical use with the employment of devices and the new method. [Brückl, E., M.P. Papí. (2016)]
The aim was to achieve the following concrete results:

Clear understanding of why the existing measurement system did not meet requirements.

- ✓ Develop a methodology that enables the detection of rockfalls from a critical size in the Spitz quarry. False alarms must be reduced to an acceptable minimum.
- ✓ The performance of the proposed alert system should be demonstrated in a field trial. In this experiment, rockfalls (to about $1\,m^3$) should be artificially triggered and detected.
- ✓ In the current research project the development of a real-time warning system was not under request. However, the method should be sufficiently fast, sensitive, robust and reliable for deciding whether it should be expanded into a real-time warning system.

8.1 Field trial with a new seismic monitoring system

In order to perform this task, a small-scale passive seismic network comprised of 7 monitoring seismic stations acquiring data in continuous mode was established in the quarry of Spitz in such a way that the rockfall hazard area was covered.

Measuring System

The following requirements were to be fulfilled by the seismic measuring system as part of the field test:

- ✓ bandwidth of the seismic signal detected at least 10-100 Hz.
- ✓ LSB (Least Significant Bit) of the measuring system should be significantly below the signal strength of the ambient noise in the planned study area.
- ✓ High-resolution A/D conversion (24 bits).
- ✓ Continuous recording in digital format, sample rate of at least 200 Hz.
- ✓ Time synchronization between the different seismic stations, or absolute time.
- ✓ Autonomous power supply for at least 24 h operation.
- ✓ Easy assembly and disassembly in the field.

The **7 seismic measuring** systems that met the requirements comprises the following components (as shown in Figure 8.1):

- ✓ Sensor: 3-component geophone, 4.5Hz, damping factor 0.7, sensitivity 81 Vms^{-1}.
- ✓ Recorder: RefTek 130 3-, or 6-channel recorder; maximum sample rate 1000 Hz; Data storage on flash disk; Time synchronization via GPS signal; LSB at high gain setting 49 nV.
- ✓ Power supply via batteries

Recording	System Geophones/Seimometers	Amount
RefTek 130 3Ch/6Ch	GS-11D 4.5Hz	7

Table 8.1. Equipment used during seismic monitoring campaign.

Figure 8.1. Seismic measurement system; a) Components: 1 .Geophone + cable, 2. Battery, 3. GPS antenna + Cable, 4. Recorder; b) Assembly in easy to transport and quickly installable systems.

Selection of monitoring stations on June 26, 2015

On the first visit to the quarry site together with Dr. Joachim Schweigl and DI Michael Bertagnoli, 8 seismic monitoring station locations were selected and carefully distributed in such a way as to enclose the rockfall hazard area. However, regrettably only 7 measuring points were occupied by seismic stations in the field test.

Figure 8.2. Location of seismic stations (red triangles) in a Google Map; the position of the laser scanner and the film camera are indicated by the red rectangle; a white cross marks the origin of the local system; seismic stations of existing measurement system are labelled with G1, G2 and G3 (yellow circles).

The terrain (Figure 8.3), which proved to be difficult to navigate at times, prompted us to construct transportable boxes (Figure 8.1b) for 6 of the measuring systems in order to facilitate the rapid installation and dismantling of the seismic stations in the field. Figure 8.2 shows the locations of the seismic stations in the area in Google Map.

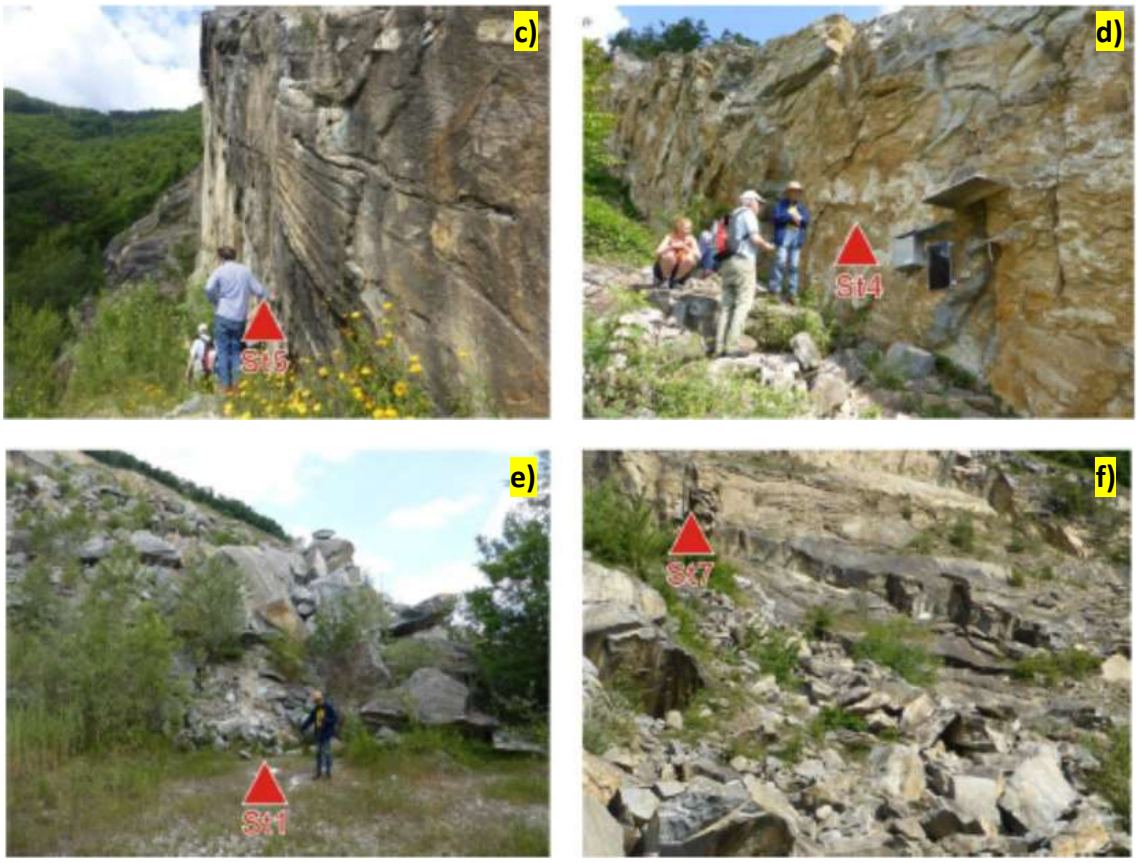

Figure 8.3. Images of the stations location in the quarry of Spitz.

Field test 1st and 2nd of October 2015

On October 1st, together with 2 employees of the working place at Schwallenbach, the 7 seismic stations were installed. At stations 4 and 5, the geophones were mounted on the rock on specially prepared mounting brackets with dowels (Figure 8.4).

Figure 8.4. Mounting of the geophone directly on the rock of station 4.

The location of seismic stations 1, 2, 3, 5 and 6 were measured with a Leica GPS unit in RKT (Real Time Kinematic) mode. RTK navigation technique processes phase measurements of the carrier wave, and provide up to centimeter-level accuracy or better.

The locations of the stations 4 and 7 could be found with sufficient accuracy from the map. In Table 2, the station and serial numbers of the recorder are allocated to the coordinates.

Each station is comprised of a geophone with three components and a natural frequency of 4.5 Hz. Recorders acquire data in continuous mode, digitized with either 500 samples per second/channel or 200 samples per second/channel. Time synchronization at individual stations is achieved using the GPS time base.

A geophone was connected to each station in order to measure the three components of the ground motion (HHE, HHN and HHZ). The geophones were either buried or placed on a (sophisticated) platform attached to the rock wall, well oriented to north by means of a compass. Boreholes were made in the rock-wall in order to fix the geophone platform.

Power supply was provided by means of batteries connected to the stations. The sample rate of the Spitz quarry stations was 500Hz, except for the stations 4 and 7 which were set to 200Hz since they were placed on hard rock and this sample rate was more appropriate. The data was saved and stored on an internal flash disk.

Gain and sample rate of the recorder was set to "high gain" and 500 Hz. On the less easily accessible stations 3, 4, 5 and 7, the recorder was started on the evening of October 1st, whereas the other stations were switched on the morning of 2nd October

Station	Serial Number	Channels	Latitude (°)	Longitude (°)	Height (m)
St1	A00D	6	48.3491137	15.4042054	261.6
St2	B4CC	6	48.3496730	15.4031862	295.0
St3	B32F	3	48.3509769	15.4021706	419.6
St4	9898	3	48.3504667	15.4036333	280.0
St5	B4C6	6	48.3505056	15.4025250	311.0
St6	A04C	6	48.3507383	15.4052684	262.7
St7	9882	3	48.3505417	15.4045194	283.0

Table 8.2. Information of the seven stations used in the experiment. Station number, serial number of the recorder, number of channels and coordinates.

Figure 8.5. Triggering of rockfalls and rockslides on the top quarry area by the troops of the local construction management.

8.2 Seismic data processing and analysis

On the 2nd of October 2015, three induced rockfall experiments were performed. The rockfall experiments began at 09:00 a.m. (local time, 07:00 UTC) and lasted about 1 hour and a half. They were carried out by a squad of the local construction company. The source area of the artificial rockfalls was the top of the cliff above the sliding surface, just below the seismic station 3. Blocks of about 100 kg to 2 $tons$ crashed to the ground (see Figure 8.5).

Raw data

The data was stored in hour files. For further evaluations and analyzes we focus on the hour 09:00 to 10:00 a.m. local time (07:00 - 08:00 UTC). The images 6a-c show the seismograms and their spectrograms for all stations and components. The stations are presented from top (rockfalls area) to bottom (traffic vibrations) of the quarry, i.e. St3, St5, St4, St2, St7, St1 and St6.

The data processing was done with the help of *pSysmon* and *Matlab®*. *pSysmon* is a seismological prototyping and processing software dedicated to non-standard seismological studies. It is written in Python and released under the GNU GPL license. pSysmon provides a modular frameset for data organization, visualization and signal processing of seismic time series. The software is built

around a primary graphical user interface using wxPython. It handles a set of packages, the *collection nodes*, providing specific functionality (e.g. data visualization, signal processing and data conversion).

Figure 8.6 shows the seismograms together with the spectrograms for the three components (EHH, NHH and ZHH) of the first hour recordings (*7:00 -8: 00 UTC)*. The seismograms are presented for the three components and sorted in the station order explained above (from top to bottom of the quarry). The black rectangles enclose the selected events for the computation of the ground motion model of the area. Furthermore, a zoom-in example of the EHH-component for the first event is presented in Figure 8.7 (the remaining representations can be found in the Appendix on the CD).

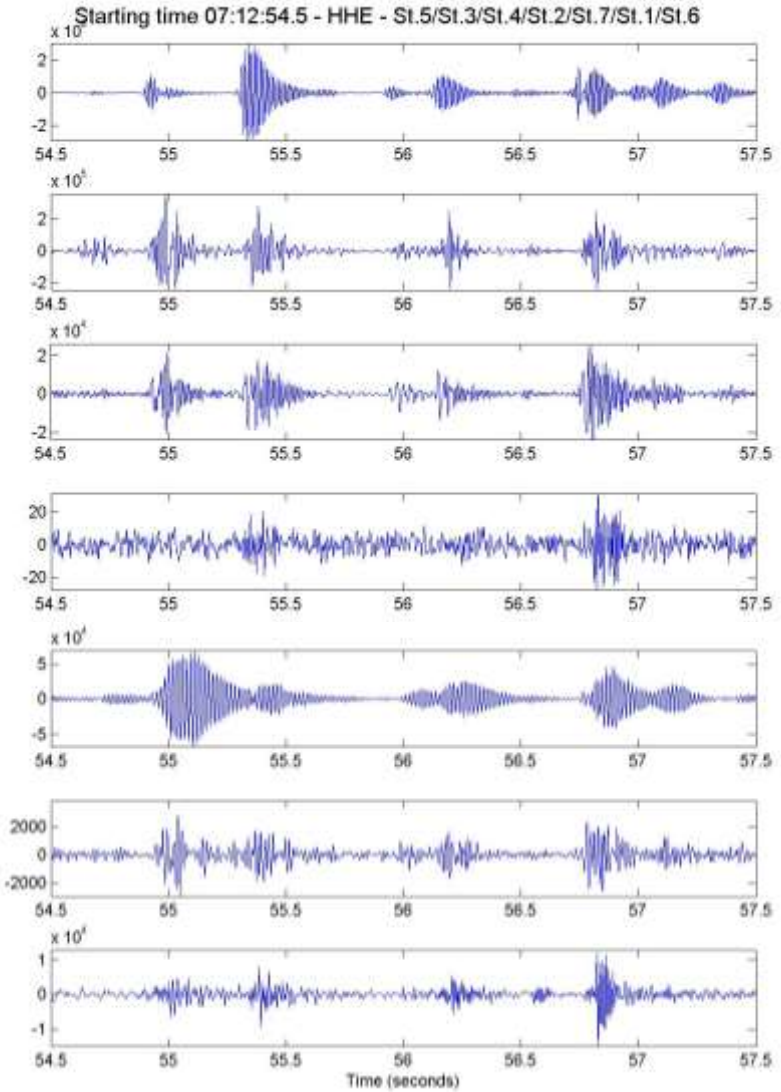

Figure 8.6: Zoom-in of the East component (HHE) first rockfall event from which distance - ground velocity relation is derived. The stations are ordered from top to bottom as previously explained.

a)

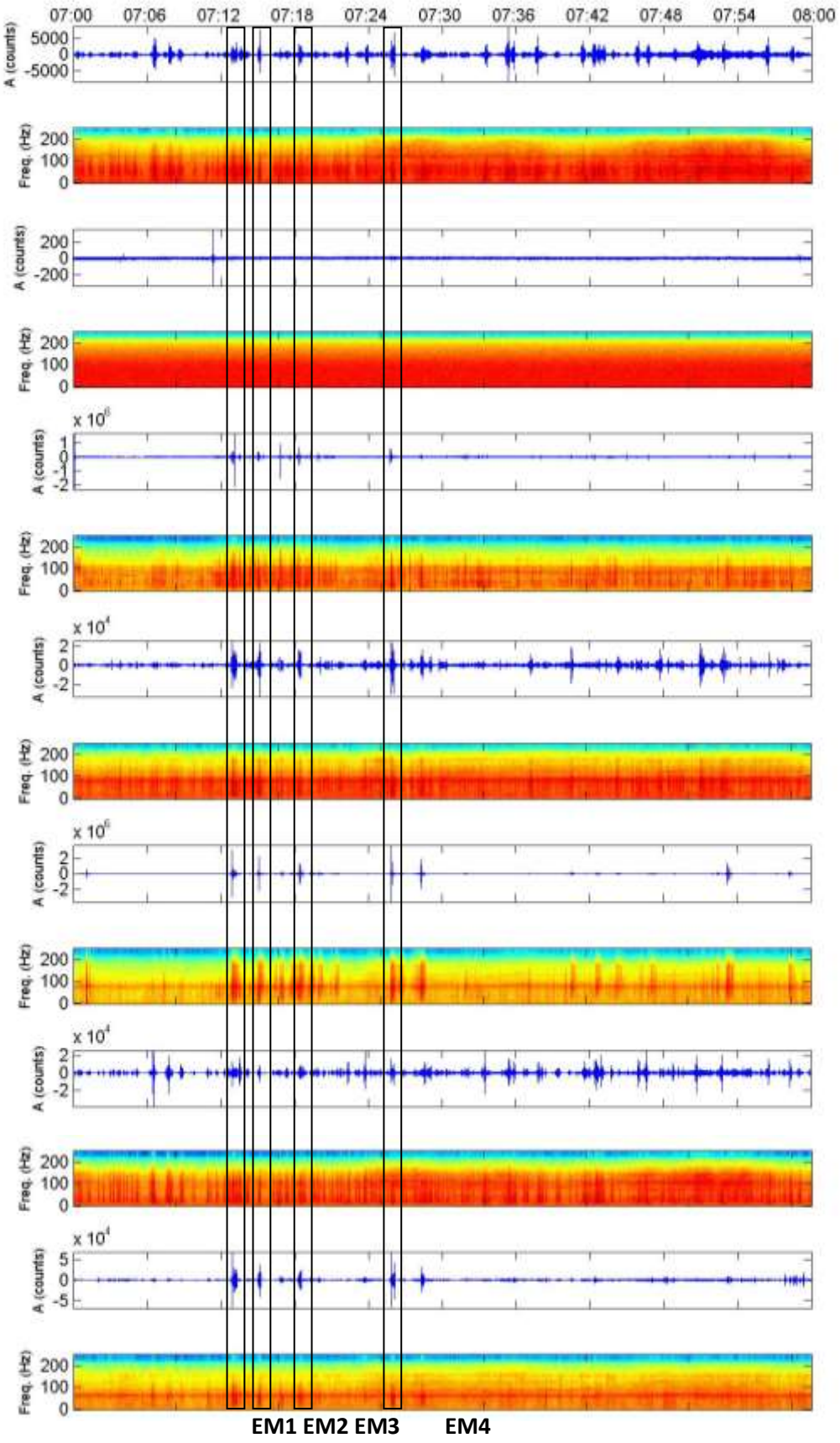
07:00
07:06
07:12
07:18
07:24
07:30
07:36
07:42
07:48
07:54
08:00
A (counts)
Freq. (Hz)
x 10^6
x 10^4
EM1
EM2
EM3
EM4

b)

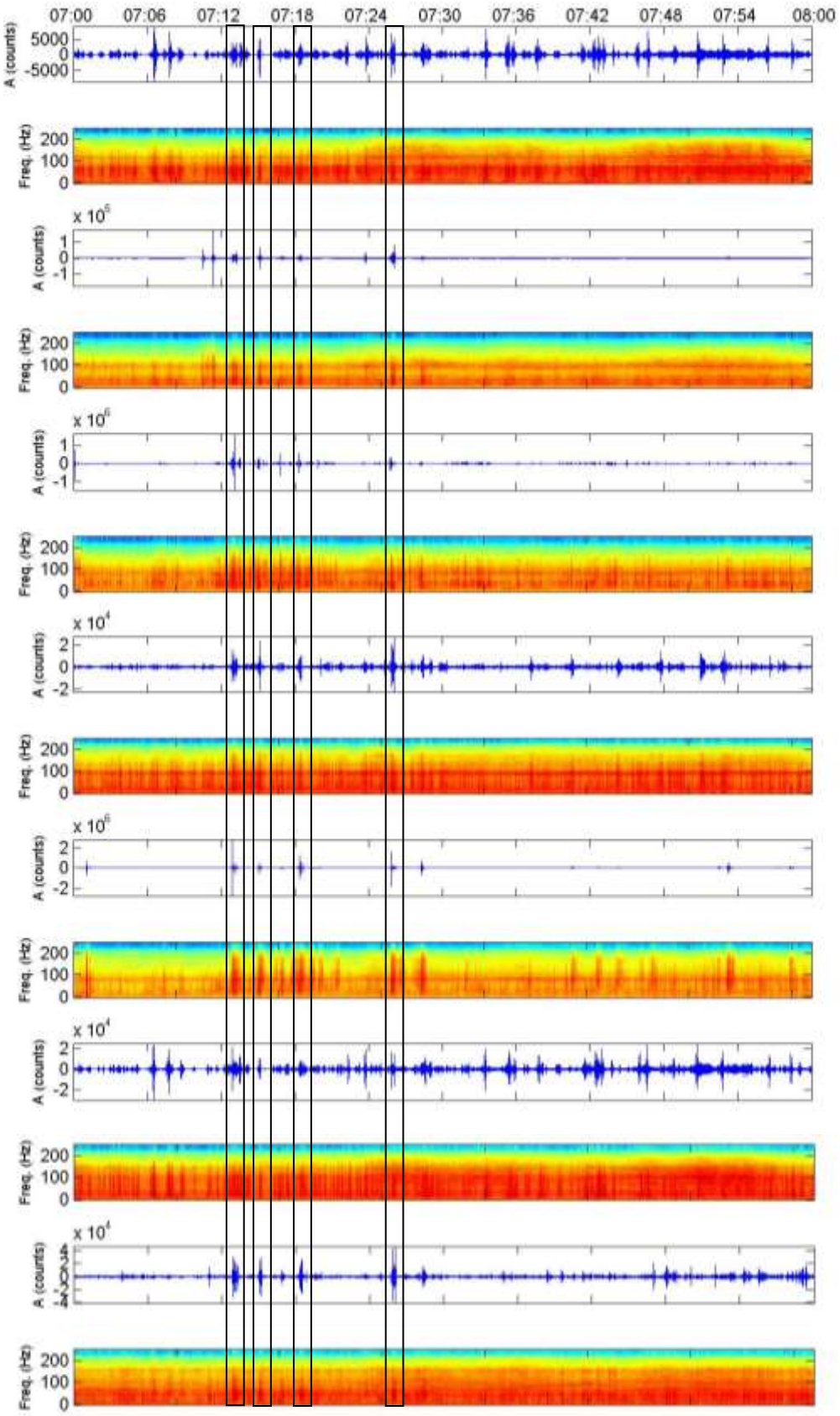
07:00
07:06
07:12
07:18
07:24
07:30
07:36
07:42
07:48
07:54
08:00
A (counts)
Freq. (Hz)
EM1 EM2 EM3
EM4

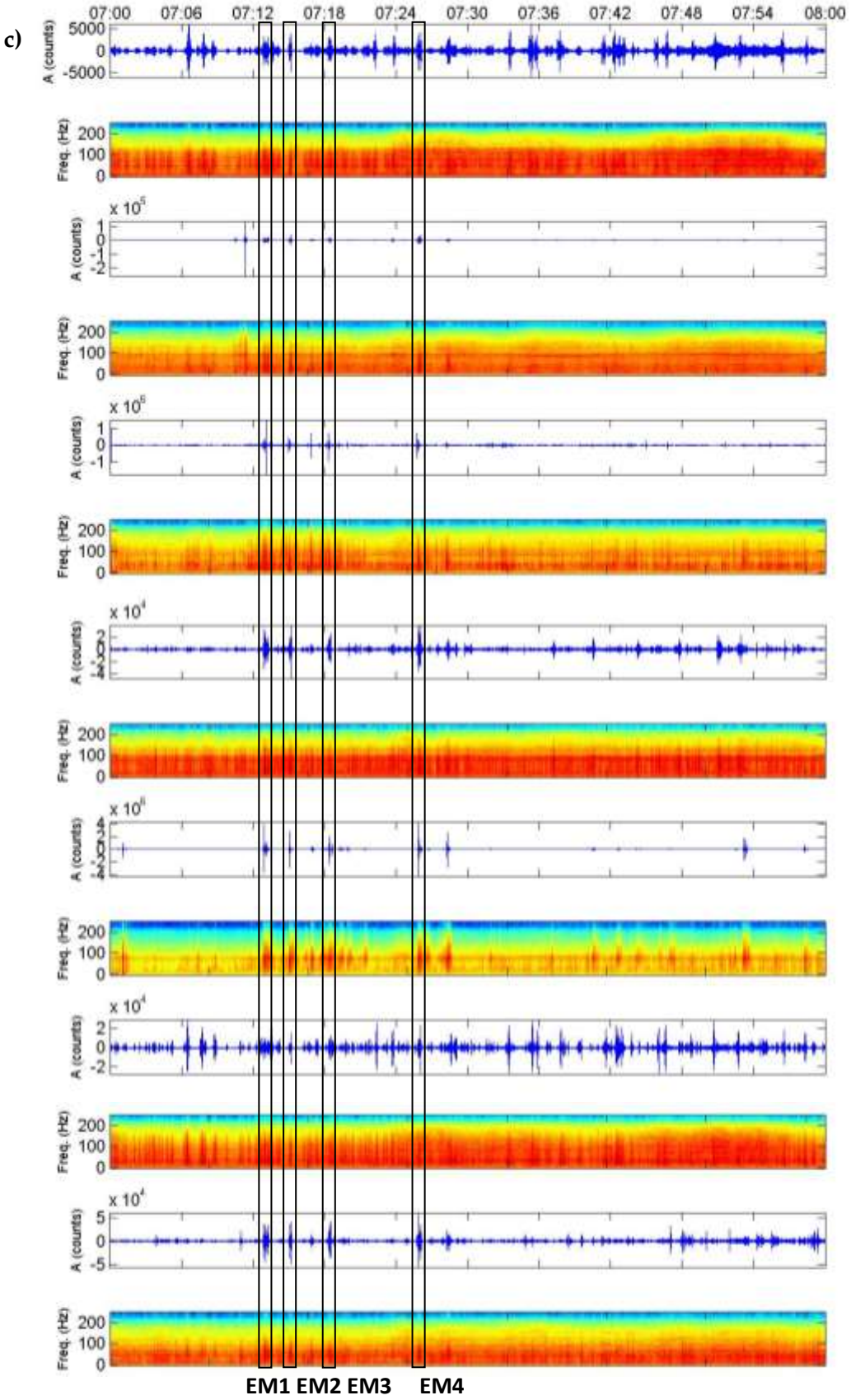

Figure 8.7. c) Seismograms, together with their spectrograms, for the 1 hour recording (7:00 -8: 00 UTC) resultant velocity for: a) HHE-component; b) HHN-component; c) HHH-component. Rectangles highlight the events chosen for computing the ground motion model.

Resultant Velocity (V)

In the first step, the resultant ground velocity (V) for each station in the network was computed using equation 4.5. Regarding the ALPAACT network, V_{xpp} in Spitz equals the EHH component, V_{ypp} the NHH and V_{zpp} the ZHH seismogram component.

Once the resulting vibration velocity is computed, Time Windows (TW) of 10 seconds, and an overlap of three quarters of the Time Window [(3/4)TW], were selected, i.e. the time interval between successive time windows was 2.5s with a resultant number of 1437 time windows for the first study hour. Figures 8.8 a) and b) show the data in logarithmic and linear scales respectively.

a)

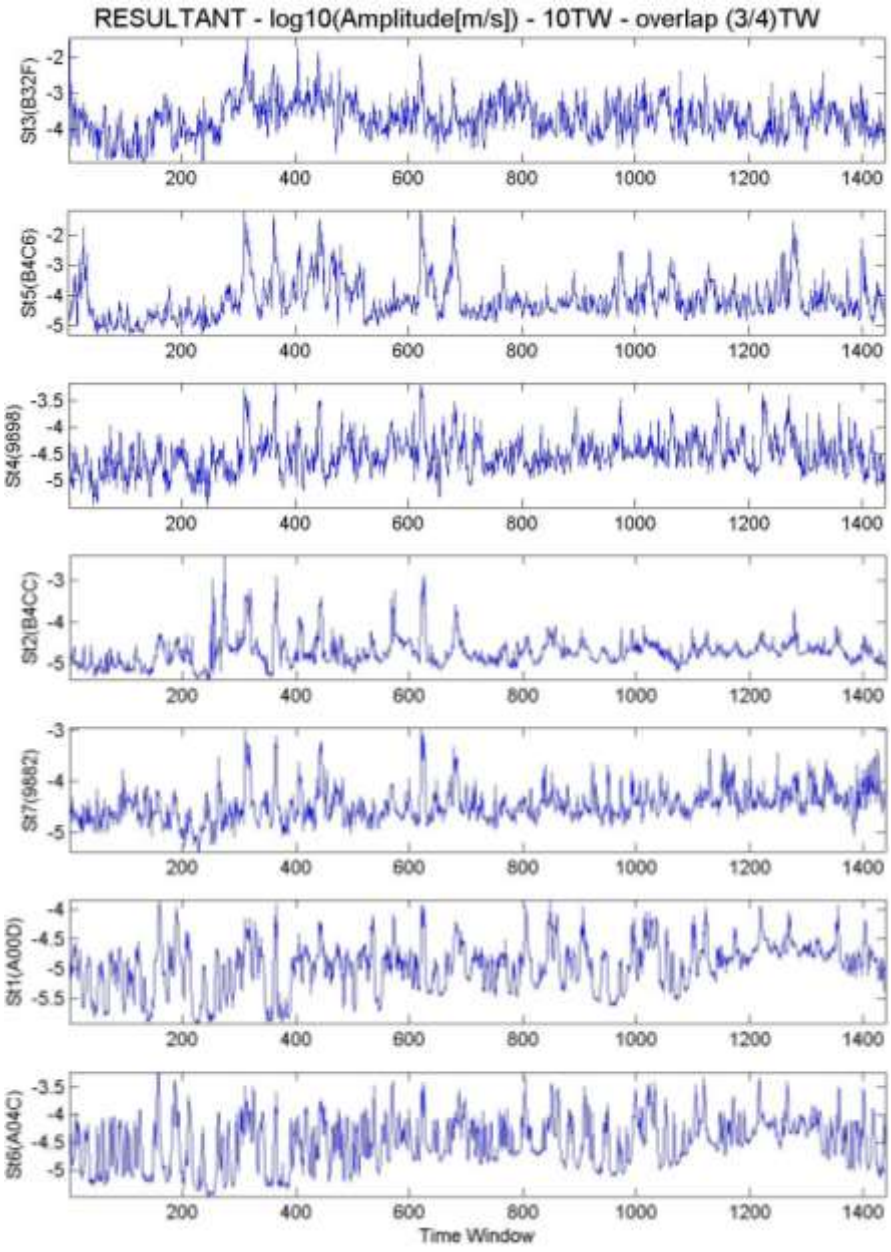

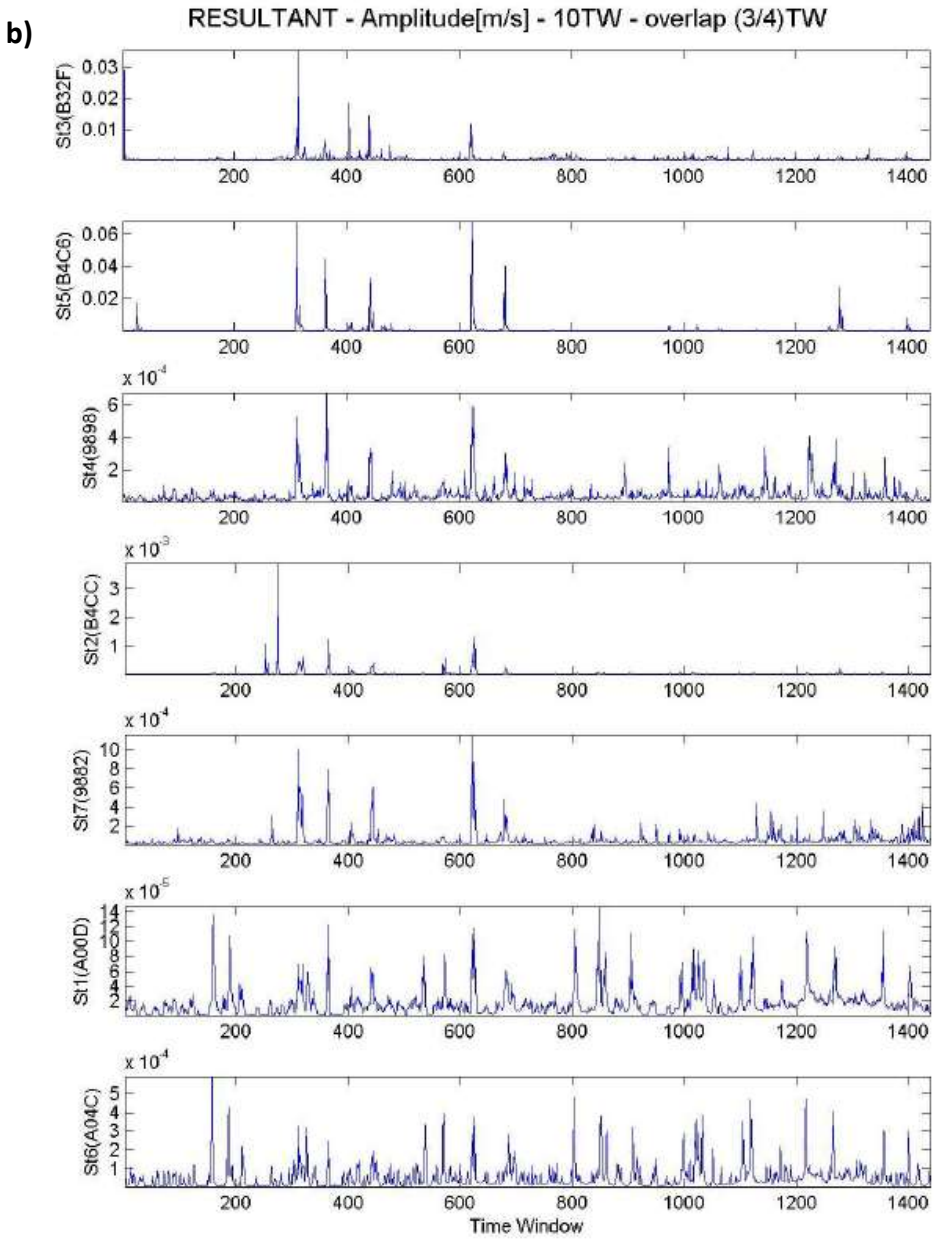

Figure 8.8. Resulting vibration velocities in 10s time windows and 2.5s step in a) logarithmic and b) linear scale.

8.3 Detection and localization of rockfalls

As mentioned before, any small seismic sources can produce indefinitely large amplitudes, as long as they are located close enough to a seismic station sensor. Therefore, the sources of the seismic waves are to be localized in order to avoid false positives.

Empirical Ground Motion Model

From the data series shown in Figure 8.7, four strong events were selected in order to determine the ground motion model parameters. Table 8.3 shows the resultant ground velocity values for the carefully selected hits used in the determination of the model. The source location (hit) was determined by monitoring the avalanche track.

Time	r_x (m)	r_y (m)	r_z (m)	V^{St1}	V^{St2}	V^{St3}	V^{St4}	V^{St5}	V^{St6}	V^{St7}
07:12:55.0	35.56	116.94	1	1.70E-05	5.66E-05	1.61E-03	9.63E-05	6.52E-03	4.07E-05	2.46E-04
07:12:55.5	37.68	115.82	1	1.38E-05	6.19E-05	1.24E-03	1.19E-04	1.54E-02	5.65E-05	2.56E-04
07:12:56.0	39.79	114.70	1	1.24E-05	4.58E-05	1.00E-03	7.63E-05	8.55E-03	4.05E-05	1.05E-04
07:12:57.0	42.91	112.55	1	1.77E-05	8.91E-05	1.10E-03	1.35E-04	1.44E-02	8.54E-05	1.82E-04
07:15:05.0	30.29	119.50	1	1.33E-05	3.78E-05	1.21E-03	6.60E-05	5.45E-03	3.54E-05	9.33E-05
07:15:07.0	33.50	115.02	1	1.95E-05	6.48E-05	6.74E-04	7.57E-05	1.16E-02	2.89E-05	1.44E-04
07:18:20.5	32.02	117.37	1	1.68E-05	7.01E-05	3.76E-03	6.43E-05	8.45E-04	2.45E-05	8.24E-05
07:18:24.5	34.30	115.23	1	1.11E-05	3.85E-05	1.49E-03	7.79E-05	7.05E-04	2.37E-05	1.19E-04
07:18:25.5	37.09	113.99	1	1.41E-05	6.70E-05	1.23E-03	7.33E-05	6.91E-03	4.42E-05	1.05E-04
07:18:26.5	39.89	108.97	1	9.78E-06	6.63E-05	5.72E-04	6.16E-05	8.73E-03	2.41E-05	9.27E-05
07:18:27.5	44.30	107.27	1	5.60E-06	5.00E-05	3.83E-04	4.62E-05	4.18E-03	2.74E-05	9.18E-05
07:25:52.5	34.82	120.88	1	2.86E-05	1.23E-04	2.11E-03	1.54E-04	1.80E-02	7.46E-05	3.03E-04
07:25:54.5	35.95	117.22	1	1.79E-05	1.10E-04	1.02E-03	9.00E-05	1.18E-02	5.56E-05	1.49E-04
07:25:57.5	37.56	116.65	1	1.32E-05	1.91E-04	3.87E-04	1.10E-04	6.71E-03	3.60E-05	8.01E-05
07:26:03.5	40.04	112.23	1	3.08E-05	3.43E-04	4.90E-04	1.52E-04	1.97E-03	1.01E-04	2.29E-04

Table 8.3. Data for calculating the amplitude -distance relationship. The hypocentral depth was set to 1m in order to avoid discontinuities. The velocities are given in (m/s).

In the calculation process, the study area was covered with a rectangular grid of $100x100$ grid points, where the grid size in the X-direction (East) is $1.845m$ and the Y-direction (North) is $2.306m$. Using the same process as before, the Back-Projection matrices are calculated for all stations before the location of the hits is performed. Figure 8.9 shows the BPM for stations 1 and 3.

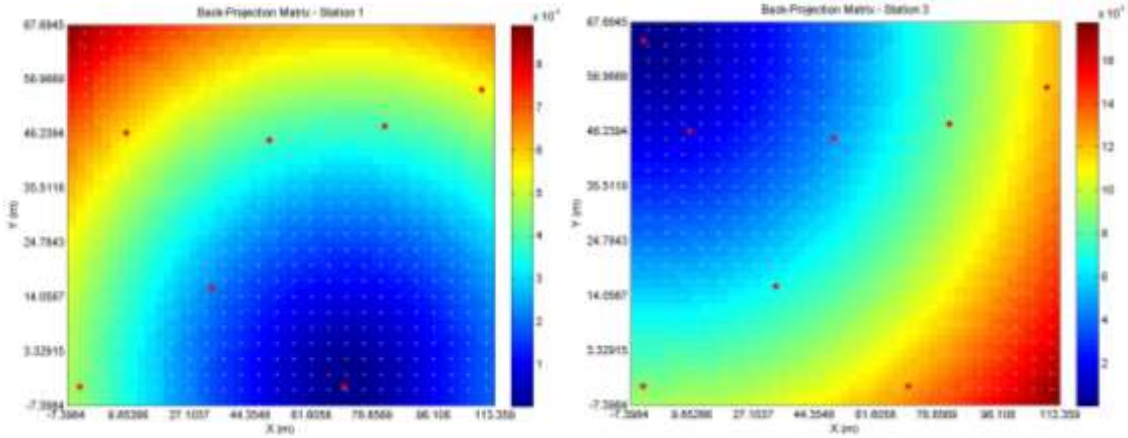

Figure 8.9. Back-Projection Matrices for stations 1 and 3. Please note the different scale in the color-bar.

Due to a possible singularity in the $\mathbf{log_{10}}(\boldsymbol{r_e^k})$ term, a hypocentral depth ($\boldsymbol{r_z}$) of 1m was established. In the case of a rock hitting the station directly, the

hypocentral depth was taken as zero, $\boldsymbol{r_e^k = 0}$ so a singularity in the logarithm function will be found.

The results of the ground motion model for the resultant velocity (V) are obtained using equation 6.5 and by solving the least square adjustment according to our new method.

pseudoMagnitude	*Station*	C^k	a
-8.06	St1	0.55	1.387
-8.00	St2	0.36	
-8.17	St3	-0.27	
-7.95	St4	0.05	
-8.18	St5	-0.03	
-8.09	St6	-0.17	
-8.24	St7	-0.49	
-8.34			
-8.13			
-8.24			
-8.37			
-7.75			
-7.95			
-8.08			
-7.90			

Table 8.4. Solution of the ground motion model for the Spitz quarry. First column: PseudoMagnitudes,; second column: Station correction; Third column: power-law factor.

The graph in figure 8.10 represents the correlation between the values logarithm in base 10 of the resultant maximum resultant vibration velocity observed at station $\boldsymbol{k}$ for every event used in the computation of the model, versus the calculated vibration velocity computed with the obtained empirical model. As we expected, a result with an almost 1:1 relationship was obtained.

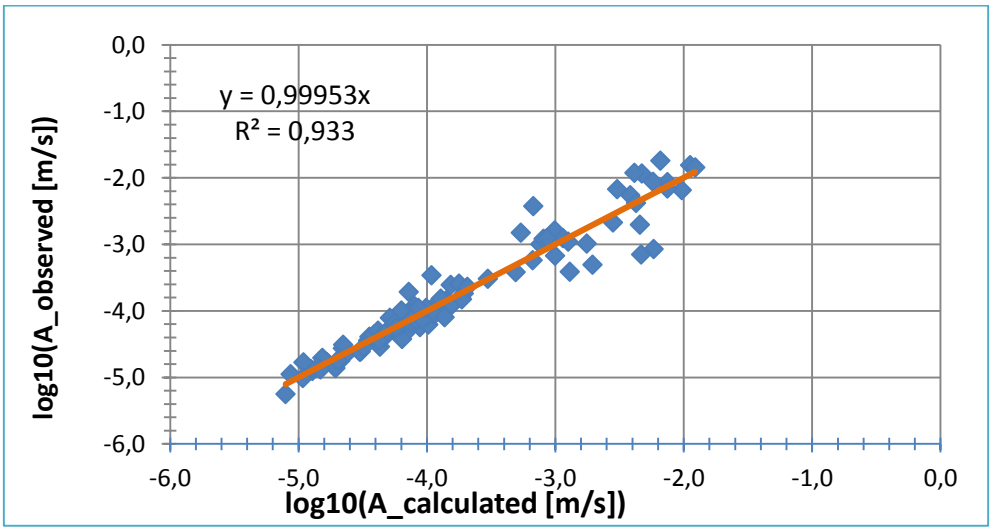

Figure 8.10. Correlation between the observed and the computed velocities.

Source MAP

The maximum pseudoMagnitude obtained by computing the minimum of all Back-Projection Amplitude Matrices, locates the rockfall impact.

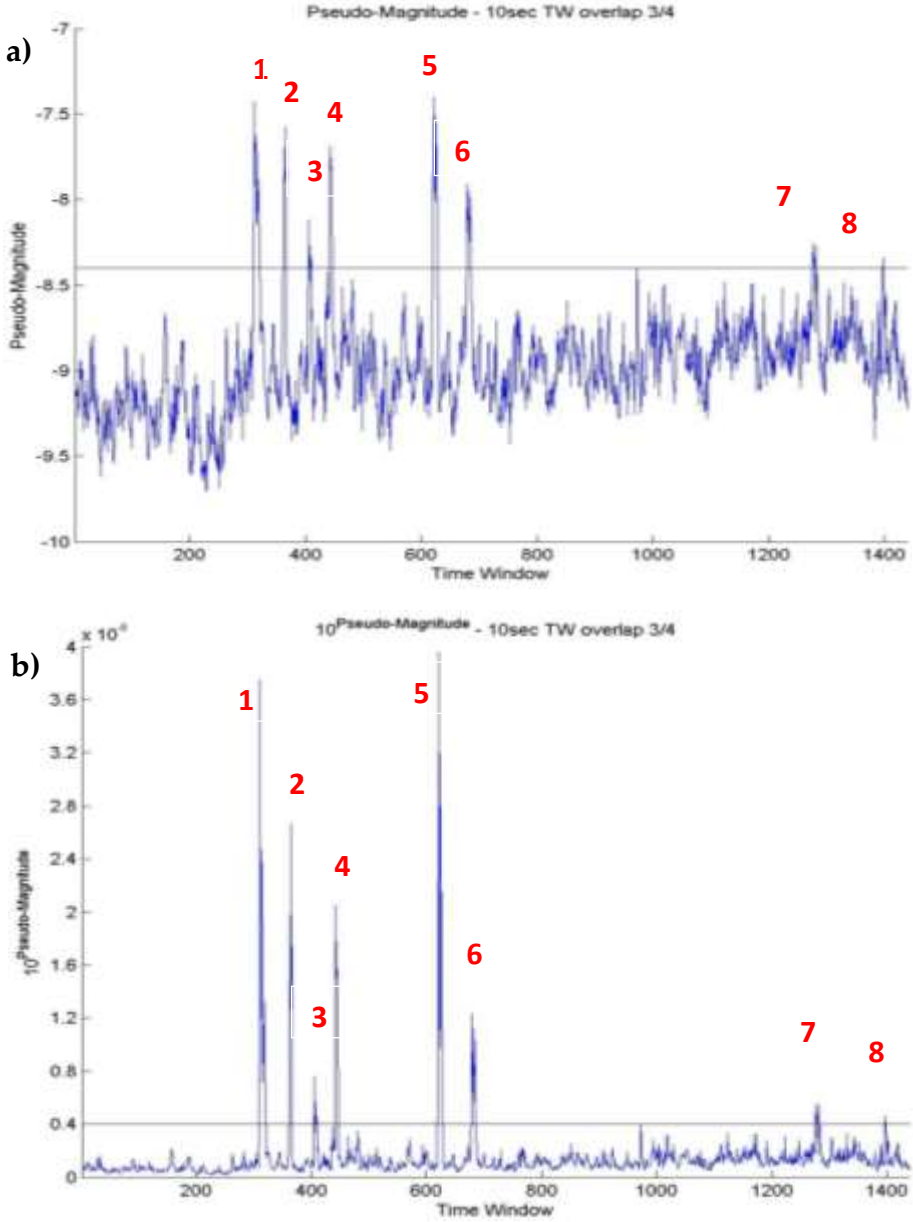

Figure 8.11. Maximum pseudo magnitudes for all time windows in a) logarithmic and; b) linear scaling. The events below the selected trigger threshold of $pseudoMagnitude = -8.4$ *will not be detected whereas the ones (1-8) will be detected by the warning system.*

After examining the results presented in Figure 8.11 and taking into account the noise level, which fluctuates around $pseudoMagnitude \sim -9$, a trigger threshold of $pseudoMgnitude = -8.4$ for a significant seismic event was selected. Eight events are above this threshold, the two strongest have a $pseudoMagnitude \sim -7.4$, an order of magnitude above the trigger threshold.

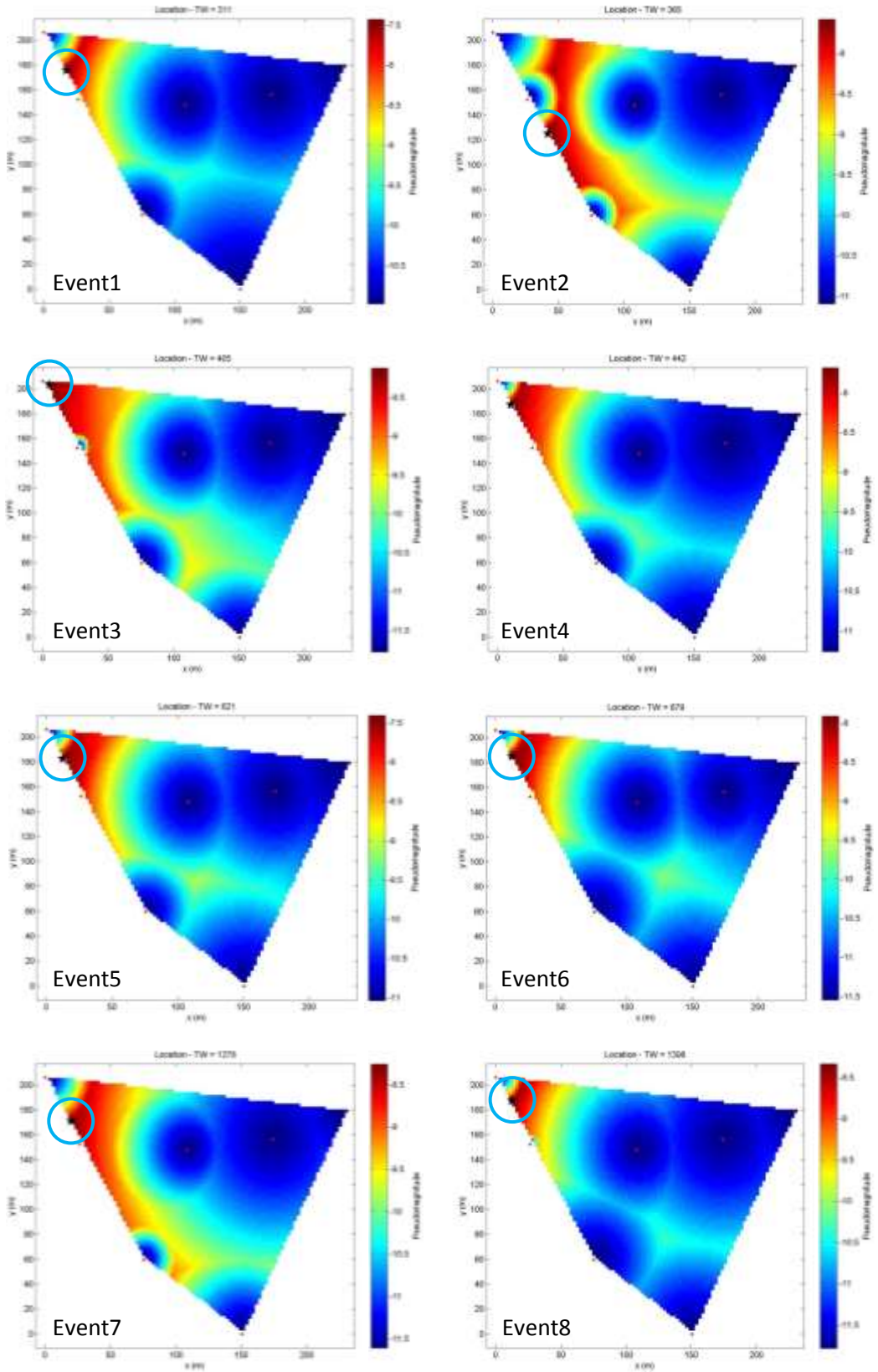

Figure 8.12. Spatial distribution of the pseudoMagnitudes of 8 events Time Windows over the trigger threshold; black stars within blue circles mark the maximum pseudoMagnitude.

Figure 8.12 shows the distribution of the PseudoMagnitude for the time windows and the location of the 8 detected events. Furthermore, it shows maxima only in the upper part of the quarry, the area in which the induced rockfalls were triggered or the strikes took place. The pseudoMagnitude of the selected events was significantly higher than the noise level and this combined with their successful location allows for an unambiguous assignment of these seismic events to the artificially released rockslides.

8.4 Terrestrial laser scanning survey

Due to partnership with the research group of photogrammetry at the Technische Universität Wien, Department of Geodesy and Geoinformation, and thanks to additional documentation of the rockfalls on the 2nd of October 2015 under the leadership of Dr. Andreas Roncat, , the rockfall loss was determined.

LIDAR (LIght Detection And Ranging) scanning technology can be used to measure small amounts of movement over large areas. LIDAR involves sending a laser pulse in a known direction and the distance is evaluated by measuring the return time of the pulse reflected by the ground surface. Scanning on a regular grid provides images of several million points. Many studies of falling rock phenomena using Terrestrial LiDAR, which we term Terrestrial laser scanning (TLS), have been realized with the intention of detecting volumetric changes along the slope after the occurrence of failures. With regards to the application of TLS monitoring on mountainous rock slopes, several authors have conducted research designed to detect rockfalls. [Royan et al, 2014]

TLS is a remote sensing technique capable of obtaining local images of the earth's 3D topography by acquiring point clouds of the ground position. The millimeter accuracy of the TLS data collection process in mines and quarries is based on sophisticated software algorithms for automatically registering images and analyzing small deformations (change detection) over time and over large fields.

For this purpose, a terrestrial laser scanning device (RIEGL VZ-2000 pulse laser scanner) and a camera (Nikon D800; 1920x1080 pixels, 30 frames/s) were also used (their location is presented in Figure 8.2), not only to draw the trajectories of the blocks of rock, but also to determine the volume of rock lost or gained in the different areas of the quarry.

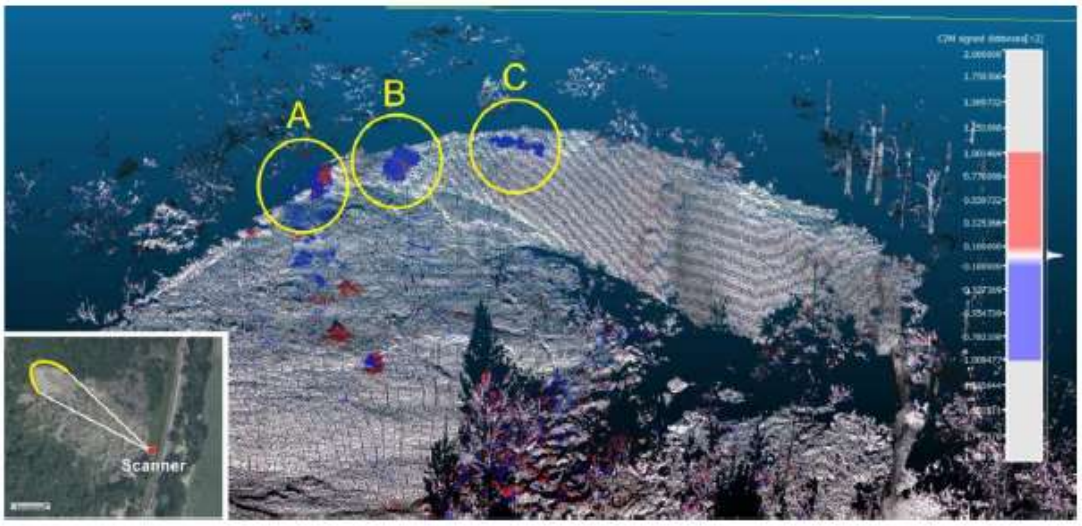

Figure 8.13. Laser Scanner difference measurement for determining the crash brought rock volume; the insert shows the location of the laser scanning - cut-out; yellow borders (A, B, C) show the outbreak areas of rockfalls.

By means of the RIEGL and the camera two measurements were taken, one before the rockfall experiments and the other one right after it. The data was processed with the RiScanProv2.1.1 software and the difference between the two images was computed. The outbreak areas of rockfalls are clearly visible in the laser scanning resultant image (Figure 8.13 Areas A, B and C). Between 09:00 to 10:00, the rockfalls were entirely induced from areas A and B and a total loss rock volume of about 2,4 m^3 (6,5 t) was released. Moreover, the crashed rock volume was estimated to be about 1,2m^3 for each of the areas.

Estimation of the rockfall volume from the pseudoMagnitude

Through the terrestrial laser scanner data, the lost (or gained) rock volume was determined for different areas of the quarry. This allowed us to relate the loss mass with the strength of the collision (pseudoMagnitude) of the rockfall, and draw and rebuild their associated trajectory. In the period from 9:00 to 10:00, rocks of around 2.4 m^3 or 6.5 $tons$, according to the results of the laser scanning measurements, with an assumed density of 2700 kg/m^3, were released from the areas A and B. Under the plausible assumption that the weight of each rockfall is proportional to $10^{pseudoM}$, we have:

$$Loss\ Mass = K \cdot 10^{pseudoM} \qquad (8.1)$$

Table 8.5 shows the hit masses of the rockfall. The constant K ($K = 4.2 \cdot 10^6\ t$) has been determined so that the sum of the calculated masses equals 6.5 t.

The maximum rockfall mass in the time interval 9:00 to 10:00 is thus 6.5 t, which corresponds approximately to the assessed value for the spot. Events with rockfall masses greater than $0.2\,t$ can be automatically detected with confidence. However, real-time analysis of the seismic data by an expert would substantially reduce the detection threshold.

Event	pseudo	Volume (m^3)	Mass (tons)
1	-7.4	0.60	1.70
2	-7.6	0.40	1.10
3	-8.1	0.10	0.30
4	-7.7	0.30	0.80
5	-7.4	0.60	1.70
6	-7.9	0.20	0.50
7	-8.3	0.10	0.20
8	-8.4	0.10	0.20
TOTAL	**-**	**2.4**	**6.50**

Table 8.5. Detected artificial rockfalls and assigned volume and masses according to equation 8.1.

These results allowed us to relate the lost mass with the strength of the hit (pseudoMagnitude) of the rockfall, since figure 8.14 shows a rather high correlation between them. As a threshold value, 0.1 *tons*, which was associated to a specific value of the pseudoMagnitude, was established in order to install an automatic and real time warning system.

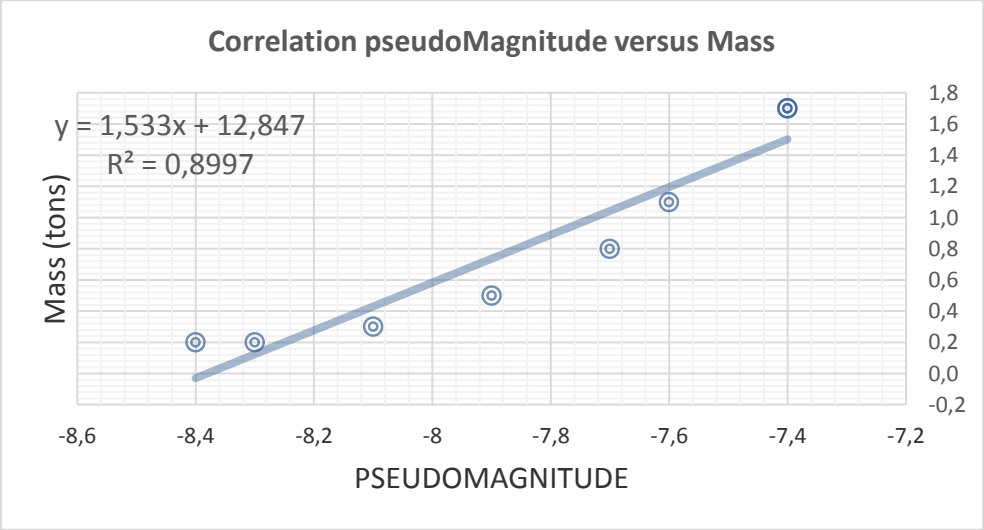

8.14. Correlation between the mass loss (tons) and the pseudoMagnitude related to that rockfall.

8.5 Analysis and evaluation of the earlier warning system

The existing seismic alert system comprised 3 seismic stations (see map Figure 2). Each of the three stations is equipped with a vibration meter from Walesch Vibras Electronic GmbH. These devices each had a 3-component geophone/seismometer with a natural frequency of 1Hz and a registration unit that digitized the analog data, pre-processed and stored it. If a trigger threshold was exceeded at a single seismic station, the alarm system was activated and a red traffic light was switched on.

For the period of March 2007 - August 2009, a total of 9363 events were provided for analysis. Based on previous experience and the information gained during the field trial on the 2nd of October 2015, the dominant signal frequencies due to possible rockfalls at a close range was selected to be between $10\,Hz$ and $200\,Hz$. Signals that cannot be linked to seismic events such as lightning, disturbances of electronics, etc. were eliminated based on the following criteria for the signal frequencies:

$$min(f_x, f_y, f_z) > 4Hz \qquad (8.2.a)$$

$$10Hz < max(f_x, f_y, f_z) < 250Hz \qquad (8.2.b)$$

$$max(f_x, f_y, f_z)/min(f_x, f_y, f_z) < 5Hz \qquad (8.2.c)$$

f_x, f_y, f_z are the maximum frequencies of the x- y- and z-component.

The data was thus reduced to 66 events (Table 8.6). The criterion is ascribed with a high probability to be a seismic source. Only once (June 26th, 2009) was an event recorded by more than one geophone. However, the relatively low registered frequencies (8 - 22Hz) are not expected to be caused by a rockfall.

On the 23rd of April 2007, rockfall tests were performed in the Spitz quarry from 09:00 until 16:00. After the supplementary analysis of the experiment recordings, they can be summarized as:

- 9:45 to 10:50: Operating geophone: 3; Artificial rockfalls $1 \times 2m^3$, $2 \times 1m^3$
- 10:40 to 11:50: Operating geophone: 2; Several artificial rockfalls $1m^3$ and $1 \times 2m^3$
- 12:00 to 12:15: Operating geophone: 1; Several artificial rockfalls of $1.5m^3$ and $1 \times 2m^3$
- 12:15 to 14:30: Operating geophone: 1; Nearly 100 rockfalls up to $3m^3$.

A total of 9 records, registered at a single station, can be correlated with an induced rockfall. An overview of these events is summarized in Table 8.7.

File	Geophon	Datum	TrigZeit	Vmax	Frq	Xmax	Ymax	Zmax	FX	FY	FZ
VI315235	2	15.03.2007	11:00:26	13,28	61	8,82	12,74	1,76	61	61	57
VI315236	2	15.03.2007	11:02:15	2,15	41	2	2	0,44	59	41	38
VI315238	2	15.03.2007	11:04:41	5,04	41	4,31	4,16	1,81	41	43	33
VI315240	2	15.03.2007	11:07:07	6,81	29	5,44	6,47	1,27	57	29	35
VI315241	2	15.03.2007	11:08:58	6,91	37	3,57	5,88	3,38	37	37	37
VI315242	2	15.03.2007	11:09:40	2,35	59	2,35	1,56	1,07	59	31	37
VI315246	2	15.03.2007	11:16:07	3,18	100	2,2	3,13	1,17	80	100	116
VI315247	2	15.03.2007	11:16:44	5,24	145	2,99	4,7	2,54	82	145	145
VI315248	2	15.03.2007	11:17:05	9,11	154	3,57	9,01	2,54	34	154	34
VI315249	2	15.03.2007	11:18:10	2,05	37	1,47	2	0,78	41	37	38
VI315250	2	15.03.2007	11:22:00	2,74	43	2,2	2,59	0,58	43	43	41
VI315251	2	15.03.2007	11:24:27	2,45	37	2,3	1,32	0,83	37	33	37
VI315252	2	15.03.2007	11:25:22	2,74	90	2,5	1,32	1,17	90	98	40
VI315253	2	15.03.2007	13:37:48	3,18	53	2,79	2,69	0,63	53	67	49
VI315254	2	15.03.2007	13:38:24	2,25	57	1,56	2,2	0,98	58	57	42
VI315255	2	15.03.2007	13:40:11	4,06	45	3,72	2,59	1,12	45	60	41
VI315256	2	15.03.2007	13:41:04	6,66	53	5,68	6,47	1,22	69	53	65
VI315257	2	15.03.2007	13:41:50	3,48	57	2,99	3,48	0,44	55	57	37
VI315258	2	15.03.2007	13:42:32	2,59	49	2,2	2,3	0,63	49	53	61
VI315259	2	15.03.2007	13:43:10	3,38	51	2,79	2,69	0,78	53	51	49
VI315261	2	15.03.2007	13:43:44	2,64	49	2	2,4	0,58	49	49	49
VI315263	2	15.03.2007	13:47:14	2,2	51	2,1	1,96	0,93	55	51	50
VI315264	2	15.03.2007	13:47:35	3,87	75	1,86	3,28	1,32	54	75	50
VI315265	2	15.03.2007	13:48:20	5,39	35	2,45	4,9	2,79	41	35	33
VI315266	2	15.03.2007	13:51:50	3,03	47	2,2	2,54	1,27	57	47	37
VI315267	2	15.03.2007	13:52:47	3,57	49	3,57	2,1	0,68	49	51	41
VI315269	3	15.03.2007	14:01:28	3,67	41	1,12	3,67	1,17	41	41	43
VI315270	3	15.03.2007	14:02:01	6,51	98	2,64	6,47	2,4	112	98	120
VI315271	3	15.03.2007	14:02:19	6,51	104	1,71	6,27	2,3	39	104	42
VI315272	3	15.03.2007	14:02:38	5,24	106	1,27	5,14	1,71	41	106	41
VI315273	3	15.03.2007	14:02:55	8,18	88	3,28	7,84	2,3	108	88	116
VI315274	3	15.03.2007	14:03:23	8,08	108	3,72	7,45	2,4	84	108	108
VI315275	3	15.03.2007	14:03:45	6,71	88	2,99	6,27	1,96	96	88	41
VI315276	3	15.03.2007	14:04:01	15,49	114	3,92	15,09	4,11	92	114	127
VI315278	3	15.03.2007	14:10:29	2,05	80	2,05	1,12	0,24	80	79	260
VI315279	3	15.03.2007	14:10:53	15,49	127	6,47	14,11	2,25	98	127	104
VI315280	3	15.03.2007	14:11:24	14,21	131	6,27	12,74	1,86	88	131	84
VI315282	3	15.03.2007	14:12:48	3,28	116	2,94	1,81	0,93	116	116	116
VI315283	3	15.03.2007	14:13:07	4,7	139	4,5	3,13	1,27	139	143	33
VI315284	3	15.03.2007	14:13:26	18,08	141	17,25	13,13	6,07	141	143	139
VI315285	3	15.03.2007	14:13:57	21,42	143	20,39	15,68	6,86	143	143	147
VI315290	3	15.03.2007	14:38:45	2,89	39	2,84	1,66	0,68	39	41	33
VI315291	3	15.03.2007	14:39:01	3,72	116	3,72	2,2	0,49	116	39	35
VI315297	3	15.03.2007	15:05:44	7,84	120	4,11	6,86	1,56	135	120	123
VI417304	2	17.04.2007	10:44:00	2,79	6	2	1,47	1,27	6	14	14
VI423315	3	23.04.2007	09:10:42	2,2	51	2,05	1,61	1,02	51	33	29
VI423316	3	23.04.2007	09:11:01	2,59	123	2,4	1,07	1,12	123	33	46
VI423320	2	23.04.2007	10:35:51	5,88	37	4,95	3,13	2,35	37	31	31
VI423321	2	23.04.2007	10:36:12	2,79	76	2,15	1,56	1,27	76	33	79
VI423323	2	23.04.2007	10:38:46	2,89	31	1,76	2,5	0,88	20	31	22
VI423324	2	23.04.2007	10:41:43	3,18	55	2,89	2,59	0,93	55	53	46
VI423325	2	23.04.2007	10:45:14	3,23	25	1,56	3,18	0,83	34	25	22
VI423326	1	23.04.2007	10:55:54	2,54	80	0,83	1,76	2,05	87	76	80
VI423327	1	23.04.2007	10:56:39	10,83	172	8,62	8,82	4,95	172	172	174
VI728554	2	28.07.2007	20:00:40	3,82	186	2,59	0,39	2,79	186	73	216
VI808678	2	08.08.2007	16:02:35	3,52	12	2,35	0,29	2,64	10	6	12
VI310692	3	10.03.2008	11:47:33	59,8	20	50	37,05	16,66	20	20	18
VI310693	1	10.03.2008	15:35:24	20,09	24	18,23	13,52	9,01	24	20	31
VI311703	3	11.03.2008	13:12:24	18,38	20	13,72	14,7	6,66	20	20	18
VI319704	3	19.03.2008	13:05:39	11,42	123	11,17	3,33	1,37	123	135	131
VIA29188	3	29.10.2008	10:05:07	7,89	125	3,92	7,05	1,07	171	125	174
VIA29191	3	29.10.2008	10:16:49	12,15	78	7,64	10,78	5,09	76	78	45
VIA29205	3	29.10.2008	12:44:01	11,12	116	9,41	10,19	3,28	116	147	198
VI626248	1	26.06.2009	01:03:44	7,15	22	4,21	3,82	5,53	8	16	22
VI626249	2	26.06.2009	01:03:44	12,69	20	9,01	5,29	7,25	20	14	22
VI802508	3	02.08.2009	19:20:23	11,91	12	8,43	5,68	6,27	12	12	12

Table 8.6. Existing Alarm System data. Seismic events corresponding to April 23, 2007. Data obtained during the rockfall experiments are highlighted in yellow, simultaneous records on more than one station are highlighted in red.

Time	Geophone	V (mm/s)	Frequency (Hz)	Distance (m)
10:10:42	3	2.2	51	9
10:11:01	3	2.59	123	8
11:35:51	2	5.88	37	5
11:36:12	2	2.79	76	8
11:38:46	2	2.89	31	8
11:41:43	2	3.18	55	7
11:45:14	2	3.23	25	7
11:55:54	1	2.54	80	8
11:56:39	1	10.83	172	3
Trigger	1,2,3	0.2	-	53

Table 8.7. Seismic data on the rockfall experiments on April 23, 2007; 5th column indicates distance to the possible source with $pseudoMagnitude = -8$*; last line shows the trigger value.*

The next step is to examine whether the observed velocity registered at a specific single station and the condition that the registered velocity must exceed the threshold $V = 0.2\,mm/s$ is compatible with a rock fall. Using the established triggering velocity at a single station, the "station rock hit" distance can be obtained according to equation (3.4). The distances are 7 m on average (Table 8.7, column 5), representing an impact of the rocks right below the cliff of the quarry and in the immediate vicinity of each geophone. According to the records of the field test, it can be assumed that the measuring system only responded to rockfalls with a $volume \geq 1m^3$. However, this does not exclude cases in which small rocks hit the immediate vicinity of a geophone, animal passing near the station or event workings taking place close to the geophones.

The question of why the trigger level ($V = 0.2\,mm/s$) was exceeded in the rockfall experiments only when the rock hit the immediately vicinity of the adjacent geophone is still left open. After the last row in Table 5, an event with $pseudoMagnitude = -8.0$, and the established trigger level of $V = 0.2\,mm/s$, an event should be located $53m$ far from the station. The actual distances between the geophones were $60m$ to $90m$. It is therefore plausible that the trigger level was never exceeded for the respective distant geophones.

After analysis of the unsatisfactory performance of the existing seismic alert system, the following two points can be made:

1) Exceeding the trigger levels at only one geophone was used as a basis for a warning system. Therefore, it was possible that small vibrations in the immediate vicinity of the geophone (e.g. movement of animals) resulted in a warning.

2) To differentiate a rockfall from a local event, recordings are needed at several locations in the quarry, e.g. the stations of network should be well distributed over the entire quarry. Moreover, when accounting for the station distribution of the previous alarm system, the trigger level would need to be several orders of magnitude below the 0.2 mm/s, or even better, the seismic data would need to be recorded continuously and with the utmost sensitivity and analyzed in real-time.

8.6 To avoid false alarms

In order to avoid false alarms, further evaluations of external factors in a rockfall can be done.

Local seismic disturbances

The amplitude-distance relationship makes it clear that every little vibration excitation can lead to arbitrarily large amplitudes, as long as the source is close enough to the seismic sensor. In many cases, an analysis of the waveform allows us to distinguish very local (micro-seismic network, distance from the source $< 10m$) eventsfrom those that occur at greater distances. However, for a real-time detection such analyzes are (at least currently) not reliable enough.

As previously discussed, for distinguishing a weak event close to a sensor, several seismic stations, or, even better, an entire seismic network, is required. A simple technique could could be to only trigger an alarm if, and only if, measurements at a certain number of stations exceed the trigger level (previously settled alarm system). However, a more meaningful and robust approach is proposed and described in section 5, since it simultaneously leads to the localization of the hits.

Transport, construction, etc.

Traffic can produce similar amplitudes of ground movement as the one for a rockfall, rockslides, etc. in our study area. An analysis of the waveform can in principle lead to discrimination of rockfall events. However, the localization of the seismic source is more suitable and robust for a warning system. Limitation arises from the fact that traffic, and similar sources such as work processes, can cause similar vibrations in the field leading to a warning. It may be assumed that such activities would in any case be monitored by direct observation.

Earthquakes

To estimate the vibration velocity in the quarry Spitz, which can be caused by earthquakes, we use the formula of local magnitude used by the ZAMG (Equation 8.3).

$$M_L = log_{10}(A) + 1.66log_{10}(D) - 0.304 \qquad (equation\ 8.3)$$

In this equation, A is the maximum amplitude of the vibration velocity in the horizontal components in the frequency range $1 - 10Hz$ $[nm/s]$ and D the epicentral-distance in degrees [°].Equation 8.3 is used for distances $10km$ - $100km$ over magnitudes 0 - 5 (Figure 8.15).

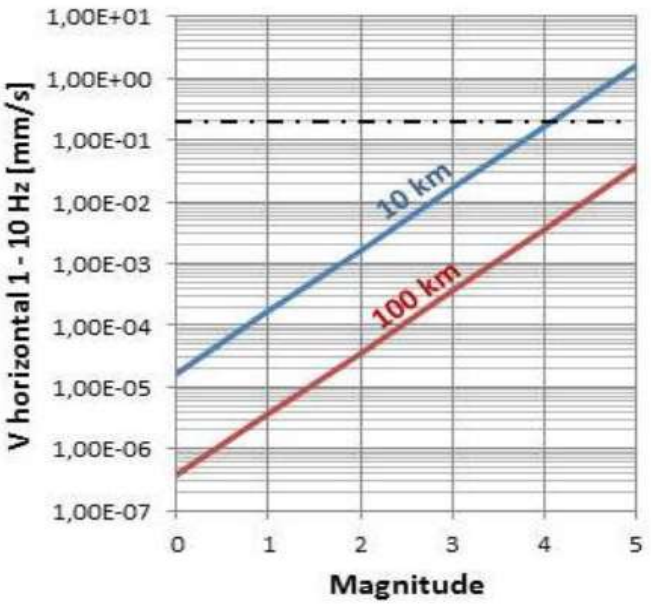

Figure 8.15. Maximum horizontal velocity in the frequency range $1 - 10Hz$ *for epicentral distances from* $10km$ *up to* $100km$*. The 0.2 mm/s value is represented by the dot black line.*

For the period 29th of March 2007 to 7th of July 2007, data from 27 earthquakes with epicenters in the immediate vicinity of the quarry Spitz were collected by the Geological Survey NÖLaReg. The local magnitudes were $1.3 \leq m_l \leq 1.9$.

From Figure 8.15, it follows that the resulting vibration velocities in the area of the Spitz quarry were at least two orders of magnitude below the trigger level of the existing system of $0.2\,mm/s$. However, it should be noted that the existing seismic warning system is based on the resulting vibration velocity in the entire frequency range of the seismic signals. Even if one takes this into account, the vibration velocities of seismic waves could not exceed this trigger level of $0.2\,mm/s$. Local earthquakes of $m_l < 4.0$ were easily defined as false alarms by the warning system.

The new seismic warning system uses the existing method looking at the entire frequency range of the seismic waves and the resultant wave velocity (equation 5.1). From figure 8.8, it can be seen that the noise level is approximately $0.02mm/s$. Therefore, it is expected that very local earthquakes with $m_l > 2.0$ and quakes from the Vienna Basin with $m_l > 3.5$ would exceed this level. Nevertheless, if an earthquake was registered, the amplitudes would increase uniformly in all the stations of the warning system. This would not be the case for a rock fall, in which the amplitude would not increase simultaneously at all stations. Taking this into consideration, a criterion, which usually prevents a false alarm due to earthquakes, can be established. However, it might be the case that perceptible earthquakes could also trigger the alarm system even if no rockfall was initiated.

Thunder

Strong sound sources in the atmosphere also stimulate seismic waves. A typical example is thunder. As with seismic waves, it would be expected that thunder should produce nearly identical signals for all stations and would be recognizable. But the inclusion of an additional noise monitoring station in the warning system proves to be more secure. In a diploma thesis from our Department (Mathias Steiner, 2015), it was shown that the ratio of the signal strengths of sound pressure and vibration velocity of the soil provide a reliable criterion for distinguishing seismic sources in the atmosphere without contact with the floor on or in the soil.

Lightning

Lightning can lead to induction in the seismic sensors, transmission and recording systems. These are at the same time at all stations, are very short and can be discarded. Together with the sound measurement station, an induction coil system that detects lightning could also be installed to exclude false alarms caused by lightning.

Electronics

Generally, responding to false alarms that could cause errors in the electronics is not possible here. However, it should be noted that modern and task adapted measurement systems should generally not provide cause for false alarms. In the data processing method proposed here however, it is necessary that "dead" traces, so non-functioning sensors - Recorder – and data transfers are recognized as such. The evaluation must include a test module.

9. *Conclusions*

In each of the studied cases, the method demonstrated efficient and reliable performance, however some aspects need supplementary investigation.

The method allows for fast determination of the location (epicenter) and magnitude (or pseudoMagnitude) of a seismic event located within a seismic network. Such an approach has two main advantages: firstly, being robust; and secondly, fast location estimates of the epicenter and local magnitude of a seismic event located within a seismic network. This is possible due to the procedure of obtaining and storing a Back-Projected Matrix (BPM), regardless of the registered amplitude, for each seismic station. As a direct consequence, we are able to save computational time for the calculation of the SourceMap. Care must be taken to ensure that no dead traces are involved in the processing.

The first results of the method applied to synthetic data verified that the method is very robust, even when outliers are present in the data. Application of the method with many stations and variable epicenter location showed variable results depending on network geometry.

According to the results presented in section 7, the [1-10Hz] band-pass filter was shown to provide better performance. As can be seen not only in the study with synthetic data but also in the ALPAACT network, the geometrical distribution of the network is a factor which requires further study. The method is strongly influenced by the geometry of the distribution of the stations in the network, and certainly also the number of available measuring stations.

The results presented for the Ebreichsdorf earthquake also show that a better performance of the network is achieved with the [1-10Hz] band-pass filter. In this event, a total number of 10 stations out of the 11 comprising the network were operative. The beneficial geometry together with the optimal position of the epicenter leads to satisfactory location of the earthquake. However, the local magnitude is slightly underestimated.

On balance, the potential of the method is shown in this section. However, further study on the geometrical network aspects is required. Furthermore, the detection matter needs additional investigation in order to be able to implement the method in real time.

The aim of the last section of this master's thesis was to determine the reasons why the previously installed seismic warning system had not been efficient enough to detect rockfalls. It was demonstrated that the deficiencies presented in the preceding warning system can be eliminated with an appropriated

seismic monitoring system and the corresponding evaluation of the results. The development of a real-time system was not included in the development of the new warning system, but it should, in principle, have the potential for such a development in the future in an economically acceptable manner.

For the period of March 2007 - August 2009, a total of 9363 characteristic events were recorded with the already existing alarm system. Based on the frequency content of the signals of most of these events, they could be attributed to non-seismic sources with a very high probability. 66 remaining events were selected for further analysis. Only once (on June 26, 2009) was an event recorded at more than one geophone.

On April 23, 2007, rockfall experiments were conducted to test the function of the existing measurement system. The alarm threshold of 0.2 mm/s was exceeded by 9 times the estimated value, which makes it such a suitable alarm system because, as shown, this threshold value is not compatible with medium rockfalls. However, larger rockfalls should have been detected by several measuring systems.

According to the data acquired using the existing measurement system, which was sensitive to rockfalls and simultaneously robust to false alarms, it was clear that the seismic warning system had to fulfill the following requirements:

- A continuous, seismological measuring system and appropriate criterion for defining a trigger threshold below 0.1 mm/s.
- If possible, a dense network in which stations are well spread out over the entire quarry.
- Further assessment for the recognition of local seismic disturbances that should not trigger a warning.
- Evaluation of the source location in order to discriminate false positives caused by traffic, industry or external causes.
- Special care must be taken when avoiding false alarms caused by earthquakes, thunder, lightning and electronic issues.

These requirements were fulfilled by the new monitoring seismic system tested on the 2nd of October 2015. Without going into detail about the method itself, it should be noted that rockfalls of an approximate size of 0.2tons were reliably detected. Furthermore, the efficient algorithms for detection and localization would allow the alarm system to be implemented in real time. However, this real time application has not yet been tested in the field, therefore further development would be required.

All in all, the location tests performed using induced rockfalls indicate that, with the deployed network and the developed location method, it is possible to provide a reliable estimate of the impact spots of the falling blocks as well as the strength of the collision. This allows us to define a robust alarm system, having

efficiently assigned a threshold value around 0.1 tons, and associating it with a specific value of the pseudoMagnitude according to the results of the field test. Even though the method has not yet been established in a real time system, the results presented in this thesis show an unquestionable potential for real time performance

To summarize, it has been seen that continuing research will provide a wealth of understanding about the influence of the geometrical distribution of the stations and the minimum number of stations required for optimal performance of the location method. Furthermore, the development of detection criteria for earthquake applications requires additional study in order to implement a real time system.

10 References

[1] *Brückl, Ewald., Weber, Robert., Apoloner, Maria-Theresia., Gottwald, Claudia., Mertl, Stefan., Möller, Groger., Schurr, Bernd., Umnig, Elke., Weginger, Stefan. ALPAACT - seismological and geodetic monitoring of ALpine-Pannonian. European Geosciences Union General Assembly 2013 Vienna, Austria. 07 – 12 April 2013.*

[2] *Hungr O, Evans SG, Bovis M, Hutchinson JN (2001) Review of the classification of landslides of the flow type. Environmental and Engineering Geoscience, VII, p.221-238.*

[3] *Deparis J, Jongmans D, Cotton F, Baillet L, Thouvenot F, Hantz D (2008) Analysis of rock-fall and rockfall avalanche seismograms in the French Alps. Bulletin of the Seismological Society of America 98 (4), p.1781-1796*

[4] *Brückl E, Brunner FK, Lang E, Mertl S, Müller M, Stary U (2013) The Gradenbach Observatory monitoring deep-seated gravitational slope deformation by geodetic, hydrological, and seismological methods. Landslides. doi: 10.1007/s10346-013-0417-1*

[5] *Kanamori H. (1993). Locating earthquakes with amplitude: application to real-time seismology. Bulletin of the Seismological Society of America, Vol. 83, No. 1, pp. 264-268.*

[6] *Udias, A. 1999. Principles of Seismology. UK. Cambridge University Press.*

[7] *Bormann, P. (Ed.). (2002) New manual of Seismological Observatory Practice (NMSOP)/IASPEI; editor, Peter Bormann- Postdam (Alemania): Geo-ForschungsZentrum.*

[8] *Wust-Bloch GH, Joswig M (2006). Pre-collapse identification of sink-holes in unconsolidated media at Dead Sea area by "Nanoseismic Monitoring" (graphical jackknife-location of weak sources by few, low-SNR records). Geophysical Journal International 167, p. 1220-1232.*

[9] *Hanks, TC, Kanamori H (1979). A moment magnitude scale. Journal of Geophysical Research, 84, 2348-50.*

[10] *Aki K, Richards PG (1980) Quantitative Seismology Theory and Methods, Vol 1, W.H. Freeman and Company, San Francisco, pp.557.*

[11] *Lowrie, W. (2007): Fundamentals of geophysics. UK. Cambridge University Press.*

[12] *Lay, T., Wallace, T. (1995): Modern global seismology, San Diego: Academic Press, Inc.*

[13] *Geiger, L. (1910). Herbsetimmung bei Erdbeben aus den Ankunfzeiten, K. Gessell. Wiss. Goett. 4, 331-349*

[14] *Moser TJ, Eck Tv, Nolet G (1992) Hypocenter determination in strongly heterogeneous earth model using the shortest path method. Journal of Geophysical Research, 97, p.6563-6572.*

[15] *Tarantola A, Valette B (1982) Inverse problems = quest for information. Journal of Geophysics, 50, p.159-170.*

[16] *Tarantola, A., 1987. Inverse problem theory: Methods for data fitting and model parameter estimation. Elsevier, Amsterdam, 613p*

[17] *Joswig M (2008) Nanoseismicmonitoring fills the gap between microseismic networks and passive seismic. First break 26, p.121-128.*

[18] *Brückl, Ewald. & Stefan Mertl. (2014). Monitoring and Predicting Acceleration and Deceleration of Large Landslides. Part of TU Wien. Final Report 2008 – 2013. ISBN-Online: 978-3-7001-7617-6 doi:10.1553/ISDR-24*

[19] *Kao, Honn and Shan, Shao-Ju. (2004) The Source-Scanning Algorithm: mapping the distribution of seismic sources in time and space. Geophys. J. Int. 157, 589–594. doi: 10.1111/j.1365-246X.2004.02276.x*

[20] *Gharti Hom, Nath, Volker Oye, Michael Roth, and Daniela Kühn. (2010). Automated microearthquake location using envelope stacking and robust global optimization. Geophysics, vol. 75, no. 4*

[21] Papí Isaba M, P. and E. Brückl. (2016) Robust method to detect and locate earthquakes by means of amplitude measurements. European Geosciences Union General Assembly 2016. (EGU 2016). Geophysical Research Abstracts. Vol. 18, ISSN: 1607-7962. EGU 2016-10354.

[22] *Brückl, Ewald., M. Puy Papí. (2016). Analyse und Weiterentwicklung des seismischen Steinschlag /Felssturz Alarmsystems im Bereich des Steinbruches Spitz. Bericht des Forschungsvertrag Report of the research contract. Technische Universität Wien Department für Geodäsie und Geoinformation, Forschungsgruppe Geophysik.*

[23] *Margrave, Gary F. (2003). Numerical Methods of Exploration Seismology with algorithms in MATLAB Department of Geology and Geophysics. The University of Calgary.*

[24] *Worboys, Michael F., Matt Duckham. (2004). GIS: A Computing Perspective, second edition. CRC Press.*

[25] *Rosenberger, A. (2009). Short note. Arrival-time order location revisited. Bull. Seism. Soc. Amer., 99, 2027-2034*

[26] *Brückl. E., Ch. Köberl, W. Lenhardt, S. Mertl, W. Rafeiner-Magor, A. Stark, G. Stickler, and R. Weber.(2015) Scientific goals of SCHOOLS & QUAKES. Geophysical Research Abstracts. Vol. 17, EGU2015-3401-4. EGU General Assembly 2015.*

[27] *Papí Isaba M, P., E. Brückl, A. Roncat, and J. Schweigl. (2016) Seismic monitoring of rockfalls at Spitz quarry (NÖ, Austria). European Geosciences Union General Assembly 2016. (EGU 2016). Geophysical Research Abstracts. Vol. 18, ISSN: 1607-7962. EGU 2016-9815.*

[28] *Mertl, S. (2015) Seismon software. Available at:*

http://www.stefanmertl.com/science/software/seismon/

[29] *Mertl, S. (2015) pSysmon software. Available at*

http://psysmon.mertl-research.at/doku.php

[30] *Royán, Manuel Jesus. Antonio Abellán. Michel Jaboyedoff. Joan Manuel Vilaplana. Jaume Calvet. (2014). Spatio-temporal analysis of rockfall pre-failure deformation using Terrestrial LiDAR. Landslides. DOI 10.1007/s10346-013-0442-0. Springer-Verlag Berlin Heidelberg.*

Web pages:

http://crack.seismo.unr.edu/feature/shakemapnews.html

http://www.stefanmertl.com/science/software/seismon/

http://psysmon.mertl-research.at/doku.php

List of Figures

Figure 2.1. Seismicity in Mur-Mürz fault (MM) and the Vienna Basin Fault (VBF)

Figure 2.2. Quarry area. Image provided by the Niederösterreich government. Red triangles show the positions where the seismic stations were placed.

Figure 4.1. Example of a local earthquake phases.

Figure 4.2. Wadati diagram. T_p is the P-wave arrival time; (T_s-T_p) is the difference in time of S and P arrival times.

Figure 4.3. Method of circles. The point where the three circles intersect is the epicenter of the earthquake.

Figure 4.4. Standard deviation map derived from Kanamori´s method. Ebreichsdorf earthquake (2013/09/20). The minimum standard deviation indicates the epicenter location.

Figure 5.1. Main steps of the localization method.

Figure 5.2. BPAM's array

Figure 5.3. Principle of the method. a) Stations without noise. b) Station 4 is noisy, however, the epicenter is still well determined making the method robust against outliers

Figure 5.4. Visibility between points x, y and z

Figure 5.5. Convex Hull of a point set (the points represent the stations).

Figure 5.6. Seismogram obtained by Sysmon and SourceMap of the Ebreichsdorf (20/09/2013) event. Black arrows indicate the maximum pseudoMagnitude. The yellow star shows the epicenter. a) Noise in the Time Window. b) Event enclosed by the Time Window.

Figure 6.1. Ricker pulse signal for a time step of 0.01 seconds, a dominant frequency of 10Hz and a seismogram length of 1.5 seconds.

Figure 6.2. a) Voronoi diagram, the sites correspond to the stations from which regions of influence are obtained. b) Voronoi diagram together with pseudoMagnitude values (colors).

Figure 6.3. Synthetic seismograms a) Wavelet without noise at each station. b) Noisy wavelet at each station.

Figure 6.4. Individual Back-Projection Matrices for the six stations used in the simulation.

Figure 6.5. Back-Projection Amplitude Matrices from each station individually to every grid point.

Figure 6.6. Location event: Step-by-step sequential procedure to determine epicentral and maximum pseudoMagnitude of an event.

Figure 6.7. SourceMap. a) Mask plus back ground are represented. b) Inner part of the convex hull.

Figure 6.8. Red: TW1. Orange: TW2. Yellow: TW3. Blue: TW4. Purple: TW5.

Figure 6.9. Localization using amplitudes of synthetic test data for different sliding time windows.

Figure 7.1. Site map of the ALPAACT seismic network.

Figure 7.2. Representation of the stations and seismic events in the study. Mercator projection.

Figure 7.3. Ebreichsdorf (20/09/2013; $m_l = 4.3$) event display with Seismon software.

Figure 7.4. Spherical coordinates

Figure 7.5. Measured velocity versus velocity obtained by the computed model. a) Band-pass filter 1-5Hz and b) Band-pass filter 1-10Hz

Figure 7.6. Stations corrections plotted as contour lines from a Krigin interpolation and stations symbols (stars) over the study area for band-pass filters, a) 1-5 Hz. b) 1-10 Hz.

Figure 7.7. Correlation of the obtained pseudoMagnitude with the local magnitude provided by ZAMG. a) Band-pass filter 1-5Hz; b) Band-pass filter 1-10Hz.

Figure 7.8. Events a) b) c) and d) Examples of epicenter location with low location error. The .5) and .10) of the labeling refers to the 1-5Hz and 1-10Hz band-pass filters respectively.

Figure 7.9. Histograms of the error in radial distance (km). a) 1-5Hz Band-pass filter. b) 1-10Hz Band-pass filter

Figure 7.10. Ebreichsdorf earthquake location.

Figure 7.11. SourceMap. a) 1-5 Hz Band-Pass Filter. b) 1-10 Hz Band-Pass Filter.

Figure 8.1. Seismic measurement system; a) components: 1 .Geophone + cable, 2. Battery, 3. GPS antenna + Cable, 4. Recorder; b) assembly in easy to transport and quickly installable systems.

Figure 8.2. Location of seismic stations (red triangles) in a Google Map; the position of the laser scanner and the film camera are indicated by the red rectangle; a white cross marks the origin of the local system; seismic stations of existing measurement system are labelled with G1, G2 and G3 (yellow circles).

Figure 8.3. Images of the stations location in the quarry of Spitz.

Figure 8.4. Mounting of the geophone directly on the rock of Station 4.

Figure 8.5. Triggering of rockfalls and rockslides on the top quarry area by the troops of the local construction management.

Figure 8.6. Zoom-in of the East component (HHE) first rockfall event from which distance - ground velocity relation is derived. The stations are ordered from top to bottom as previously explained

Figure 8.7. Seismograms, together with their spectrograms, for the 1 hour recording (7:00 -8: 00 UTC) resultant velocity for: a) HHE-component; b) HHN-component; c) HHH-component. Rectangles highlight the events chosen for computing the ground motion model.

Figure 8.8. Resulting vibration velocities in 10s time windows and 2.5s step in a) logarithmic and b) linear scale.

Figure 8.9. Back-Projection Matrices for stations 1 and 3. Please note the different scale in the color-bar.

Figure 8.10. Correlation between the observed and the computed velocities.

Figure 8.11. Maximum pseudo magnitudes for all time windows in a) logarithmic and; b) linear scaling. The events below the selected trigger threshold of $pseudoMagnitude = -8.4$ will not be detected whereas the ones (1-8) will be detected by the warning system.

Figure 8.12. Spatial distribution of the pseudoMagnitudes of 8 events Time Windows over the trigger threshold; black stars within blue circles mark the maximum pseudoMagnitude.

Figure 8.13. Laser Scanner difference measurement for determining the crash brought rock volume; the insert shows the location of the laser scanning - cut-out; yellow borders (A, B, C) show the outbreak areas of rockfalls.

Figure 8.14. Correlation between the mass loss (tons) and the pseudoMagnitude related to that rockfall.

Figure 8.15. Maximum horizontal velocity in the frequency range 1 – 10Hz for epicentral distances from 10km up to 100km. The 0.2 mm/s value is represented by the dot black line.

List of Tables

Table 6.1. Resultant velocity for the synthetic network stations.

Table 6.2. Theoretical epicenter coordinates and the ones obtained with the model.

Table 6.3. BPA values for each of the five time windows of figure 6.9.

Table 7.1. Locations of the ALPAACT network stations.

Table 7.2. Information on the analyzed events.

Table 7.3. Power-law factors for both of the band-pass filters.

Table 7.4. Obtained pseudoMagnitude from the two models corresponding to the two band-pass filters (1-5Hz and 1-10Hz).

Table 7.5. Computed pseudoMagnitude correction factors for the seismic stations of the ALPAACT network.

Table 7.6. Coordinates and error in the radial distance (d) of the events that lay inside the network. Band-pass filters 1-5Hz and 1-10Hz**.**

Table 7.7. Obtained magnitude for events lying inside the network and its relative error, where the value provided by the ZAMG was taken as the accepted value. 1-5Hz Band-pass filter.

Table 7.8. Obtained magnitude for events laying inside the network and its relative error, where the value provided by the ZAMG was taken as the accepted value. 1-10Hz Band-pass filter.

Table 7.9 Ebreichsdorf earthquake coordinates provided by the ZAMG and obtained by the two models.

Table 8.1. Equipment used during seismic monitoring campaign.

Table 8.2. Information of the seven stations used in the experiment. Station number, serial number of the recorder, number of channels and coordinates.

Table 8.3. Data for calculating the amplitude-distance relationship. The hypocentral depth was set to 1m in order to avoid discontinuities. The velocities are given in (m/s).

Table 8.4. Solution of the ground motion model for the Spitz quarry. First column: PseudoMagnitudes,; second column: Station correction; Third column: power-law factor.

Table 8.5. Detected artificial rockfalls and assigned volume and masses according to equation 8.1.

Table 8.6. Existing Alarm System data. Seismic events corresponding to April 23, 2007. Data obtained during the rockfall experiments are highlighted in yellow, simultaneous records on more than one station are highlighted in red.

Table 8.7. Seismic data on the rockfall experiments on April 23, 2007; 5th column indicates distance to the possible source with pseudoMagnitude $= -8$; last line shows the trigger value.

Source code

The source code was written in Matlab and is presented as a part of the master thesis.

The code was implemented in a simple way. However, improvements might be done in order to improve the efficiency of the code. In case of a real-time used the code should be change accordingly to the needs of the user and its application.

Common functions

Distance in geographic coordinates

```
%% Distance in geographic coordinates
function [dist_degrees, dist_meters] = dist_geog_coord(long, lat, long_epi,
lat_epi)
% The input parameters must be given in degrees
R = 6.371e6;        % Earth radius (m)

% Let long and lat be the longitude and latitude for the stations (or grid
points) and
% long_epi and lat_epi the longitude and the latitude for the epicenter (or
one specific point)

% "non-prime" letters refer to St. parameters while "prime" to the
epicenter
A = sind(90-lat).*cosd(long);
A_prime = sind(90-lat_epi).*cosd(long_epi);
B = sind(90-lat).*sind(long);
B_prime = sind(90-lat_epi).*sind(long_epi);
C = cosd(90-lat);
C_prime = cosd(90-lat_epi);

% distance to the picentre, not taking into account the depth
dist_degrees_epi = acosd(A.*A_prime + B.*B_prime + C.*C_prime);

% depths  --> average of 9km depth --> in degrees
depth = 360*9000/(2*pi*R);

dist_degrees = sqrt(dist_degrees_epi.^2 + depth.^2);
dist_meters = sqrt((dist_degrees.*2*pi*R./360).^2+(9000)^2);
```

Resultant Velocity. Note: the "10HZ"-construction must be changed all over the code when using the 5Hz Band-Pass filter y "5Hz" for ALPAACT and nothing for Spitz.

```
close all; clear all; clc;
%% Loading the ALL the data
% % data = load(input('Please load the txt file with all the data (between
comas): '));
data = load('data_10Hz.txt');
% 1.column --> Longitude St (°)            2.column --> Latitude St (°)
% 3.column --> Longitude Epicentre (°)     4.column --> Latitude Epicentre
(°)
% 5.column --> HHZmax(m/s)                 6.column --> HHZmin(m/s)
% 7.column --> HHNmax(m/s)                 8.column --> HHNmin(m/s)
% 9.column --> HHEmax(m/s)                 10.column --> HHEmin(m/s)
long_St = data(:,1);          lat_St = data(:,2);
long_epi = data(:,3);         lat_epi = data(:,4);
HHZmax = data(:,5);           HHZmin = data(:,6);
HHNmax = data(:,7);           HHNmin = data(:,8);
HHEmax = data(:,9);           HHEmin = data(:,10);
```

```
% Difference between the components
HHZ_diff = HHZmax - HHZmin;
HHN_diff = HHNmax - HHNmin;
HHE_diff = HHEmax - HHEmin;
% Resultant
resultant_max = sqrt(HHZ_diff.^2 + HHN_diff.^2 + HHE_diff.^2);

%% Distance from the epicentre to the stations
[epi_dist_deg,epi_dist_m] = dist_geog_coord(long_St, lat_St, long_epi,
lat_epi);  % Epicentral distance in DEGREES and METERS

non_log = [epi_dist_deg,epi_dist_m,resultant_max];
save('DistHipoDegree_DistHipoMeter_Amplitude.txt','non_log','-ASCII', '-
tabs')

Log = [log10(epi_dist_deg),log10(epi_dist_m),log10(resultant_max)];
save('LOG_DistHipoDegree_DistHipoMeter_Amplitude.txt','Log','-ASCII', '-
tabs')
```

ALPAACT network codes

Least Square Adjustment, ALPAACT network:

```
close all; clear all; clc;

%% Loading the DESING MATRIX (A)
% % data = load(input('Please load the txt file with all the data (between
comas): '));

% Desing matrix A for all events
desing = load('Desing_Matrix_A_all_events_10Hz.txt');
A = desing(:,:);

%% Loading the OBSERVATIONS VECTOR (l) - Maximum of the amplitude (m/s)
% % obs = load(input('Please load the txt file with all the data (between
comas): '));
obs = load('observations_10Hz.txt');
l = obs(:,:);

%% Loading the MAGNITUDES obtained from the ZAMG
% % mag = load(input('Please load the txt file with all the data (between
comas): '));

% Magnitude for all events
mag = load('mag_used_events.txt');
M = mag(:,:);


%% The least square solution ==> x = (At * P * A)^(-1) * At * P * l
x = inv(A'*A)*A'*l;

%% Magnitudes, "a" coefficient and correction coefficient
X = x(1:length(x)-1);    % X == Pseudomagnitude
a = x(length(x));        % the last coeff. of the least squate solution is
the "a" coeff.
mean_X = mean(X);

epi_dist = A(:,size(A,2));
mag_zamg = exp(M);
```

Back-Projection Matrices (BPMs) ALPAACT network: please note that, depending on the Band-Pass filter applied, the 10Hz should be changed to 5Hz.

```
%% BACK PROJECTION MATRICES
clear all, clc
% A file with the coordinates if the stations is needed:
% 'St_coord_all txt'
St_coord = load('Stations_coord_all.txt');
% 1.column --> Longitude (°)
% 2.column --> Latitude (°)
long = St_coord(:,1);
lat = St_coord(:,2);

% Names of the used stations
Stations = ['ALBA'; 'ARSA'; 'BISA';'CONA'; 'CSNA'; 'GILA'; 'GUWA';
'MARA';'PUBA'; 'SITA'; 'SOP '];

% A file with the coordinates if the stations is needed
% 'Stations_corr_all.txt'
St_corr = load('Stations_corr_all.txt');

% The area is defined by latitudes(47°,48.6°) and longitides(15°, 17.5°)
long_grid = linspace(15, 17, 50);
lat_grid = linspace(47, 48.6, 50);

%% Computation of the coordinates for X and Y
[X_long_grid,Y_lat_grid] = meshgrid(long_grid,lat_grid);

%% Calculation of the back-projection amplitude factor for each station
% A_BP_factor will afterward be multiplied by the maximum amplitude
% measured at each station

% A file with the calculated attenuation factor is needed
% 'Stations_corr_all.txt'
St_corr = load(Attenuation_fac.txt');

%% Distance from the stations to all grid points
for j = 1:length(long)
    [d_grid_deg(:,:,j), d_grid_m(:,:,j)] = dist_geog_coord(X_long_grid,
Y_lat_grid, long(j,1), lat(j,1));   % distance in degrees and meters

    % Back Projected Amplitude from the stations to all grid points
    A_BP_factor(:,:,j) = (d_grid_deg(:,:,j).^a)./10^St_corr(j);
    save(['back_projected_factor_10Hz_', Stations(j,:),'.txt'], '-ASCII',
'-tabs')
% plot back-projected factor for each station
    figure(j)
%     contour(X_long_grid,Y_lat_grid,A_BP_factor(:,:,j),50);
    pcolor(X_long_grid,Y_lat_grid,A_BP_factor(:,:,j));
    hold on
    St = plot(long(j,1), lat(j,1),'o', 'Color', [0 0 1], 'MarkerFaceColor',
[0 0 1], 'MarkerSize', 6);
    title(['Back-projected factor for 10Hz filtering of ' Stations(j,:)])
    xlabel('longitude (°)')
    ylabel('latitude (°)')
%     legend([St],Stations(j,:))
    colorbar
    for ii = 1:length(lat_grid)
        plot(X_long_grid(ii,:),Y_lat_grid(ii,:), '.', 'Color', [0.8 0.8
0.8], 'MarkerSize', 3)
        xlim([min(long_grid) max(long_grid)]); ylim([min(lat_grid)
max(lat_grid)]);
    end
    hold off
    saveas(figure(j), strcat('surf_10Hz_',Stations(j,:),'.jpg'));
end
```

SourceMap ALPAACT network:

```
% function source_map
 close all; clear all; clc;

%% Loading the data
str = input('Please load the DATE of the event (date between single quotes)
');

% % % % St_coord = load(input('Please load the stations LOCATION data (name
between comas) '));
St_coord = load(strcat('St_coord_',str,'.txt'));
% Usually the file will be called: 'St_coord_"date of the event".txt'
% 1.column --> Longitude (°)
% 2.column --> Latitude (°)
long = St_coord(:,1);
lat = St_coord(:,2);

% % % % St_ampli_dist = load(input('Please load the stations CORRECTED
AMPLITUDE data (name between comas) '));
St_ampli_dist = load(strcat('ResultantA_',str,'.txt'));
% Usually the file will be called: 'velocities_"date of the event".txt'
% 1.column --> Resultant amplitude (m/s)
result_A = St_ampli_dist(:,1);


% % % % epi_data = load(input('Please load the EPICENTRE data (name between
comas) '));
epi_data = load(strcat('epicentre_', str,'.txt'));
% Usually the file will be called: 'epicentre_"date of the event".txt'
% 1.column --> Longitude (°)
% 2.column --> Latitude (°)
long_epi = epi_data(1,1);       lat_epi = epi_data(1,2);

% % % %
% Station corrections
St_corr = load(strcat('St_corr_', str,'.txt'));

tic
%% &&&&&&&&&&&& GRID witht he coordinates &&&&&&&&&&&&
% The area is defined by maximum and minimum latitudes and longitides of
% each event
long_grid = linspace(min(min(long),long_epi)-0.05,
max(max(long),long_epi)+0.05, 100);
lat_grid = linspace(min(min(lat),lat_epi)-0.05, max(max(lat),lat_epi)+0.05,
100);

%% I compute the coordinates for X and Y
[X_long_grid,Y_lat_grid] = meshgrid(long_grid,lat_grid);

% A file with the calculated attenuation factor is needed
% 'Stations_corr_all.txt'
a = load(Attenuation_fac.txt');

%% Distance from the stations to all grid points
for ii = 1:length(long)
    [d_grid_deg(:,:,ii), d_grid_m(:,:,ii)] =
dist_geog_coord_2016_04_12_Lat(X_long_grid, Y_lat_grid, long(ii,1),
lat(ii,1));   % distance in degrees and meters

% A file with the calculated attenuation factor is needed
% 'Stations_corr_all.txt'
a = load(Attenuation_fac.txt');

%% Distance from the stations to all grid points
for ii = 1:length(long)
```

```
    [d_grid_deg(:,:,ii), d_grid_m(:,:,ii)] =
dist_geog_coord_2016_04_12_Lat(X_long_grid, Y_lat_grid, long(ii,1),
lat(ii,1));   % distance in degrees and meters

    % Back Projected Amplitude from the stations to all grid points
    Pseudomag_10(:,:,ii) =
(10.^St_corr(ii)).*result_A(ii,1)./(d_grid_deg(:,:,ii).^f);
    Pseudo_Mag (:,:,ii) = log10(result_A(ii,1)) -
(f*log10(d_grid_deg(:,:,ii))) + St_corr(ii);
end

%% Resultant Log10(pseudo-mag), Pseudo-mag & Real mag.
Pseudomag_10_min = Pseudomag_10(:,:,1);   % initial value for the log of
the pseudo-magnitude
Pseudo_Mag_min = Pseudo_Mag(:,:,1);      % initial value for the pseudo-
magnitude
for j = 1:(length(long)-1)
    Pseudomag_10_min = min(Pseudomag_10_min, Pseudomag_10(:,:,j+1));
    Pseudo_Mag_min = min(Pseudo_Mag_min, Pseudo_Mag(:,:,j+1));
end
Real_mag  = 0.8605749374.*Pseudo_Mag_min + 7.2690111093;  % Real magnitude
of the source

%%%% PCOLOR Log(Pseudomag) - REAL SCALE
figure(3)
% For the color bar
maxbar = max(max(Pseudomag_10_min)); minbar = min(min(Pseudomag_10_min));
barbar = (maxbar - minbar)/6;   % in order to have 6 mark lines in the
colorbar
for jj = 1:7;
    CB1(jj) = minbar+(jj-1)*barbar;   % log10(pseudomag)
end
CB = 0.8605749374*(log10(CB1)) + 7.2690111093;   % Scaled to Real magnitude
cbar = colorbar;
set(cbar, 'YTickLabel', {CB(1,1) CB(1,2) CB(1,3) CB(1,4) CB(1,5) CB(1,6)
CB(1,7)});
hold on
pcolor(X_long_grid,Y_lat_grid,Pseudomag_10_min);
hold on
% % I plot the STATIONS  [RGB]
for i = 1:length(lat_grid)
    plot(X_long_grid(i,:),Y_lat_grid(i,:), '.', 'Color', [0.8 0.8 0.8],
'MarkerSize', 2)
    xlim([min(long_grid) max(long_grid)]); ylim([min(lat_grid)
max(lat_grid)]);
    hold on
end
% % I plot the STATIONS  [RGB]
for k = 1:length(long)
    hold on,
    h(k)=plot(long(k), lat(k),'o', 'Color', [0 0 1], 'MarkerFaceColor', [0
0 1], 'MarkerSize', 5);
    % I locate the EPICENTRE in the grid with a point
    Epi=plot(long_epi, lat_epi,'p', 'Color', [0 1 0], 'MarkerFaceColor', [0
1 0], 'MarkerSize', 8);
    % legend
    title(['Source map - 10^{m_L} - ', str(1,1:4) '/',  str(1,6:7) '/',
str(1,9:10)])
    xlabel('longitude (°)'),    ylabel('latitude (°)')
%     legend([h(k) Epi],'ARSA','BISA', 'CONA', 'CSNA', 'GILA', 'GUWA',
'MARA', 'PUBA', 'SITA', 'SOP','Epicentre')
end
```

```
%% &&&&&&&&&&&      CONVEX HULL MASK      &&&&&&&&&&&
% convex Hull
CH = convhull(long,lat, 'simplify', false);
% closest value to find --> St cood.
for kk = 1:length(CH);
    val_lat = lat(CH(kk));
    val_long = long(CH(kk));

    tmp_lat = abs(lat_grid - val_lat);
    tmp_long = abs(long_grid - val_long);

    [IDx_lat, IDy_lat] = min(tmp_lat);
    [IDx_long, IDy_long] = min(tmp_long);

    ID_lat_mask(kk) = IDy_lat;
    ID_long_mask(kk) = IDy_long;
end

% % % Pseudo Magnitude - Real Scale - Convex Hull
mask_in = poly2mask(ID_long_mask,ID_lat_mask, length(long_grid),
length(lat_grid));
Pseudo_mag10_mask = Pseudomag_10_min.*mask_in;
Pseudo_mag10_mask(Pseudo_mag10_mask == 0)=NaN;

Real_mag_mask = Real_mag.*mask_in;
Real_mag_mask(Real_mag_mask == 0)=NaN;

Pseudo_mag_mask = Pseudo_Mag_min.*mask_in;
Pseudo_mag_mask(Pseudo_mag_mask == 0)=NaN;

%% PLOTS %%
%% PLOT SOURCE-MAP 10^Pseudomagnitude
figure(5)
p5 = pcolor(X_long_grid,Y_lat_grid, Pseudo_mag10_mask);

set(p5, 'EdgeColor', 'none');
ratio = [2,1,1];
pbaspect(ratio)
hold on
c5 = colorbar;
ylabel(c5,'10^{Pseudomagnitude}')
% grid points
plot(X_long_grid(1:20:end,1:20:end),Y_lat_grid(1:20:end,1:20:end), '.',
'Color', [0.8 0.8 0.8], 'MarkerSize', 2)
xlim([min(min(X_long_grid)) max(max(X_long_grid))]);
ylim([min(min(Y_lat_grid)) max(max(Y_lat_grid))]);
% Stations
St = plot(long(:,:),lat(:,:), 'o', 'MarkerFaceColor', [1 0 0],
'MarkerSize', 3);
% Epicenter
epi=plot(long_epi, lat_epi,'p', 'Color', [0 0 0], 'MarkerFaceColor', [0 1
0], 'MarkerSize', 8);
xlabel('x (km)'),    ylabel('y (km)')
legend([St,epi], 'Stations', 'Epicenter', 'Location', 'NorthWest')
title(['SourceMap - ',  str(1,1:4), '/',  str(1,6:7), '/',  str(1,9:10)])
hold off
saveas(figure(5), strcat('SourceMap_PseudoMag_CH_', str, '.jpg'));

%% POSITION OF THE MAXIMUM AND VALUE
[num idx] = max(Pseudo_mag10_mask(:));
[Epi_y Epi_x] = ind2sub(size(Pseudo_mag10_mask),idx);
MaxPM = Pseudo_mag10_mask(Epi_x, Epi_y);
Long_Epi = long_grid(Epi_x);
Lat_Epi = lat_grid(Epi_y);
```

Source code

```
% format long e
MODEL = [Long_Epi Lat_Epi MaxPM];
fileID = fopen(strcat('MODEL_Results_10Hz_',str,'.txt'),'w');
fprintf(fileID,'%10.15f\r\n',MODEL);
fclose(fileID);

%% PLOT SOURCE-MAP 10^Pseudomagnitude MASK
figure(7)
p7 = pcolor(X_long_grid,Y_lat_grid, Pseudo_mag10_mask);

set(p7, 'EdgeColor', 'none');
% contour(X, Y, BP_A_min_mask, 50);
ratio = [2,1,1];
pbaspect(ratio)
hold on
c7 = colorbar;
ylabel(c7,'10^{Pseudomagnitude}')

p7 = pcolor(X_long_grid,Y_lat_grid, Pseudomag_10_min);
set(p7, 'EdgeColor', 'none');
alpha(p7, 0.5);
toc;
```

Spitz network codes

Least Square Adjustment, Spitz network:

```
close all; clear all; clc;

%% Loading the DESING MATRIX (A)
% % data = load(input('Please load the txt file with all the data (between
comas): '));

% Desing matrix A for all events
desing = load('Desing_Matrix_A_a_fixed_161.txt');
A = desing(:,:);

%% Loading the OBSERVATIONS VECTOR (l) - Maximum of the amplitude (m/s)
% % obs = load(input('Please load the txt file with all the data (between
comas): '));
obs = load('observations_a_fixed_161.txt');
l = obs(:,:);

%% The least square solution ==> x = (At * P * A)^(-1) * At * P * l
x = inv(A'*A)*A'*l;

%% Magnitudes, "a" coefficient and correction coefficient
X = x(1:length(x)-1);    % X == Pseudomagnitude
a = x(length(x));        % the last coeff. of the least squate solution is
the "a" coeff.
mean_X = mean(X);

epi_dist = A(:,size(A,2));
```

Spectograms.

```
%% SPITZ - 1hour data
close all, clear all, clc
tic, format long;
t = (7:0.002/3600:8-0.002/3600)';    % f = 500Hz, sample-rate = 0.002 sec
                                     % 3600sec*500Hz = 1 800 000
%% Import the data
% % St. 1
St1_A00D_HHE = importdata('Spitz_Stei_A00D_04_HHE_2015-10-
02T070000.ascii',' ');
St1_A00D_HHN = importdata('Spitz_Stei_A00D_04_HHN_2015-10-
02T070000.ascii',' ');
St1_A00D_HHZ = importdata('Spitz_Stei_A00D_04_HHZ_2015-10-
02T070000.ascii',' ');
A1_A00D_HHE = St1_A00D_HHE.data(1:1800000);
A1_A00D_HHN = St1_A00D_HHN.data;
A1_A00D_HHZ = St1_A00D_HHZ.data;

% % St. 2
St2_B4CC_HHE = importdata('Spitz_Stei_B4CC_05_HHE_2015-10-
02T070000.ascii',' ');
St2_B4CC_HHN = importdata('Spitz_Stei_B4CC_05_HHN_2015-10-
02T070000.ascii',' ');
St2_B4CC_HHZ = importdata('Spitz_Stei_B4CC_05_HHZ_2015-10-
02T070000.ascii',' ');
A2_B4CC_HHE = St2_B4CC_HHE.data;
A2_B4CC_HHN = St2_B4CC_HHN.data;
A2_B4CC_HHZ = St2_B4CC_HHZ.data;

% % St. 3
St3_B32F_HHE = importdata('Spitz_Stei_B32F_01_HHE_2015-10-
02T070000.ascii',' ');
St3_B32F_HHN = importdata('Spitz_Stei_B32F_01_HHN_2015-10-
02T070000.ascii',' ');
St3_B32F_HHZ = importdata('Spitz_Stei_B32F_01_HHZ_2015-10-
02T070000.ascii',' ');
A3_B32F_HHE = St3_B32F_HHE.data;
A3_B32F_HHN = St3_B32F_HHN.data;
A3_B32F_HHZ = St3_B32F_HHZ.data;

% % St. 4
St4_9898_HHE = importdata('Spitz_Stei_9898_02_HHE_2015-10-
02T070000.ascii',' ');
St4_9898_HHN = importdata('Spitz_Stei_9898_02_HHN_2015-10-
02T070000.ascii',' ');
St4_9898_HHZ = importdata('Spitz_Stei_9898_02_HHZ_2015-10-
02T070000.ascii',' ');
A4_9898_HHE = St4_9898_HHE.data;
A4_9898_HHN = St4_9898_HHN.data;
A4_9898_HHZ = St4_9898_HHZ.data;

% % St. 5
St5_B4C6_HHE = importdata('Spitz_Stei_B4C6_06_HHE_2015-10-
02T070000.ascii',' ');
St5_B4C6_HHN = importdata('Spitz_Stei_B4C6_06_HHN_2015-10-
02T070000.ascii',' ');
St5_B4C6_HHZ = importdata('Spitz_Stei_B4C6_06_HHZ_2015-10-
02T070000.ascii',' ');
A5_B4C6_HHE = St5_B4C6_HHE.data;
A5_B4C6_HHN = St5_B4C6_HHN.data;
A5_B4C6_HHZ = St5_B4C6_HHZ.data;

% % St. 6
St6_A04C_HHE = importdata('Spitz_Stei_A04C_07_HHE_2015-10-
02T070000.ascii',' ');
```

Source code

```
St6_A04C_HHN = importdata('Spitz_Stei_A04C_07_HHN_2015-10-
02T070000.ascii',' ');
St6_A04C_HHZ = importdata('Spitz_Stei_A04C_07_HHZ_2015-10-
02T070000.ascii',' ');
A6_A04C_HHE = St6_A04C_HHE.data;
A6_A04C_HHN = St6_A04C_HHN.data;
A6_A04C_HHZ = St6_A04C_HHZ.data;

% % St. 7
St7_9882_HHE = importdata('Spitz_Stei_9882_03_HHE_2015-10-
02T070000.ascii',' ');
St7_9882_HHN = importdata('Spitz_Stei_9882_03_HHN_2015-10-
02T070000.ascii',' ');
St7_9882_HHZ = importdata('Spitz_Stei_9882_03_HHZ_2015-10-
02T070000.ascii',' ');
A7_9882_HHE = St7_9882_HHE.data;
A7_9882_HHN = St7_9882_HHN.data;
A7_9882_HHZ = St7_9882_HHZ.data;

%% specgrams plots
%%% PLOT Z COMPONENT SEISMOGRAM TRACE + specgram
figure(1)
subplot(6,1,1), plot(t,A1_A00D_HHZ,'b'), %xlim([min(t8)-30, max(t8)+30])
ylim([min(A1_A00D_HHZ),max(A1_A00D_HHZ)]),
set(gca,'XAxisLocation','top'), %set(gca, 'TickDir', 'out'),
set(gca,'XTickLabel',str2mat('07:00','07:06','07:12','07:18','07:24','07:30
','07:36','07:42','07:48','07:54','08:00'))
ylabel('A (counts)', 'FontSize', 8),
subplot(6,1,2), specgram(A1_A00D_HHZ,500,500),
ylabel('Freq. (Hz)', 'FontSize', 8), xlabel(''), set(gca,'XTickLabel',[])
subplot(6,1,3), plot(t,A2_B4CC_HHZ,'b'), %xlim([min(t8)-30, max(t8)+30])
ylim([min(A2_B4CC_HHZ), max(A2_B4CC_HHZ)]), set(gca,'XTickLabel',[])
ylabel('A (counts)', 'FontSize', 8),
subplot(6,1,4), specgram(A2_B4CC_HHZ,500,500),
ylabel('Freq. (Hz)', 'FontSize', 8), xlabel(''), set(gca,'XTickLabel',[])
subplot(6,1,5),plot(t,A3_B32F_HHZ,'b'),

ylabel('A (counts)', 'FontSize', 8),
subplot(6,1,6), specgram(A3_B32F_HHZ,500,500),
ylabel('Freq. (Hz)', 'FontSize', 8), xlabel(''), set(gca,'XTickLabel',[])
saveas(figure(1), '1hour_specgramsHHZ_St1_St2_St3.jpg');

figure(2)
subplot(6,1,1), plot(t,A4_9898_HHZ,'b'),%xlim([min(t8)-30, max(t8)+30])
ylim([min(A4_9898_HHZ), max(A4_9898_HHZ)]), set(gca,'XTickLabel',[])
ylabel('A (counts)', 'FontSize', 8),
subplot(6,1,2), specgram(A4_9898_HHZ,500,500),
ylabel('Freq. (Hz)', 'FontSize', 8), xlabel(''), set(gca,'XTickLabel',[])
subplot(6,1,3),plot(t,A5_B4C6_HHZ,'b'), %xlim([min(t8)-30, max(t8)+30])
ylim([min(A5_B4C6_HHZ), max(A5_B4C6_HHZ)]), set(gca,'XTickLabel',[])
ylabel('A (counts)', 'FontSize', 8),
subplot(6,1,4), specgram(A5_B4C6_HHZ,500,500),
ylabel('Freq. (Hz)', 'FontSize', 8), xlabel(''), set(gca,'XTickLabel',[])
subplot(6,1,5), plot(t,A6_A04C_HHZ,'b'),%xlim([min(t8)-30, max(t8)+30])
ylim([min(A6_A04C_HHZ), max(A6_A04C_HHZ)]),set(gca,'XTickLabel',[])
ylabel('A (counts)', 'FontSize', 8),
subplot(6,1,6), specgram(A6_A04C_HHZ,500,500),
ylabel('Freq. (Hz)', 'FontSize', 8), xlabel(''), set(gca,'XTickLabel',[])
saveas(figure(2), '1hour_specgramsHHZ_St4_St5_St6.jpg');
```

Single eventdetection.

```
%% SPITZ - 1hour data - SHAKE MAP
close all, clear all, clc
%% St coordinates
St_coord = load('St_coord.txt');
% 1.column --> Y (m)
% 2.column --> X (m)
long = St_coord(:,2);
lat = St_coord(:,1);
Y_st = [lat - min(lat)]*111325;        % In latitude 1° == 111.325 [m]
X_st = [long - min(long)]*73984;       % In longitude 1° == 73.984 km [m]

%% Station corrections
St_corr = load('St_corr.txt');

%% Resultant in m/sec
result_A = load('A_resultant10sec_over3%4.txt');

tic
%% GRID witht he coordinates
% The area is defined by maximum and minimum latitudes and longitides of
% each event
long_grid = linspace(min(long)-0.0001, max(long)+0.0001, 100);
lat_grid = linspace(min(lat)-0.0001, max(lat)+0.0001, 100);

X_min = (min((long - min(long))-0.0001)*73984);
X_max = (max((max(long) - long)+0.0001)*73984);
Y_min = (min((lat - min(lat))-0.0001)*111325);
Y_max = (max((max(lat) - lat)+0.0001)*111325);
X_grid = linspace(X_min, X_max, 100);
Y_grid = linspace(Y_min, Y_max, 100);

%% I compute the coordinates for latitude and longitude
[X_long_grid,Y_lat_grid] = meshgrid(long_grid,lat_grid);

% A file with the calculated attenuation factor is needed
% 'Stations_corr_all.txt'
a = load(Attenuation_fac.txt');


TW = size(result_A,1);  % number of TW used
for ij = 1:TW
    %% Distance from the stations to all grid points
    for ii = 1:length(long) % number of stations
        % Back Projected Amplitude from the stations to all grid points
        Pseudomag_10(:,:,ij,ii) =
(10.^St_corr(ii)).*result_A(ij,ii)./(d_grid_deg(:,:,ii).^a);
        Pseudo_Mag (:,:,ij,ii) = log10(result_A(ij,ii)) -
(a*log10(d_grid_deg(:,:,ii))) + St_corr(ii);
    end
    Pseudomag_10_min1 (:,:,ij) = min(Pseudomag_10(:,:,ij,1),
Pseudomag_10(:,:,ij,2));
    Pseudomag_10_min2 (:,:,ij) = min(Pseudomag_10_min1(:,:,ij),
Pseudomag_10(:,:,ij,3));
    Pseudomag_10_min3 (:,:,ij) = min(Pseudomag_10_min2(:,:,ij),
Pseudomag_10(:,:,ij,4));
    Pseudomag_10_min4 (:,:,ij) = min(Pseudomag_10_min3(:,:,ij),
Pseudomag_10(:,:,ij,5));
    Pseudomag_10_min5 (:,:,ij) = min(Pseudomag_10_min4(:,:,ij),
Pseudomag_10(:,:,ij,6));
    Pseudomag_10_min (:,:,ij) = min(Pseudomag_10_min5(:,:,ij),
Pseudomag_10(:,:,ij,7));
    Pseudo_Mag_min(:,:,ij) = log10(Pseudomag_10_min(:,:,ij));
Real_mag(:,:,ij) = 0.8605749374.*Pseudo_Mag_min(:,:,ij) + 7.2690111093;
```

```
% Real magnitude of the source
end

%% &&&&&&&&&&&      CONVEX HULL MASK      &&&&&&&&&&&
% convex Hull
CH = convhull(long,lat, 'simplify', false);
% closest value to find --> St cood.
for kk = 1:length(CH);
    val_lat = lat(CH(kk));
    val_long = long(CH(kk));

    tmp_lat = abs(lat_grid - val_lat);
    tmp_long = abs(long_grid - val_long);

    [IDx_lat, IDy_lat] = min(tmp_lat);
    [IDx_long, IDy_long] = min(tmp_long);

    ID_lat_mask(kk) = IDy_lat;
    ID_long_mask(kk) = IDy_long;
end
mask_in = poly2mask(ID_long_mask,ID_lat_mask, length(long_grid),
length(lat_grid));

    Pseudomag_10_mask(:,:,jj) = Pseudomag_10_min(:,:,jj).*mask_in;
    Pseudomag_10_mask(Pseudomag_10_mask(:,:,:) == 0) = NaN;
    Max_PM10 = max(max(Pseudomag_10_mask));
    % PSEUDOMAGNITUDE
    Pseudomag_mask(:,:,jj) = log10(Pseudomag_10_min(:,:,jj)).*mask_in;
    Pseudomag_mask(Pseudomag_mask(:,:,:) == 0) = NaN;
    Max_PM = max(max(Pseudomag_mask));

    % REAL MAGNITUDE
    Realmag_mask(:,:,jj) = Real_mag(:,:,jj).*mask_in;
    Realmag_mask(Realmag_mask(:,:,:) == 0) = NaN;
    Max_RM = max(max(Realmag_mask));
end

Max_PM10_ALL = Max_PM10(:);
figure
hold on
plot(Max_PM10_ALL, 'b')
plot([1,size(Max_PM10_ALL,1)], [3.9811e-9, 3.9811e-9], 'k')
title('10^{Pseudo-Magnitude} - 10sec TW overlap 3/4')
xlabel('Time Window'),
xlim([1 size(Max_PM10_ALL,1)])
ylabel('10^{Pseudo-Magnitude}')
set(gca,'YTick',(0:0.4e-8:4e-8))
saveas(figure(1), strcat('10sec_max_PM10_lines04line39811e-9.jpg'))

Max_RM_ALL = Max_RM(:);
figure
plot(Max_RM_ALL, 'b')
title('Real Magnitude - 10sec TW overlap 3/4')
xlabel('Time Window'),
xlim([1 size(Max_RM_ALL,1)])
ylabel('Real Magnitude')
saveas(figure(3), strcat('10sec_max_RM.jpg'))

%% %%%% Plot from top St to bottom St
tt = [1:1:TW];
A1 = result_A(:,1); A2 = result_A(:,2);
A3 = result_A(:,3); A4 = result_A(:,4);
A5 = result_A(:,5); A6 = result_A(:,6);
A7 = result_A(:,7);
```

Source code

```
%% HITS 2D plots
for ii = 311
    % %%%%% Location of the maximum magnitude (10^PM and PM)
    % Maximum value 10^PM
    max_PM_10 = Max_PM10(1,1,ii);
    % Location of the maximum
    [rPM10,cPM10] = find(Pseudomag_10_mask(:,:,ii) == max_PM_10);

    % Maximum value PM
    max_PM = Max_RM(1,1,ii);
    % Location of the maximum
    [rPM,cPM] = find(Pseudomag_mask(:,:,ii) == max_PM);
    % %%%%% 10^PM
    figure(ii), hold on
    p1 = pcolor(X_grid, Y_grid, Pseudomag_10_mask(:,:,ii));
    set(p1, 'EdgeColor', 'none');
    c1 = colorbar;
    maxbar = 4e-8; minbar = 0.4e-8;  % min and max of the color bar
(logarithm of the pseudomag)
    caxis([minbar, maxbar])
    ylabel(c1,'10^{Pseudomagnitude}')

    % grid points
    plot(X_long_grid(:,:),Y_lat_grid(:,:), '.', 'Color', [0.8 0.8 0.8],
'MarkerSize', 2)
    xlim([min(X_grid) max(X_grid)]); ylim([min(Y_grid) max(Y_grid)]);
    % Stations
    St = plot(X_st(:),Y_st(:), 'o', 'Color', [1 0 0], 'MarkerFaceColor', [1
0 0], 'MarkerSize', 3);
    % maximum magnitude
    maxPM10 = plot(X_grid(cPM10),Y_grid(rPM10), 'p', 'Color', [0 0 0],
'MarkerFaceColor', [0 0 0], 'MarkerSize', 13);
    xlabel('x (m)'),    ylabel('y (m)')
    title('Location - TW = 311')
    hold off
    saveas(figure(ii), strcat('PM_10_location_TW311.jpg'))

    % %%%%% Pseudomagnitude
    figure(ii+1)
    p1 = pcolor(X_grid, Y_grid, Pseudomag_mask(:,:,ii));
    set(p1, 'EdgeColor', 'none');
    hold on
    c1 = colorbar;
    maxbar = -7.4; minbar = -8.4;  % min and max of the color bar
    caxis([minbar, maxbar])
    ylabel(c1,'Pseudomagnitude')
    % grid points
    plot(X_long_grid(:,:),Y_lat_grid(:,:), '.', 'Color', [0.8 0.8 0.8],
'MarkerSize', 2)

    xlim([min(X_grid) max(X_grid)]); ylim([min(Y_grid) max(Y_grid)]);
    % Stations
    St = plot(X_st(:),Y_st(:), 'o', 'Color', [1 0 0], 'MarkerFaceColor', [1
0 0], 'MarkerSize', 3);
    maxPM10 = plot(X_grid(cPM10),Y_grid(rPM10), 'p', 'Color', [0 0 0],
'MarkerFaceColor', [0 0 0], 'MarkerSize', 13);

    xlabel('x (m)'),    ylabel('y (m)')
    title('Location - TW = 311')
    hold off
    saveas(figure(ii+1), strcat('PM_location_TW311.jpg'))
end
```